https://doi.org/10.15388/vu.thesis.714
https://orcid.org/0000-0001-8637-1328

VILNIUS UNIVERSITY
STATE RESEARCH INSTITUTE CENTER FOR PHYSICAL SCIENCES AND TECHNOLOGY

Justina Anulytė

Strongly Coupled Extended Plasmonic States for Coherent Energy Exchange

DOCTORAL DISSERTATION

Natural Sciences
Physics (N 002)

VILNIUS 2025

The dissertation was prepared between 2020 and 2024 at the State Research Institute Center for Physical Sciences and Technology.

Academic supervisor – Prof. Dr. Zigmas Balevičius **(**State Research Institute Center for Physical Sciences and Technology, Natural Sciences, Physics, N 002).

This doctoral dissertation will be defended in a public/closed meeting of the Dissertation Defence Panel:

Chairman – Prof. Dr. Aidas Matijošius (Vilnius University, Natural Sciences, Physics, N 002).
Members:
Prof. Habil. Dr. Proc. Jonas Gradauskas (State Research Institute Center for Physical Sciences and Technology, Natural Sciences, Physics, N 002),
Prof. Dr. Saulius Juodkazis (Swinburne University of Technology, Natural Sciences, Physics N 002),
Prof. Habil. Dr. Sigitas Tamulevičius (Kaunas University of Technology, Natural Sciences, Physics N 002),
Dr. Mindaugas Gedvilas (State Research Institute Center for Physical Sciences and Technology, Natural Sciences, Physics, N 002).

The dissertation shall be defended at a public meeting of the Dissertation Defence Panel at 10 (hour)/ on 23 January 2025 in meeting room D401 of the State Research Institute Center for Physical Sciences and Technology..
Address: Saulėtekis ave., 3, D401, Vilnius, Lithuania
Tel. +37052649211; e-mail: office@ftmc.lt

The text of this dissertation can be accessed at the libraries of State research institute Center for Physical Sciences and Technology and Vilnius University as well as on the website of Vilnius University:
www.vu.lt/lt/naujienos/ivykiu-kalendorius

https://doi.org/10.15388/vu.thesis.714
https://orcid.org/0000-0001-8637-1328

VILNIAUS UNIVERSITETAS
VALSTYBINIS MOKSLINIŲ TYRIMŲ INSTITUTAS FIZINIŲ IR TECHNOLOGIJOS MOKSLŲ CENTRAS

Justina Anulytė

Koherentiniai energijos mainai išplėstinėse plazmoninėse būsenose esančiose stipriojoje sąveikoje

DAKTARO DISERTACIJA

Gamtos mokslai,
Fizika (N 002)

VILNIUS 2025

Disertacija rengta 2020–2024metais Valstybinis mokslinių tyrimų institutas Fizinių ir technologijos mokslų centras.
Mokslinius tyrimus rėmė Lietuvos mokslo taryba, gauta stipendija už akademinius pasiekimus (Nr. P-DAP-23-68).

Mokslinis vadovas – prof. dr. Zigmas Balevičius (Valstybinis mokslinių tyrimų institutas Fizinių ir technologijos mokslų centras, gamtos mokslai, fizika, N 002).

Gynimo taryba:
Pirmininkas – prof. dr. Aidas Matijošius (Vilniaus universitetas, gamtos mokslai, fizika, N 002).
Nariai:
Prof. habil. dr. proc. Jonas Gradauskas (Valstybinis mokslinių tyrimų institutas Fizinių ir technologijos mokslų centras, gamtos mokslai, fizika, N 002),
Prof. dr. Saulius Juodkazis (Svinburno technologijų universitetas, gamtos mokslai, fizika, N 002),
Prof. habil. dr. Sigitas Tamulevičius (Kauno technologijų universitetas, gamtos mokslai, fizika, N 002),
Dr. Mindaugas Gedvilas (Valstybinis mokslinių tyrimų institutas Fizinių ir technologijos mokslų centras, gamtos mokslai, fizika, N 002).

Disertacija ginama viešame Gynimo tarybos posėdyje 2025 m. sausio mėn. 23 d. 10 val. Valstybinio mokslininkų tyrimų instituto Fizinių ir technologijos mokslų centro D401 posėdžių salėje.
Adresas: Saulėtekio al. 3, D401, Vilnius, Lietuva, tel. +37052649211 ; el. paštas office@ftmc.lt

Disertaciją galima peržiūrėti Valstybinio mokslininkų tyrimų instituto Fizinių ir technologijos mokslų centro bei Vilniaus universiteto bibliotekose ir VU interneto svetainėje adresu:
https://www.vu.lt/naujienos/ivykiu-kalendorius

LIST OF ABREVIATIONS

AOI – angles of incidence
ATR – attenuated total reflection
BSW – Bloch surface waves
CVD – chemical vapor deposition
DBR – distributed Bragg reflectors
DLW – direct laser writing
FLIM – fluorescence lifetime imaging microscopy
FRET – Förster resonance energy transfer
HLPP – hybrid lattice plasmon polaritons
IBS – ion beam sputtering
IRF – instrument response function
ISC – intersystem crossing
LED – light-emitting diodes
LRSP – long-range surface plasmon polaritons
LSP – localized surface plasmon
PBG – photonic bandgap
PC – photonic crystal
PL – photoluminescence
PMMA – poly(methyl methacrylate)
PSLPR – Propagated Surface Lattice Plasmonic Resonance
PVD – physical vapor deposition
Q-factor – quality factor
R6G – Rhodamine 6G
RIU – refractive index unit
SE – Spectroscopic ellipsometry
SEM – scanning electron microscopy
SLPR – surface lattice plasmon resonances
SP – surface plasmon
SPAD – single photon avalanche diode
SPASER – SP amplification by stimulated emission of radiation
SPCE – Surface Plasmon-Coupled Emission
SPP – surface plasmon polaritons
TCSPC - time-correlated single-photon counting
TE – transverse electric
TIR – Total Internal Reflection
TIRE – Total Internal Reflection Ellipsometry
TM – transverse magnetic
TPP – Tamm plasmon-polariton
TPP-SPP – Tamm plasmon polariton-surface plasmon polariton

CONTENTS

ACKNOWLEDGMENT

It would be very difficult to implement and complete doctoral studies without support and assistance from my colleagues and family, I am very grateful that they have been there all these years. First of all, I would like to thank my supervisor, Prof. Dr. Zigmas Balevičius, for giving me the opportunity to prepare my dissertation on this topic. I am grateful for the opportunity to discuss scientific issues, for the strong support and help in analyzing the results and writing the dissertation. I am also thankful to my colleague dr. Ernesta Bužavaitė-Vertelienė, who invited me to the Plasmonics and Nanophotonics laboratory, shared her experience and knowledge, helped me in all areas, and didn't let me give up. It is a great privilege to have such wonderful colleagues.

Many thanks to the entire collegues of the Center for Physical Sciences and Technology for their help, advice, and friendly environment. Especially to dr. Vilius Vertelis for fruitful discussion about modeling and advice for manuscript preparation, to dr. Evaldas Stankevičius and dr. Lina Grinevičiūtė for the preparation of the samples and to dr. Vytautas Žičkus for the opportunity to come to the University of Glasgow and meet many wonderful scientists, try new measurement methods, and get new knowledge and results.

Finally, I want to thank my wonderful, inspiring family, especially to my grandfather, whose faith in me kept me from giving up and purposefully pursuing my goal. I also want to thank my bachelor and master degree supervisor prof. habil. dr. Kęstutis Arlauskas for motivation, knowledge and opportunities to learn about science. I want to thank all my family and friends for their patience and endless support.

1. INTRODUCTION

The fundamental understanding of coherent energy exchange via strong light-matter interaction between nanophotonic cavity and emitter opens various applications in modification of chemical reactions rate [1], conceptually new type of nano lasers [2], Bose-Einstein condensation at room temperature [3] , quantum optical nanodevices [4], advanced optical sensing [5].

The basic assumptions of strong coupling is that two harmonic oscillators, become strongly coupled if there is some way for them to exchange energy faster than the rate of energy losses occur [6]. If this happens the energy levels of the hybrid system may be different from those of the uncoupled emitter or the optical system individually. In such coupled systems the interaction strength between two harmonic oscillators exceeds the damping rate and as a result, the eigenstate of the system is polaritonic mode [1]. These hybrid states offer the possibility to explore light-matter interactions, they also give opportunities to exploiting various nano-fabrication techniques to design quantum optical devices [5, 7].

Generally, the rate of the emission process can be modified by placing the emitter in a structured environment (cavity). The enhancement of spontaneous emission (Purcell effect) [8] widely used in conventional lasers, which is an example of weak coupling case where emission energy remaining unaltered. But if the interaction is strong enough then energy levels responsible for emission are also altered. They become inextricably linked with the modes of the local optical environment. The difference between the original and the new energies depends on the strength of the coupling. The energy separation between the normal modes at the avoided crossing is called the normal mode splitting or the Rabi splitting [9]. Usually for photonic systems strong coupling achieved when Rabi gap is experimentally detected. Strong coupling phenomena it is a signature of entering a regime where coherence play an important role. Thus, it closely connected to such phenomena as stimulated emission, gain and lasing for example, tresholdless lasing. The mode volume of conventional photonic cavity cannot be reduced lower than diffraction limit, what restrict the interaction strength in strong coupling regime. Meanwhile, plasmonics allow to subwavelength confinement and overcome the diffraction limit, thus the mode volume can be reduced even more than in purely photonic mode. Additional advantage that plasmonics+emitters provide possibility to employ the so called “open cavity”, i.e. enabling easy access to the mode volume in which strong coupling takes place [6]. Light interaction with metals at the nanoscale demonstrates enhancement of local electromagnetic field at the metal-dielectric interfaces

[10] and is generally known as plasmonics. Plasmons are collective oscillations of conduction electrons in the metal and can couple with light photons, forming the polariton state. Surface plasmon polaritons (SPPs) are electromagnetic modes that arise from interaction between light and conduction electrons in metals [10]. Surface plasmons (SP) are the most collective material oscillations known in nature, which implies they are the most harmonic [2]. This fundamental property predicts many advancements related with increased coherence of nanophotonic structures where plasmonic resonances interact strongly with matter.

This PhD thesis is dedicated for study of fundamental properties of extended plasmon polaritonic states in strong coupling regime during the coherent energy exchange occur, and their applications for fluorescence lifetime microscopy and optical sensing technologies. In this study, we investigate the influence of room temperature strong coupling between SPP and excitons on fluorescence lifetimes and photobleaching effects. The plasmonic-photonic structure, comprising of thin silver (Ag) and gold (Au) layers with a Rhodamine 6G (R6G) dye layer, shows a clear shift in the plasmon resonance and R6G absorption lines with varying incident angles, indicative of strong coupling, with a measured Rabi splitting of approximately 90 meV. Fluorescence lifetime imaging microscopy (FLIM) for the first time was employed to assess photobleaching, revealing a significant reduction in photobleaching effect in strongly coupled plasmonic-excitonic structures compared to single R6G layers (Chapter 4.1).

Another part of PhD thesis investigates samples with lattice arrays of gold nanobumps in which surface lattice plasmonic resonances coupled strongly with other plasmonic modes and organic dye excitons. The total internal reflection ellipsometry (TIRE) method was used for the excitation and study of strong coupling between Tamm plasmon polariton (TPP) and SPP in nanophotonic structures with 1D photonic crystal (PC) and lattice of gold nano-bumps on the top. The optical dispersion and propagation features of extended plasmon polaritonic states in 1D PC with uniform gold layer and the lattice of gold nano-bumps array were analyzed by two coupled oscillator model and wave-vector vs. energy broadening (Chapter 4.2).

Lastly, the influence of the strong coupling regime between Tamm (TPP) and propagated plasmon polaritons in the hybrid plasmonic modes on the refractive index sensitivity was analyzed. TIRE method was used for optical response of the gold film without laser modification and secondly, on the area with gold nanobumps produced by the Direct Laser Writing (DLW) technique. The optical signal sensitivity of hybrid plasmonic resonances was compared with traditional surface plasmon resonance (SPR) on a single gold layer.

OBJECTIVES

- Examine the strong coupling regime between SPP and excitons in a hybrid plasmon-exciton polariton structure, focusing on energy level modification and optical dispersion alteration.
- Investigate the influence of strong coupling on photobleaching suppression in fluorescent molecules (R6G dye) using surface plasmon-exciton polaritons in FLIM method.
- Investigate the effects of surface lattice arrays on the coupling between Tamm plasmons and surface plasmons polaritons, and their impact on the propagation length, Q-factor and coherence properties.
- Analyze the hybrid TPP-SPP plasmonic modes' optical properties and sensitivity to refractive index changes by comparing uniform gold layers with structures modified by nano-bumps.

Tasks to achieve the objectives

- Measure the TIRE spectra of ellipsometric parameters (Ψ and Δ) to map the hybrid exciton-SPP mode and compare the optical dispersion of single SPPs with and without dye excitons, identifying shifts in the reflection intensity maps.
- Evaluate the photobleaching effect on fluorescence lifetime in strongly coupled and non-coupled structures using FLIM, determining the extent photobleaching suppression in the presence of strong coupling between SPPs and R6G dye excitons.
- Quantify the Rabi splitting and strong coupling strength through modeling and fitting the dispersion curves of upper and lower polariton branches, comparing the coupling strength (g) with damping (γ) to confirm the strong coupling regime.
- Measure and compare the TIRE spectra of ellipsometric parameters (Ψ and Δ) for both uniform gold layers and nano-bumps-modified areas to evaluate the spectral shifts, strong coupling, and generation of new hybrid plasmonic modes.
- Model the dispersion behavior of hybrid TPP-SPP and Bragg modes using coupled oscillator model, analyzing the impact of nano-bumps lattice on the Rabi splitting and coupling strength between TPP and SPP components.
- Quantify the changes in Q-factor and propagation length (δ) for the SPP and TPP components, identifying the differences in resonance broadening, wave-vector uncertainty (Δk), and coherence properties between uniform gold layers and lattice structures.

- Perform TIRE spectra analysis of ellipsometric parameters (Ψ and Δ) in both uniform gold layers and gold nano-bumps samples, determining the wavelength shift and sensitivity to refractive index changes in deionized water and ethanol.
- Analyze the dispersion map of hybrid TPP-SPP modes and PSLPR (Propagated Surface Lattice Plasmonic Resonance) excitation, comparing the spectral features and Q-factor (quality factor) for structures with and without nano-bumps array.
- Compare the sensitivity of ellipsometric parameters (Ψ and Δ) to ambient refractive index changes for both uniform and modified areas, determining the increase in sensitivity and Q-factor due to nano-bump lattice modifications.

SCIENTIFIC NOVELTY

The experimental studies conducted in this PhD thesis belongs to the topic of nanophotonic devices in which polaritonic states with extended coherence properties are employed.

The main novelty of these PhD thesis is demonstrated property of strong light-matter interaction to reduce the photobleaching of organic dye molecules and stabilization of the fluorescence intensities in a hybrid SPP and R6G dye exciton mode (SPP-exciton) and it's applications for FLIM measurements.

The suppression of photobleaching by strongly coupled localized plasmons and J-aggregates were showed previously [18]. Here two measuring techniques were used, the TIRE measurements together with FLIM complement each other, thus, both verifying the influence of the strong coupling between SPP and exciton polaritons on the photobleaching. It was demonstrated that the fluorescence signal intensity for hybrid SPP-exciton polaritonic state was reduced by 5% compared with weak coupling regime (25-30%) in FLIM. This shows the strongly coupled SPP-exciton polaritons potential impact on the development of polaritonic devices with enhanced stability and performance. During this study the TIRE method was used to determine the strong coupling between SPP and R6G excitons by using optical filter method and the FLIM demonstrated that strong coupling leads to reduced photobleaching. To the best of our knowledge, the combination of strongly coupled based polaritonic nanostructures to suppress photobleaching in FLIM method was applied for the first time.

The obtained results demonstrate novel approach to control and change the propagation length under strong coupling regime between TPP and SPP

components in the hybrid plasmonic mode by using surface lattice arrays. The fabricated nanophotonic-plasmonic structures demonstrate the potential impact of DLW method as cost effective, fast and large area for creating integrated photonic devices with designed properties in this case changing the propagation length and coherence properties in the hybrid plasmonic mode. The application of surface lattice resonances together with strong coupling regime leads to decreasing losses, what resulting in the increasing propagation length and better coherence properties of such plasmonic excitations which in turn promises advanced properties for thresholdless plasmonic based coherent emission nano sources. Attention to the nanophotonic – plasmonic structures which are able to support extend coherence properties under strong coupling arises from their promising applications to the plasmonic lasing, information processing, and using such polaritonic structures for new generation of biosensing.

PRACTICAL VALUE

The application of strongly-coupled plasmon-exciton polaritonic states in Fluorescence Lifetime Image Microscopy allow remarkably suppress photobleaching effect in organic dye molecules and thus decrease the influence of photobleaching to the fluorescence life time decay. It was observed that the strong coupling between SPP and dye excitons plays a pivotal role in suppressing photobleaching, a phenomenon that often impedes fluorescence-based studies. The plasmon-exciton polaritonic nanostructures exhibit a remarkable ability to stabilize photobleaching mechanisms, thereby offering a promising avenue for the development of quantum multiparticle nanophotonic devices with organic molecules.

The fabrication of gold nano-bumps lattice array on the structures supporting strong coupling between TPP and SPP allow to modify the coherence length of the extended plasmon polaritonic states.

The influence of the strong coupling between Tamm (TPP) and propagated SPP in the extended plasmon polaritonic modes on the increased sensitivity to the refractive index changes was demonstrated. This optical property of extended plasmon polaritonic mode was successfully applied for real time, non-destructive optical sensing technologies.

STATEMENTS TO DEFENCE

- The normal mode splitting of 90 meV confirms the strong coupling regime between the surface plasmon polaritons and R6G dye excitons, exceeding the damping (52 meV) of coupled plasmon-exciton hybrid mode, which is described as the sum of quarter linewidths.
- Strong coupling regime between plasmons and excitons suppress the photobleaching effect of rhodamine 6G molecules and thus fluorescence intensity of FLIM signal decreases 25% less compared with weak coupling samples without metallic layer.
- Surface lattice resonances together with strong coupling regime leads to decreasing losses of polaritonic states, resulting in the increasing propagation length and spatial coherence of such polaritonic states.
- Strong coupling regime increases optical signal sensitivity to the refractive index changes by approximately 27% compared to traditional surface plasmon resonance sensors.

Structure of the dissertation

This dissertation is organized into five main chapters, each addressing critical aspects of the research on hybrid plasmonic modes and their applications in sensing and photobleaching suppression.

Chapter 1 provides an overview of the research, outlining the motivations, objectives, and structure, while introducing key concepts like strong coupling and plasmonics.

Chapter 2 reviews the relevant literature, covering topics such as harmonic oscillators, 1D PC, and various hybrid plasmonic modes, along with photobleaching and laser dye characteristics.

Chapter 3 details the experimental methods, including spectroscopic ellipsometry (SE), TIRE, and sample fabrication techniques like spin-coating and DLW.

Chapter 4 presents the experimental findings, exploring the effects of gold nano-bumps on TPP-SPP modes, biosensing applications and photobleaching suppression in hybrid plasmon-exciton structures.

Finally, Chapter 5 summarizes the key results and discusses their contributions to hybrid plasmonics and potential applications in biosensing and nanophotonics.

List of the scientific publication

P1. J. Anulytė*, E. Bužavaitė-Vertelienė, V. Vertelis, E. Stankevičius, K. Vilkevičius, Z. Balevičius, Influence of gold nano-bumps surface lattice array to the propagation length of strongly coupled Tamm and surface plasmon polaritons, *Journal of Materials Chemistry C* (2022), **10**, 13234 – 13241. Q1 (IF:8.067)

P2. J. Anulytė, E. Bužavaitė-Vertelienė, E. Stankevičius, K. Vilkevičius, Z. Balevičius*, High Spectral Sensitivity of Strongly Coupled Hybrid Tamm-Plasmonic Resonances for Biosensing Application, *Sensors* (2022), **22**(23), 9453. Q2 (IF:3.847)

P3. J. Anulytė*, V. Žičkus, E. Bužavaitė-Vertelienė, D. Faccio, Z. Balevičius, Strongly coupled plasmon-exciton polaritons for photobleaching suppression, *Nanophotonics* vol. 13, no. 22, 2024, pp. 4091-4099. Q1 (IF: 6.5).

Other publications during this PhD

P4. E. Bužavaitė-Vertelienė, V. Mačiulis, I. Plikusienė, J. Anulytė, T. Tolenis, A. Baškys, Z. Balevičius, Total internal reflection ellipsometry approach for Bloch surface waves biosensor applications, *Biosensors* **12**(8), 584, (2022). Q1 (IF:5.743)

Conference

C1. V. Gradauskas, J. Anulytė, E. Bužavaitė-Vertelienė, I. Plikusienė, Z. Balevičius. (In-situ) Study of immobilized receptor binding kinetics by using planar photonic-plasmonic nanostructures for biosensing. *64th International conference for students of physics and natural sciences "Open Readings"*, Vilnius, 2021 March 16-19.

C2. J. Anulytė, E. Bužavaitė-Vertelienė, I. Plikusienė. Z. Balevičius. Hybrid Tamm-surface plasmon polaritons mode based on planar plasmonic photonic nonostructure for highly sensitive real time biosensing of GsCF and BSA proteins. *23-rd International Conference – School, "Advanced materials and technologies"*, Palanga, 2021 August 23-27.

C3. J. Anulytė, E. Bužavaitė-Vertelienė, Z. Balevičius. Modelling of plasmon – exciton strong coupling in silver/gold film with R6G dye in polymethyl methacrylate layer. *65th International conference for students of physics and natural sciences "Open Readings"*, Vilnius, 2022 March 15-18.

C4. J. Anulytė, E. Bužavaitė-Vertelienė, Z. Balevičius. Application of hybrid Tamm and surface plasmon polariton modes to optical sensors. Lietuvos mokslų akademijos *11-oji konferencija „Fizinių ir technologijos mokslų tarpdalykiniai tyrimai“* reikšmė ir rezultatai, Vilnius, 2023 March 23th.

C5. J. Anulytė, E. Bužavaitė-Vertelienė, V. Vertelis, E. Stankevičius, K. Vilkevičius, Z. Balevičius. Optical response of the hybrid Tamm-surface plasmon polariton modes on the surface lattice array of gold nanobumbs *66th International conference for students of physics and natural sciences "Open Readings",* Vilnius, 2023 April 18-21.

C6. J. Anulytė, E. Bužavaitė-Vertelienė, Z. Balevičius. Study of the strongly coupled Tamm-plasmon polariton states in the surface lattice array of gold nano-bumps. *6th International Conference on Optics, Photonics and Lasers (OPAL' 2023),* 17-19 May 2023 Funchal (Madeira Island), Portugal.

C7. E.Bužavaitė-Vertelienė, S. Juciūtė, I. Plikusienė, J. Anulytė, Z. Balevičius. Application of strongly coupled plasmonic excitation for sensing of dye-labelled Bovine Serum Albumin, *IOP Photon 2024, Swansea,* United Kingdom, 2024 September 2-6.

C8. P. Jurkšaitis, J. Anulytė, D. Banevičius, E. Bužavaitė-Vertelienė, Z. Balevičius. Surface Plasmon Coupled Emission of Rhodamine 6G Dye in Strong Coupling Regime, *IOP Photon 2024, Swansea,* United Kingdom, 2024 September 2-6.

Authors contribution

The author of this PhD Thesis performed spectroscopic ellipsometry presented in all scientific publications of dissertation. Also participating in design optical scheme configuration and experiments of fluorescence life time measurements. Sample preparation, the deposition of metallic layer by magnetron sputtering and organic dye molecules in PMMA matrix layers with different thicknesses and concentrations by spin coating method was done by the author. All first drafts manuscripts were prepared by the author in detailed discussions with supervisor and co-authors, as well as, further participating in discussions and improving the manuscripts during review process. In two scientific publications on which this PhD Thesis is based J. Anulytė is corresponding author and in all publications she is the first author.

2. LITERATURE OVERVIEW

2.1. Strong Coupling Between Two Harmonic Oscillators

In recent decades, the study of strong coupling in light-matter interaction systems has garnered substantial interest due to its profound implications in both fundamental physics and technological applications. Strong coupling occurs when two or more oscillators interact so intensely that their individual energy levels are significantly modified, leading to the formation of hybrid modes [6,11]. This phenomenon is observed across various systems, including molecules in optical cavities and SPP [1]. Understanding the mechanisms and consequences of strong coupling is crucial for developing advanced photonic devices, quantum technologies, and enhancing the control of chemical reactions [6,11].

Generally, three different approaches are used to describe the strong coupling phenomenon: classical, semiclassical and quantum. In the classical approach splitting of energy levels due to strong coupling between emitter and surface plasmon polariton described as Lorentz oscillator substituted into the SPP dispersion relation. For semiclassical approach, emitter is described as the two-level system instead of Lorentz oscillator and is alternative to the conventional SPP dispersion relation. For fully quantum case, the emitter and SPP mode are considered as two-level system and quantum field, respectively. In quantum case splitting appears when appropriate Hamiltonian of the described system is solved. The Hamiltonian describing two coupled harmonic oscillators is expressed as,

$$H = \frac{p_1^2}{2m_1} + \frac{p_2^2}{2m_2} + \frac{1}{2}k_1x_1^2 + \frac{1}{2}k_2x_2^2 + k_{12}x_1x_2\,, \qquad (2.1)$$

where p_i and x_i are the momentum and position operators of the i-th oscillator, m_i is the mass, k_i is the spring constant, and k_{12} represents the coupling strength between the oscillators [6]. A critical indicator of strong coupling is the Rabi splitting in which the coupling strength exceeds the dissipation rates of the system and the energy is therefore coherently exchanged between atom and cavity photon. This phenomenon results in the formation of a Rabi gap, which can be observed in systems such as quantum dots (two-level system) embedded in optical cavities [12,13] (Fig 2.1.1). The Rabi splitting Ω_R,

$$\Omega_R = \sqrt{(\omega_1 - \omega_2)^2 + 4g^2}, \qquad (2.2)$$

where ω_1 and ω_2 are the frequencies of oscillators and the parameter g represents the coupling strength between them.

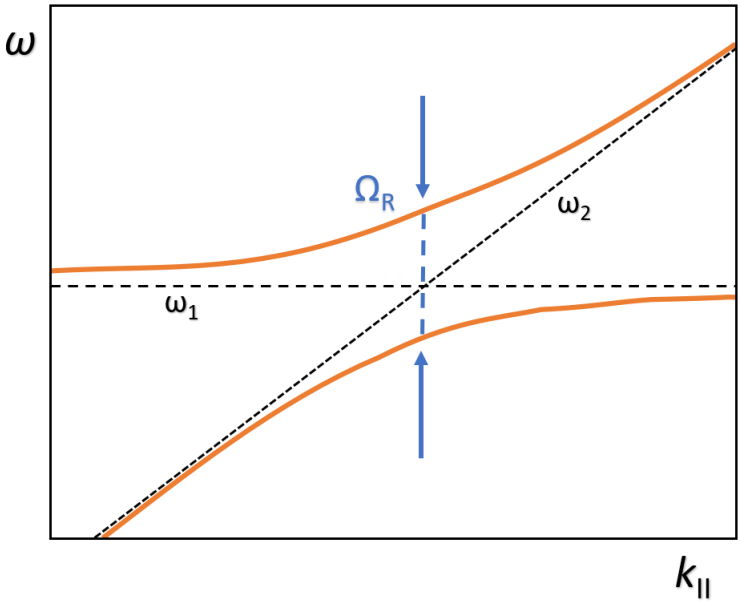

Figure 2.1.1. Hybrid mode (orange lines) dispersion **(**strong coupling regime) and single (dashed lines) emitter and optical cavity modes.

In quantum and semiclassical systems, Rabi splitting can also be expressed as [6],

$$\Omega_R = d\sqrt{\frac{N}{V}}\sqrt{\frac{\omega_0}{\hbar\varepsilon_0}}, \tag{2.3}$$

where N is the number of molecules or atoms in volume V, ε is the dielectric permittivity, ω_0 is the resonant frequency, and d is the dipole moment [14] $\hbar$ – reduced Planck constant. However, vacuum Rabi splitting obtained from fully quantum theory is similar to normal mode splitting at the resonance point in classical (Lorentzian oscillator) emitter and becomes,

$$\Omega = \sqrt{\frac{N}{V}}\frac{e}{\sqrt{\varepsilon_0 m}}. \tag{2.4}$$

The splitting is proportional to $\frac{e}{\sqrt{\varepsilon_0 m}}$ and $\sqrt{\frac{N}{V}}$. For both cases quantum and classical splitting depends on the square root of the concentration of the emissive molecules. Thus, the size of the splitting gap as function of number density of the emissive species does not allow distinguish between quantum or classical fields. Other term in the Ω is general, namely $\frac{e}{\sqrt{\varepsilon_0 m}}$, described only by electron charge and mass. In particular experimental case the features of the emissive species can be derived more specifically.

The practical implications of strong coupling are vast and varied, spanning from advanced photonic and quantum devices to enhanced chemical reaction control. Strong coupling enables precise control over light-matter interactions, which is crucial for quantum computing [14], sensing, and communication technologies [15], as well as the development of plasmonic lasers (surface plasmon amplification by stimulated emission of radiation - SPASER) [16]. For strong coupling to achieve, the coupling strength g must exceed the decay rates γ of the oscillators [12],

$$g > \frac{1}{4}(\gamma_1 + \gamma_2). \qquad (2.5)$$

In optical systems, strong coupling is identified by a significant frequency shift relative to the oscillator's linewidth, with distinct dispersion curves indicating its presence [17]. One of the most compelling examples of strong coupling is the interaction between SPP and excitons. To fully grasp the significance of strong coupling, it is essential to understand how it alters the energy landscape of interacting systems. When two harmonic oscillators couple strongly, they must efficiently exchange energy, leading to the creation of new hybrid modes with frequencies distinct from the original oscillators. The strong light-matter interaction between SPPs and organic dye molecule excitons results in a large Rabi splitting, typically around 100-300 meV, significantly larger than those achieved in inorganic semiconductors [18,19]. For efficient coupling, which depends on the distance between the dye molecule and the metal surface, the wave vectors of the SPPs and excitons must match. However, if the molecule is too close to the metal surface, energy dissipation into the metal occurs, necessitating an optimal distance of 10-20 nm [10]. SPPs, however, face rapid coherence decay due to their dissipative nature, allowing only a few Rabi oscillations before phase matching is lost, typically within 10-100 femtoseconds. To mitigate losses, long-range SPP (LRSPs) are employed, which have propagation lengths up to 250 micrometers [20]. These surface modes appear in thin metal layers surrounded

by dielectric. When the metal layer is thin, plasmonic modes at the two metal/dielectric interfaces interact to create hybrid modes. Recent studies have explored the benefits of strong coupling in hybrid systems for enhancing photobleaching suppression and sensor sensitivity. Munkhbat et al. demonstrated the suppression of photo-oxidation of organic chromophores by strongly coupling them to plasmonic nanoantennas. This study underscores the potential of strong coupling to mitigate photobleaching, which is crucial for extending the lifetime of fluorescent biomarkers. Similarly, Nefedkin et al. [22] explored the role of strong coupling in suppressing photobleaching, further emphasizing the benefits of controlled coupling strength in enhancing the stability and performance of photonic systems. Additionally, surface lattice plasmon resonances (SLPR) offer another avenue for reducing losses. In SLPR samples, coupling is achieved through the interaction between phase-matched nanoparticles arranged periodically, enhancing the Q-factor and compensating for energy losses in the metal [17]. SLRP can be utilized in various applications, including sensing, imaging, and photonic devices, further reinforcing the importance of strong coupling phenomena in modern science and technology.

The field of strongly coupled oscillators is rapidly evolving, with ongoing research exploring new coupling regimes and enhancing coherence in hybrid systems. Future studies may focus on integrating strongly coupled systems into scalable quantum networks, developing new materials and device architectures to improve coupling strength and coherence, and investigating non-linear and non-equilibrium dynamics in coupled systems to understand their fundamental properties and potential applications [6]. Understanding and harnessing strong coupling between harmonic oscillators is crucial for advancing quantum optics, photonics, and materials science. This knowledge forms the foundation for developing devices capable of manipulating light and matter interactions at the quantum level, paving the way for future technological innovations.

2.2. One-Dimensional Photonic Crystals

One-dimensional (1D) PC (also known as a Bragg mirror or distributed Bragg reflectors (DBR)) are materials with periodic optical nanostructures for photons mimicking the electron propagation in periodic structure of real crystal. Among these, 1D PC are the simplest form, where the periodicity is in a single direction. These structures are significant due to their unique ability to control and manipulate light, making them essential in various optical applications such as optical fibers [23], sensing [24], waveguides [25]. 1D PC

consist of alternating layers of materials with different refractive indices. The periodic structure creates a photonic bandgap (PBG), a range of wavelengths where light propagation is forbidden (Fig. 2.2.1. a). This bandgap is analogous to the electronic bandgap in semiconductors, but it applies to photons instead of electrons. The control over the PBG allows for the manipulation of light in innovative ways, leading to numerous practical applications The fabrication of 1D PC involves creating thin films of alternating materials using various deposition techniques [26]. These techniques include chemical vapor deposition (CVD), physical vapor deposition (PVD), sol-gel, thermal evaporation, and ion beam sputtering (IBS) [27,28].

Photolithography and electron-beam lithography are used to define precise periodic structures at the nanoscale, while self-assembly methods can also form periodic structures under suitable conditions [29,30]. Materials commonly used in these processes include silicon and other semiconductors, silicon dioxide (SiO_2), titanium dioxide (TiO_2), organic polymers [31], and metal derivatives [32], chosen for their optical properties and compatibility with fabrication processes. Efficient DBRs, a type of 1D photonic crystal, are produced using high-purity dielectric materials to suppress absorption and by precisely controlling the thickness of the layers to select the desired wavelength of reflection [33]. Smooth interfaces and surfaces are essential to prevent scattering. The formation of SiO_2 and TiO_2 layers (Fig. 2.2.1 b) is typically carried out using ion fiber sputtering on non-heated substrates, followed by an annealing step in a tube furnace with the addition of oxygen to reduce visible light absorption of TiO_2 [33,34]. Bragg mirrors consist of several layers of periodic dielectric pairs, each with an optical path length of a quarter wavelength, which imparts unique properties suitable for optoelectronic applications. The reflectivity of these devices can be tuned from 0% to almost 100% by adjusting the number of mirror stacks and the

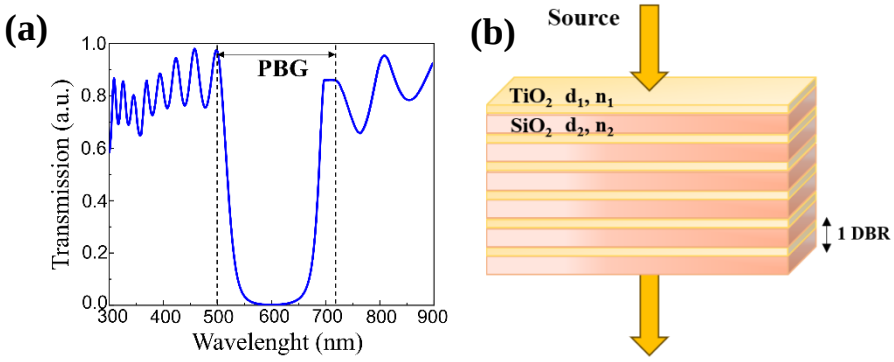

Figure 2.2.1. (a) The transmission spectra of light after passing through the PC structure and (b) the schematic structure of 1D photonic crystal.

total wavelength [27]. Their high reflectance and low internal absorption coefficient result from the constructive interference of incident and reflected light, a result of Fresnel reflection [35].

A simple equation to calculate a single DBR reflectance under normal light incidence is

$$R = \left[\frac{1 - \left(\frac{n_1}{n_2}\right)^{2m}}{1 + \left(\frac{n_1}{n_2}\right)^{2m}}\right]^2, \tag{2.6}$$

where m is the index number of quarter-wave DBR pairs, n_1 and n_2 are the refractive indices of the materials used for different DBR layers [35].

DBRs are widely used in applications such as optical filters, micro-cavities, vertical cavity surface-emitting lasers, PC, organic light-emitting diodes (LED), and for enhancing radiation efficiency [24]. The angle and wavelength dependence of DBR transmission are measured and compared with numerical simulations, while the optical properties of the evaporated layers are analyzed using ellipsometry and spectrometry [27].

One of the most promising applications of 1D PCs is in sensing, particularly biosensing. These crystals can be designed to have high sensitivity to environmental changes, making them ideal for detecting biological molecules, gases, and other analytes. For instance, a recent study utilized 1D PCs as biosensors for SARS-CoV-2 detection, showcasing their potential in medical diagnostics [36]. In optical communication systems and laser technology, 1D PCs enhance the performance of optical fibers and laser cavities [37]. A notable example is the development of a 1D PC nanobeam laser, demonstrating high efficiency and compact size [37]. Beyond sensing and communication, 1D PCs are being explored for use in displays, energy harvesting, and quantum computing. Their versatility and tunable properties make them suitable for a wide range of innovative applications [38].

Their ability to control light in unique ways opens up numerous applications in sensing, communication, and beyond. Continued advancements in fabrication and integration techniques are expected to further enhance their capabilities, making them a vital component of future optical technologies.

2.3. Plasmon Polaritons States

Surface plasmons (SP) are quasiparticles resulting from the collective oscillations of free electrons at a metal-dielectric or metal-air interface, that can interact with an external electromagnetic field, and create SPP [39]. Following Ritchie's pioneering work on plasma losses in the 1950s [40], SPs have become crucial in surface science, particularly in forming SPPs. SPP have garnered significant attention due to their promising applications across various fields such as medicine, chemistry, photonic devices, subwavelength optics, and photonics for electronic circuit elements. Advances in nanotechnology have enhanced the study and application of plasmonics, enabling unprecedented control over electromagnetic waves at the nanoscale [39].

Plasmon polariton excitation occurs when electromagnetic fields interact with free electrons in a metal, causing collective oscillations at the metal-dielectric interface [41]. This interaction confines light to the boundary, generating SPPs. These confined electromagnetic waves are highly sensitive to changes in the surrounding dielectric environment, making them useful in various applications, including biosensing, data storage, optics, and solar cells [42,43]. A key aspect of plasmon polariton excitation is plasmon resonance, which happens when the frequency of incident light matches the natural frequency of surface electron oscillations. The theoretical understanding involves solving Maxwell's equations with boundary conditions at the metal-dielectric interface [44,45]. The dispersion relation for surface plasmons can be expressed as,

$$k = \frac{\omega}{c}\sqrt{\varepsilon(\omega)}\,, \tag{2.7}$$

where k is the wave vector, ω is the angular frequency, c is speed of light in vacuum and $\varepsilon(\omega)$ is the dielectric function. This relation shows (Eq. 2.7) that as the frequency of incident light approaches the plasmon resonance frequency, the wave vector increases significantly, leading to stronger confinement of electromagnetic fields at the interface.

Further in this chapter, various polariton modes will be discussed: TPP, SPP, hybrid TPP-SPP modes, hybrid lattice plasmon polaritons (HLPP).

2.3.1. Tamm Plasmon Polaritons

TPPs are optical modes that occur at the boundary between a metal and a 1D PC. Unlike traditional SPPs, TPPs have a dispersion relation that lies entirely within the light cone, allowing them to be easily excited with both transverse electric (TE) and transverse magnetic (TM) polarized light at various angle of incidence (AOI) (Fig. 2.3.1) [46]. This unique property eliminates the need for complex configurations typically required to couple light into SPPs, such as prisms or metal gratings. The Tamm plasmon concept was first proposed theoretically by Kaliteevski et al. [47] and later verified experimentally by Sasin et al. [48].

TPPs are formed due to the coupling of electromagnetic waves at the interface of a metal and a DBR. The DBR, consisting of alternating layers of dielectric materials, creates a PBG that confines light. When a metal is placed adjacent to the DBR, SP at the metal surface couple with the photonic modes of the DBR, leading to the formation of TPPs. These modes exhibit characteristics of both SP and cavity modes, leading to unique dispersion properties [49]. A key feature of TPPs is their resistance to dissipative losses within the metal, as the majority of their electromagnetic fields are concentrated in the non-absorbing Bragg mirror. This robustness makes TPPs an appealing alternative to SPPs, offering enhanced stability and versatility in various applications.

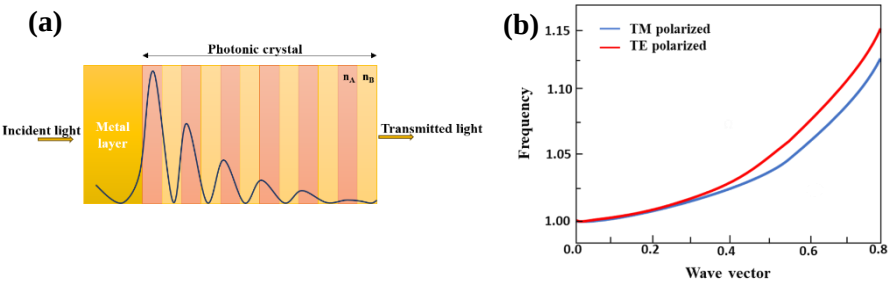

Figure 2.3.1. (a) The electric field distribution in the 1D PC/metal structure and (b) the dispersion of TPP for both p-pol and s-pol states [46].

The Bragg mirror, or DBR, consists of alternating dielectric layers with different refractive indices (n_A and n_B), and thicknesses (d_A and d_B). These layers are designed to satisfy the quarter-wavelength condition,

$$n_A d_A = n_B d_B = \frac{\pi c}{2\omega_{Br}}. \qquad (2.8)$$

The Bragg frequency (ω_{Br}) is a crucial parameter in defining the PBG and is determined by the refractive indices and thicknesses of the layers [47].

The normal modes can be imagined as two virtual interfaces introduced within one of the uniform layers. The amplitude reflection coefficient for a leftward-propagating wave at the left virtual interface is referred to as r_{left} while the coefficient for a rightward-propagating wave at the right virtual interface is known as r_{right}. Using the transfer matrix method, which allows for the analysis of wave propagation in layered media, it is possible to derive an equation that describes the field of the eigenmode in terms of these reflection coefficients for rightward- and leftward-propagating waves. This approach provides a framework to understand the behavior of electromagnetic waves in complex structures with multiple layers and interfaces [47],

$$K\begin{pmatrix} 1 \\ r_{left} \end{pmatrix} = \begin{pmatrix} \exp i\Phi & 1 \\ 1 & \exp -i\Phi \end{pmatrix}\begin{pmatrix} r_{right} \\ 1 \end{pmatrix}, \tag{2.9}$$

where K is a constant, r_{left} and r_{right} are the leftward and rightward propagating waves respectively, and $\Phi = n_x\omega/c$ is the phase change between different interfaces of the wave with angular frequency ω. The electric field in PC and metal structure is intensified at the interface between the PC and the metal. To determine the condition for the resonant mode, consider the following relation derived from the reflection coefficients for leftward- and rightward-propagating waves

$$r_{left}r_{right}\exp(2i\Phi) = 1\,, \tag{2.10}$$

with zero phase difference ($2i\Phi$=0), since there's no propagation distance. The reflection amplitudes can be expressed as r_{M} , representing the coefficient for the wave incident on the metal from the A layer of the photonic crystal (PC), and r_{Br} representing the coefficient for the wave incident on the Bragg mirror from the A layer, so the Eq. 2.10 can be rewritten as,

$$r_M r_{Br} = 1, \tag{2.11}$$

where r_M is the reflection coefficient for the wave incident from the PC's A layer onto the metal, and r_{BR} is the reflection coefficient for the wave incident from the same A layer onto the Bragg mirror. This condition indicates that if the product of these two reflection coefficients is 1, a resonant mode is created

at the metal/PC interface (Fig. 2.3.2). This condition guides the analysis of resonant modes in PC/metal structures [47].

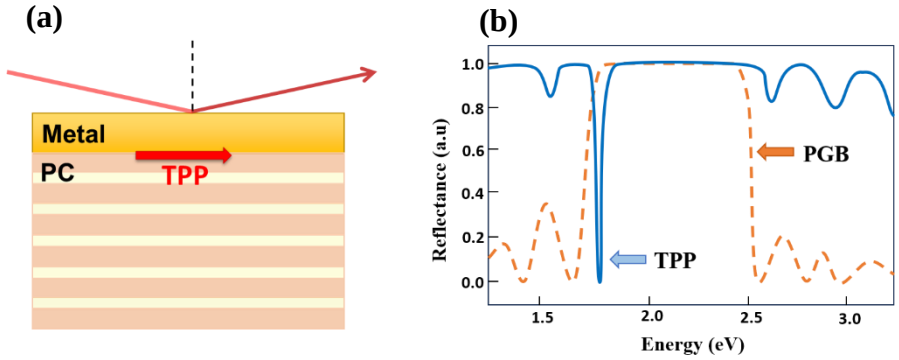

Figure 2.3.2. (a) The TPP excitation scheme. (b) The optical response of the TPP, where TPP mode appears in the PBG.

The reflection coefficient r_M for a wave incident on a metal from the PC's A layer is given by the Fresnel formula,

$$r_M = \frac{n_A - n_M}{n_A + n_M}\,, \tag{2.12}$$

where n_A is the refractive index of the PC's A layer, and n_M is the refractive index of the metal. This reflection coefficient indicates the proportion of the wave's amplitude that is reflected at the metal interface, influenced by the contrast in refractive indices [47]. The reflection coefficient r_{BR} for a Bragg mirror can be found using the transfer matrix method. If the Bragg mirror has many layers and the wave's frequency ω is near the Bragg frequency, the reflection coefficient is

$$r_{BR} = \pm \exp\left[i\beta \frac{(\omega - \omega_{Br})}{\omega_{Br}}\right], \tag{2.13}$$

where the positive or negative sign depends on whether $n_A > n_B$ or $n_A < n_B$. For a wave incident from a medium with refractive index n_A, the phase change β is

$$\beta = \frac{\pi n_A}{|n_A - n_B|}. \tag{2.14}$$

This phase shift affects wave reflection in a Bragg mirror with alternating layers. For a solution close to the Bragg frequency, when the decay is minimized, this condition leads to an expression for the frequency as follows,

$$\omega_{TPP} \approx \frac{\omega_{Br}}{1 + \frac{2n_A\omega_{Br}}{\sqrt{\varepsilon_B}\,\beta\omega_P}}, \tag{2.15}$$

where ε_B is the background dielectric constant, and ω_P is the plasma frequency [47].

TPPs unlike conventional surface plasmon resonance sensors, do not require intricate setups and offer a more straightforward approach due to their dispersion characteristics. This makes them ideal for a wide range of applications, including optical switches, semiconductor lasers, light emitters, temperature and refractive index sensors [49,50]. Given their unique advantages and versatility, TPP are expected to play an increasingly significant role in photonics and optoelectronics. Their combination of easy excitation, reduced sensitivity to metal-induced losses, and broader application scope marks them as a promising area of research and innovation [52].

Recent advances have explored topological insulator-based TPPs, leading to the creation of robust modes that are less susceptible to defects [53]. Additionally, research has shown the existence of hybrid modes that combine TPPs with other photonic states, such as microcavity exciton polaritons, leading to new possibilities in light-matter interaction studies [54].

2.3.2.Surface Plasmon Polaritons

To excite SPP, the magnitude of the parallel component of incident light wave vector ($\overrightarrow{k_x}$) needs to be matched with the surface plasmon wave vector ($\overrightarrow{k_{SPP}}$) at the metal/dielectric interface (Fig. 2.3.3 a).

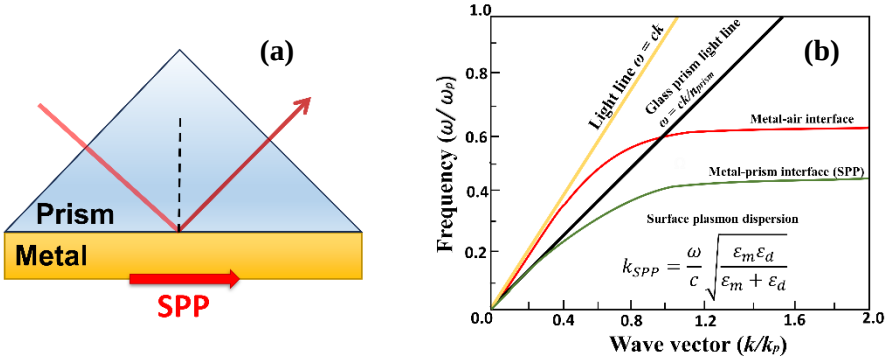

Figure 2.3.3. (a) The SPP excitation scheme and (b) SPP dispersion relation, where $\omega=k/c$ is the light cone in vacuum, $\omega=kc/n$ is the light dispersion in prism coupler.

The component of the incident wave $\overrightarrow{k_x}$ depends on the wavelength (λ), refractive index of the prism (n_p), and the AOI (θ_i),

$$\overrightarrow{k_x} = \frac{2\pi}{\lambda} n_p sin\theta_i \,. \tag{2.16}$$

From the boundary conditions one can obtain the dispersion relation for the SPP wave (ε_m – metal dielectric constant, ε_d – dielectric constant) [55],

$$\overrightarrow{k_{SPP}} = \overrightarrow{k_x}\sqrt{\frac{\varepsilon_m \varepsilon_d}{\varepsilon_m + \varepsilon_d}} \,. \tag{2.17}$$

The wave vector k_{SPP} of the SPP is complex due to the absorbing nature of metals, where the SPP wavelength λ_{SPP} is inversely proportional to k_{SPP}. The penetration depths of the electric field into the dielectric (δ_d) and metal (δ_m) materials can be derived from k_d and k_m, respectively [56],

$$\delta_d = \frac{1}{k_d} = \frac{\lambda}{2\pi}\sqrt{\varepsilon_d + \varepsilon'_m - \varepsilon_d^2} \,, \tag{2.18}$$

$$\delta_m = \frac{1}{k_m} = \frac{\lambda}{2\pi}\sqrt{\varepsilon_d + \varepsilon'_m - \varepsilon_m^2}\,. \qquad (2.19)$$

Surface plasmonic excitations can be classified into propagating SPP and non-propagating, localized surface plasmons (LSP). LSPs involve interactions between electrons within particles and incident photons when light falls on metallic nanoparticles [39]. SPPs are excited by p-polarized light (TM), generated when photons interact with free electrons on metal surfaces, typically in the visible or infrared wavelength range [10]. SPPs exhibit a strong dependency on polarization. While TM polarization supports the existence of SPPs, TE polarization does not, as Maxwell's equations yield no solution for SPPs in this case [57]. As k_{SPP} approaches infinity, the dispersion curve nears the plasma frequency value (Figure 2.3.3 b). SPP propagates along the metal-dielectric interface as non-radiative modes until their energy dissipates as heat within the metal. The propagation length of SPPs can reach up to the order of centimeters, making them suitable for various applications. Achieving wave vector matching is essential for the excitation of SPPs. The wave vector component of the incident light parallel to the interface must be increased, and that can be achieved through various optical configurations. The most common mechanisms for coupling light to SP are prism configurations and grating couplings.

Otto configuration - in this setup, the prism is positioned near the metal surface, with a gap between the prism base and the metal layer (Fig. 2.3.4 a). The higher refractive index of the prism compared to free space increases the wave vector of the incident light,

$$k = \frac{\omega}{c} n_p sin\theta_i\,, \qquad (2.20)$$

where θ_i is the AOI and n_p is the refractive index of the prism. Total internal reflection (TIR) at the prism base can transfer energy to excite SPPs if the gap is on the order of the penetration depth in dielectrics.

And another one is the **Kretschmann configuration** which relies on the principle of TIR. In this setup, a metal layer is deposited onto a dielectric prism, and p-polarized light is transmitted through the prism (Fig. 2.3.4 b). When light passes from a denser optical medium with refractive index n_1 to a rarer medium with refractive index n_2, at a certain angle called the critical angle (θ_c), light is totally reflected from the interface. By adjusting the angle θ_c, the wave vector of the incident light can be aligned with the SP wave vector at the metal-dielectric (air) interface [58].

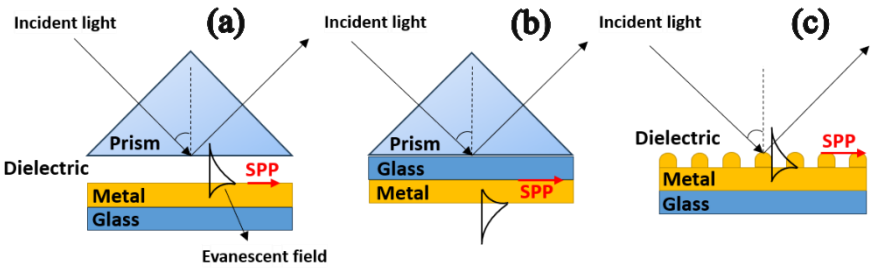

Figure 2.3.4. (a) Otto configuration scheme, (b) Kretschmann configurations scheme for the SPP excitation using prism coupler. (c) The SPP excitation using grating coupler.

The tangential component of the wave vector (k_x) corresponds to attenuated total reflection (ATR) and is close to the SP wave vector, which propagates parallel to the metal layer surface [58,59],

$$k_x = \frac{\omega}{c}\sqrt{\varepsilon_{prism}} * sin\theta_i \,. \qquad (2.21)$$

Grating coupling involves forming grooves on the metal surface with a period *a* (Fig. 2.3.4 c). Incident light upon the grating satisfies the wave matching condition if,

$$k_{SPP} = k_0 n\, sin\theta_i \pm \frac{2\pi m}{a}. \qquad (2.22)$$

where *m* is an integer and *n* is the refractive index of the ambient medium.

SPPs enhance sensor performance, improve photovoltaic efficiency, and enable optical devices like plasmonic waveguides and modulators. In biosensing, SPPs detect biomolecules at very low concentrations due to their sensitivity to refractive index changes near metal surfaces [47]. They also boost surface-enhanced Raman spectroscopy by increasing Raman signal strength [61]. Additionally, SPPs enable compact light sources, such as plasmonic lasers, suitable for high-speed, miniaturized optical components [17].

Recent advances include new materials and nanostructures, like graphene, which reduce losses and improve SPP performance. However, challenges like intrinsic metal losses and integration into existing systems remain [57]. Despite these, SPPs' unique properties continue can lead to promising significant impacts in sensing, imaging, and communications.

2.3.3. Hybrid Tamm Plasmon-Surface Plasmon Polaritons

Surface Plasmon Resonance (SPR) is widely utilized in optical sensing due to its sensitivity to changes in the refractive index near metal surfaces. However, as mentioned in previous section, SPR faces limitations due to the broad resonance widths caused by metal layer losses, which can affect sensitivity and precision [62]. To address these challenges, hybrid modes combining TPP and SPP offer a promising solution. These hybrid Tamm plasmon-surface plasmon polariton (TPP-SPP) modes can potentially reduce losses, thereby enhancing sensitivity and precision in optical sensing applications [51,62,63].

Hybrid modes form when TPP and SPP are coupled under specific conditions. This coupling occurs in setups where a glass prism is optically connected to PC with a thin metal layer (Fig. 2.3.5 a). At certain light angles of incidence (AOI) on the prism, the wave vectors of SPPs and TPPs align, resulting in strong coupling between these modes. This strong coupling regime can lead to significant changes in the dispersion relations of the involved plasmons [6,64].

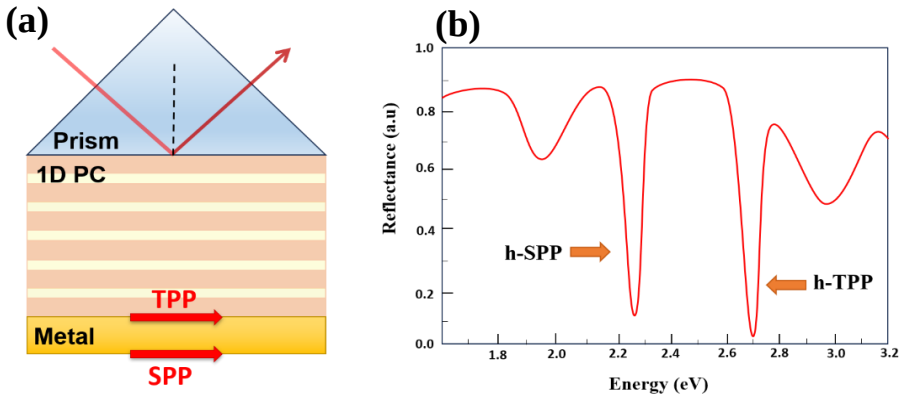

Figure 2.3.5. (a) The exitation configuration of the hybrid TPP-SPP and (b) the p-pol reflection spectra of the hybrid SPP (h-SPP) and hybrid TPP (h-TPP) componentes.

In the strong coupling regime, energy transfers between plasmons and emitters, such as quantum dots or dye molecules, occurs faster than the damping rates. This results in the formation of hybrid modes, also known as polaritons, which blend the characteristics of both plasmons and excitons, leading to a modified energy spectrum distinct from the individual resonances in uncoupled systems. These hybrid modes can be observed through changes

in the reflectance spectrum and mode splitting, although direct observation in the time domain is challenging due to the rapid decay times of plasmons, typically around 100 femtoseconds [66].

The first experimental discovery of the hybrid mode of Tamm plasmon-polariton and surface plasmon-polariton was reported by Afinogenov et al. [67]. This hybrid state was excited in a one-dimensional PC terminated by a semitransparent metal film under TIR conditions for TM-polarized light. The coupling between Tamm and surface plasmon-polaritons results in dispersion curve repulsion, controlled by the metal film thickness. These findings suggest potential for developing tunable plasmonic filters and sensors [66].

The coupling between SPP and TPP at metal-dielectric and metal-PC interfaces creates unique plasmonic properties. This interaction offers new ways to manipulate energy transfer and light propagation, leading to novel applications in photonics and optoelectronics [61,64,67].

A hybrid TPP-SPP plasmonic mode can be excited when a PC has a semi-transparent metal layer attached to the base of a PC. A p-polarized hybrid mode of p-TPP and p-SPP can be generated on the same metal layer when suitable conditions are satisfied for both states. They are excited on different interfaces of the same metal layer, thereby revealing the anti-crossing effect of their dispersion curves. This anti-crossing effect indicates a strong coupling regime, where the energy spectrum is modified, and splitting between the TPP and SPP components corresponds to their coupling strengths [63,68].

The excitation of this hybrid plasmonic mode requires conditions of TIR and is polarization-sensitive. A detailed analysis of the polarization properties in a TIR setup can be achieved using polarization sensitive TIRE method. Since the SE setup in its TIR configuration with a glass prism coupler is useful for monitoring ambient refractive index changes and interactions between proteins at solid/liquid interfaces [70] it can be applied for enhanced TPP-SPP sensing.

TPP-SPP present a significant advancement over individual TPP and SPP modes. By reducing losses and enhancing sensitivity, these hybrid modes hold and optoelectronics. The strong coupling mechanism and the unique properties of hybrid TPP-SPP modes open new avenues for developing advanced plasmonic devices with improved performance and functionality [67].

2.3.4. Hybrid Lattice Plasmon Polariton

Metallic nanostructures have emerged as exceptional tools for manipulating light at the nanoscale, thanks to their capacity to support SP [44]. These excitations arise from the collective motion of conduction electrons within the nanostructure, leading to a strong interaction with light and confinement into subwavelength volumes. Consequently, SP generate significant field enhancements, which have been harnessed for various applications, including solar energy harvesting, photocatalysis, and photothermal cancer therapies. However, due to their large radiative cross-sections and the inherent nonradiative losses in metals, the SP of individual nanostructures typically exhibit relatively broad line shapes with modest Qs [70,71].

To address these limitations, arranging plasmonic nanoparticles into one-dimensional (1D) and two-dimensional (2D) arrays has been shown to reduce radiative losses and support lattice plasmon resonances with much higher Q ($Q > 200$) compared to single nanoparticles ($Q < 20$) [73]. These approaches are critical for enhancing the longevity and efficiency of SPP-based devices. For seamless device integration, the grating coupler approach stands out as an ideal method. Grating couplers can be directly fabricated on metal films that support SPPs, enabling the integration of complex plasmonic systems that support multiple plasmon modes. These systems, including metallic nanodimers, nanoshells, nanotubes, and nanoparticles near metal films, exhibit plasmon hybridization where LSP can interact with SPP. The ability to manipulate these interactions opens up new possibilities for designing sophisticated nanophotonic devices with enhanced functionalities. Significant

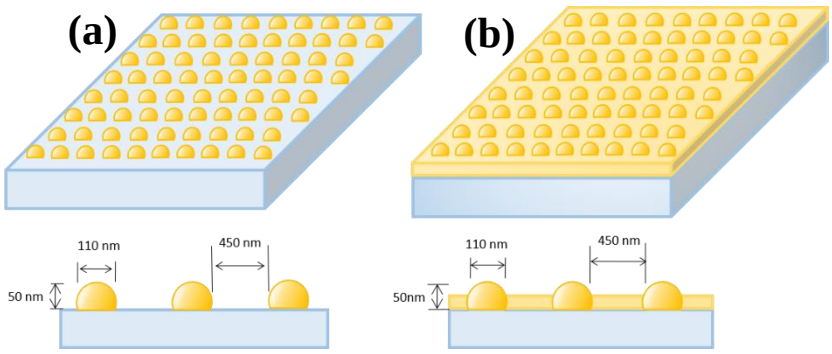

Figure 2.3.6. Two different schematics: (a) the SLPR and (b) the HLPP array structure.

advancements in the field focus on the interactions between LSPs, SLPR (Fig. 2.3.6 a), and hybrid localized plasmon polaritons (HLPPs) (Fig. 2.3.6 b).

One of the pivotal discoveries in plasmonic nanoparticle research is the observation that well-ordered nanoparticle arrays exhibit significantly narrower resonance half-widths (high Q-factor) compared to their disordered counterparts. This narrow resonance is indicative of lower plasmonic excitation losses and allows for longer surface wave propagation lengths. The resonance width of disordered nanoparticles typically exceeds the 80–100 nm full-width at half-maximum (FWHM) [73,74], of nanostructure LSPs, compared to the 50 nm spectral width of propagating plasmons. The enhanced optical properties of these ordered arrays are crucial for applications requiring high precision and low energy losses. SLPR is a phenomenon observed when the periodicity of nanoparticle arrays matches the wavelength of the incident light. This matching satisfies the Bragg condition, resulting in multiple periodic reflections and interactions between neighboring particles. The hybrid waves formed by local plasmons and Bragg reflections compensate for phase losses due to metal dissipation, thereby enhancing the Q of the resonances. This effect is pivotal in reducing plasmonic excitation losses and extending surface wave propagation lengths, making it highly beneficial for optical applications. HLPPs are formed through the interaction of the local plasmon resonance of one nanoparticle with its neighboring particles, leading to multiple periodic reflections. These reflections create a hybrid wave that combines local plasmon resonances with Bragg reflections, significantly enhancing the Q-factor and reducing energy losses. Achieving this effect requires that the nanoparticle lattice period is comparable to the wavelength of the incident light, facilitating efficient coupling and energy transfer between particles. This principle is central to designing advanced plasmonic devices with superior performance.

In well-ordered nanoparticle arrays, HLPPs exhibit significantly narrowed resonance half-widths compared to disordered nanoparticles. Narrower resonance indicates lower plasmonic excitation losses and longer surface wave propagation lengths. When the period of nanoparticles in a lattice matches the wavelength of incident light, interactions between neighboring particles and multiple periodic reflections satisfy the Bragg condition [73]. This results in the formation of hybrid waves of local plasmons and Bragg reflections, compensating for SLPR phase losses due to metal losses [17,73]. The narrowing of the half-width indicates lower plasmonic excitation losses and longer surface wave propagation lengths. Then the local plasmon resonance of one particle interacts with neighboring particles and the surface

wave experiences multiple periodic reflections that satisfy the Bragg condition.

HLPPs are formed when the local plasmon resonance of one nanoparticle interacts with neighboring particles, causing the surface wave to undergo multiple periodic reflections. These reflections create a hybrid wave that combines local plasmon resonances with Bragg reflections, enhancing the Q of the resonances and reducing losses.

The production of metal nanoparticles, essential for creating well-ordered arrays, involves techniques such as colloidal chemistry and nanosphere lithography [75]. Colloidal chemistry allows for precise control over nanoparticle size, shape, and arrangement through the reduction of metal salts [74]. Nanosphere lithography, on the other hand, provides a template-based approach to fabricate periodic nanoparticle structures. Additionally, DLW technology has emerged as a cost-effective and versatile method for fabricating periodic nanostructures [76]. DLW enables the precise formation of plasmonic nanostructures, paving the way for advancements in nanophotonic devices, including nanolasers.

2.3.5. Hybrid Exciton-Plasmon Polaritons States

In the realm of nanophotonics, the interaction between excitons and plasmons has garnered significant attention due to its potential applications in sensing, imaging, and light-harvesting technologies. Excitons, which are bound states of electrons and holes in semiconductors, and plasmons, which are collective oscillations of free electrons in metals, exhibit unique optical properties. When these two quasiparticles interact, they can form hybrid states that enhance the capabilities of nanophotonic devices [76,77].

Excitons are generated when photons are absorbed by a semiconductor, promoting an electron to a higher energy state and leaving behind a positively charged hole. The Coulomb attraction between the electron and the hole leads to the formation of an exciton. These quasiparticles are crucial in understanding the optical properties of semiconductors and are fundamental to devices like solar cells and LEDs [79].

The coupling between excitons and plasmons occurs when their electromagnetic fields interact. In the weak coupling regime, the exciton and plasmon maintain their individual identities, leading to energy transfer processes such as Förster resonance energy transfer (FRET). In the strong coupling regime, the interaction is so intense that new hybrid states are formed, exhibiting characteristics of both excitons and plasmons. In the weak coupling regime, the emission primarily comes from the excitonic material,

but it is significantly enhanced by the localized electromagnetic field of the plasmonic nanostructures. This results in increased emission intensity and potentially faster emission rates, while the spectral profile of the emission remains largely similar to that of the uncoupled excitonic material [80]. In contrast, in the strong coupling regime, the emission spectrum is profoundly altered due to the formation of hybrid exciton-plasmon states. These states lead to a distinct Rabi splitting in the emission spectrum, characterized by two new peaks corresponding to the new hybrid energy levels [77]. This spectral modification reflects the coherent exchange of energy between the excitons and plasmons, resulting in unique optical properties that are not present in the weak coupling regime [80]. When the interaction strength between excitons and photons exceeds the damping rates, exciton-plasmon polaritons form, entering a strong coupling regime. This results in phenomena such as vacuum Rabi splitting and hybridization, creating new quasiparticles with mixed light-matter properties [9]. Excitons in these systems can be tightly bound Frenkel excitons, common in organic materials, or loosely bound Wannier-Mott excitons, typical in inorganic semiconductors [6]. Hybrid excitons-plasmon polaritons have lower effective mass and enhanced propagation distances [81].

For example, R6G is an organic dye noted for strong fluorescence and high quantum yield. In hybrid structures with thin silver layers, R6G interacts with SP to form plasmon-exciton polaritons [82]. For example, thin metal layer silver or gold, superior plasmonic properties enhance these interactions at the nanoscale, improving optical characteristics. The interaction between R6G and thin metal layers involves key processes: surface plasmon coupling, FRET, and radiative coupling. These mechanisms form plasmon-exciton-polaritons and modify the emission properties of R6G [81,82]. Experimental techniques like optical spectroscopy, photoluminescence (PL) measurements, and surface-enhanced Raman spectroscopy study exciton-plasmon polaritons in hybrid systems. These techniques reveal insights into interactions, coupling strength, emission properties, and polariton dispersion [83,84].

Exciton-plasmon polaritons are suitable for various optoelectronic applications, including low-threshold lasers and light-emitting devices. They offer efficient, low-power solutions for photonics. Additionally, hybrid modes enhance plasmonic sensor sensitivity and light-harvesting efficiency, benefiting environmental monitoring, biological detection, and chemical sensing [6]. Research on these hybrid systems advances understanding of strong coupling phenomena and paves the way for developing advanced photonic and optoelectronic devices. Future research will focus on optimizing these modes and exploring practical applications [85].

2.3.5.1. Photoluminescence

PL is the emission of light from a material following the absorption of photons. It is observed in various materials, including semiconductors, organic compounds, and biological materials [86]. PL can be classified into two main types: fluorescence, which occurs almost instantaneously (within nanoseconds) after the material absorbs photons, and phosphorescence, which involves delayed emission (ranging from microseconds to minutes) due to the trapping of electrons in metastable states before they return to the ground state (Fig. 2.3.7). The mechanism of PL involves the absorption of photons, which excites electrons from the ground state to higher energy states. These excited electrons can relax back to lower energy states through non-radiative processes (heat dissipation) or radiative processes. During radiative relaxation, the electrons emit photons, which are observed as PL. PL has a wide range of applications, including material characterization, where it is used to study the electronic and optical properties of materials, particularly semiconductors and nanomaterials [87]: biological imaging, where fluorescent dyes and proteins are used to label and visualize biological structures and processes optoelectronics [88], where PL is crucial in the development of LED's and laser diodes; and sensing, where photoluminescent

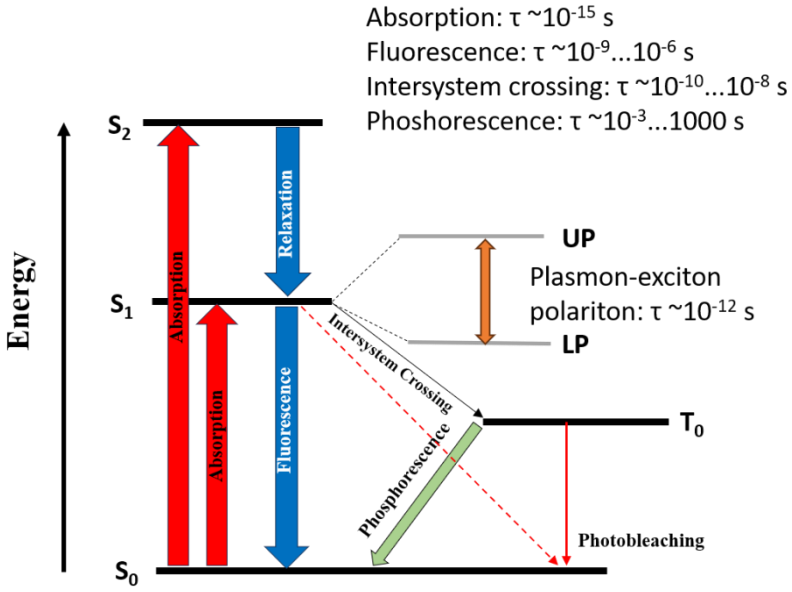

Figure 2.3.7. Schematic energy diagram for spontaneous fluorescence relaxation and transition pathways between exciton and plasmon in strong coupling regime.

materials are employed in sensors to detect various chemical and biological substances [89].

PL in dyes is influenced by several factors, including the chemical structure of the dye, with the chromophore being critical for light absorption and emission; solvent effects, as solvents can affect the PL properties by influencing the dye's environment, concentration, as higher dye concentrations can lead to quenching effects, where the proximity of dye molecules leads to non-radiative energy transfer, and temperature, as higher temperatures can increase non-radiative decay processes, reducing PL intensity [90].

During electron relaxation from excited to ground state photons can be emitted, where such phenomena is applied in many optical and electronic technologies. In hybrid plasmon-exciton systems, also known as exciton polariton systems, this emission is significantly influenced by the coupling between excitons electron-hole pairs in semiconductors or organic molecules and plasmons [6]. These hybrid systems are exceptional for their enhanced emission properties. The Purcell effect plays a pivotal role, where the local density of optical states near plasmonic structures increases, boosting the spontaneous emission rate of excitons [91]. This enhancement is most pronounced when the resonance frequencies of the plasmons and excitons align. Another key feature is Rabi splitting, indicative of strong coupling, where the hybrid modes split into two distinct energy levels, observable as separate peaks in the emission spectrum [92]. Photon are emitted along the metal-dielectric interface through Surface Plasmon-Coupled Emission (SPCE) channels, resulting in emission that is both directional and polarized [93].

The emission spectra of hybrid plasmon-exciton systems can be finely tuned. This tuning is achieved by adjusting the size, shape, and material of the plasmonic nanostructures, as well as the properties of the excitonic materials [94]. Such control allows precise manipulation of emission wavelengths and line shapes, that are crucial for specific applications. However, achieving high quantum efficiency can be challenging due to potential non-radiative losses, including plasmonic quenching [95]. Enhancing quantum yield involves strategies such as optimizing spacer layers between the plasmonic and excitonic components, using materials with lower inherent losses, and designing nanostructures to minimize energy dissipation [96]. The unique emission characteristics of these hybrid systems have various applications. In optical sensing, they provide high sensitivity to environmental changes, such as variations in refractive index or the detection of specific molecules [97]. In lighting and display technologies, these systems can improve color purity and

brightness, offering tunable emission spectra and controlled polarization [98]. Additionally, in quantum information technologies, the controlled emission properties are valuable for developing quantum emitters for communication and computing applications [99]. Future research is likely to focus on discovering new materials with improved properties, such as lower losses and higher quantum yields, as well as integrating these systems into photonic circuits for compact and efficient device applications [100]. This integration could lead to significant advances in optical computing, communication, and sensing technologies [101].

Organic dyes used as the active medium in early lasers can be applied for novel nanolasers based on strong coupling between cavity mode and exciton of the organic dye molecules. These dyes, including R6G, Rhodamine B, and fluorescein, are suitable gain media for producing coherent light over a wide range of wavelengths [102]. The effectiveness of these dyes is determined by several key properties: strong absorption at the excitation wavelength and minimal absorption at the emission wavelength, ensuring efficient energy transfer and minimizing losses, high quantum yield values (0.5–1.0) which indicate efficient conversion of absorbed light into emitted light and photochemical stability, as dyes should be stable under prolonged exposure to light preventing photobleaching induced photodegradation. Minimizing population of fluorophores in the triplet state increases photochemical stability and reduces photobleaching.

2.3.5.2. Photobleaching

As mention above one of the fundamental phenomena appearing in many organic molecules is the photobleaching effect, which can suppress the fluorescence of the dye molecule due to the transition of singlet excited state electrons to the atmospheric triplet oxygen state. Because the lifetime of the triplet state is long, the excited molecules have high probability to interact with oxygen in the environment and during this interaction fluorophores are damage and no longer can emit light. Photobleaching is the irreversible loss of fluorescence from molecules due to prolonged exposure to light. This phenomenon limits the duration and quality of fluorescence microscopy and imaging. Understanding photobleaching and developing suppression methods are crucial for enhancing fluorescence-based techniques [104,105]. Key mechanisms include the generation of reactive oxygen species and triplet state reactions. Fluorophores can transfer energy to molecular oxygen, producing singlet oxygen, which oxidizes the fluorophores [105] (Fig. 2.3.7 red arrows).

In the triplet state, fluorophores are more reactive and likely to interact with oxygen, leading to degradation [106]. Localized heating, especially near metallic nanostructures, can also accelerate photobleaching [107].

Mitigating photobleaching extends imaging duration in fluorescence microscopy, significant for studying dynamic processes in living cells and materials. It also maintains fluorescence signal intensity and quality, essential for accurate data collection and interpretation [109,110]. In quantitative studies such as fluorescence recovery after photobleaching, understanding photobleaching kinetics allow accurate interpretation of molecular dynamics and interactions [107].

Strong coupling between plasmons and excitons offers a promising approach to suppress photobleaching. Studies have demonstrated that strong coupling can significantly reduce photobleaching rates, enabling longer exposure time and more stable signal [22]. Theoretical research indicates that strong coupling between organic J-aggregated chromophores and plasmonic nanostructures effectively stabilize chromophores by an order of magnitude. Moreover, it has been shown that there is an optimal value of red detuning between the plasmon resonance frequency and the frequency of the dipole transition in the J-aggregate, for which the photobleaching suppression is most effective [22]. Furthermore, experimental evidence supports that strong coupling to plasmonic nanoantennas can suppress photo-oxidation and thereby photobleaching of organic chromophores [21]. This practical implementation of strong coupling enhances photostability, with significant implications for biological imaging and material science research. Enhancing photostability through strong coupling allow longer observations and more accurate data. This approach can also lead to advanced photonic devices with enhanced performance and durability [104,105].

Photobleaching is a challenge in fluorescence-based techniques. Strong coupling between plasmons and excitons offers a promising solution, redistributing excitation energy and significantly suppressing photobleaching. This advancement extends the utility and effectiveness of fluorescence imaging in scientific research [110].

3. METHODS

3.1. Spectroscopic Ellipsometry

SE is a powerful optical technique used to characterize thin films and surfaces by measuring the change in polarization as light reflects off a sample. This method provides detailed information about a material's thickness, optical constants (refractive index and extinction coefficient), and other properties [27,112,113]. SE involves analyzing the change in the polarization state of light upon reflection from a sample. The technique measures two primary parameters: Psi (Ψ), which represents the amplitude ratio, and Delta (Δ), which denotes the phase difference between p- and s-polarized light components. These parameters are defined by the equation,

$$\rho = \frac{r_p}{r_s} = tan\Psi e^{i\Delta}, \tag{3.1}$$

where r_p and r_s are the reflection coefficients for p-polarized and s-polarized light, respectively [113]. The complex reflection coefficients for a single interface are given by:

$$r_p = \frac{n_t cos\theta_i - n_i cos\theta_t}{n_t cos\theta_i + n_i cos\theta_t}, \tag{3.2}$$

$$r_s = \frac{n_i cos\theta_i - n_t cos\theta_t}{n_i cos\theta_i + n_t cos\theta_t}, \tag{3.3}$$

where n_i and n_t are the refractive indices of the mediums where the beam is incident and transmitted, respectively. θ_i is the AOI, and θ_t is the angle of transmission, related by Snell's law [114].

SE is extensively used to measure thin film thickness with sub-nanometer precision, which is crucial in semiconductor manufacturing, coatings, and biofilms. It also provides the optical constants (n and k) necessary for understanding the material's optical behavior. Additionally, it can characterize material composition, crystallinity, and other properties [115]. Measurements can be performed over a broad spectral range, from ultraviolet to infrared, offering comprehensive material characterization [116].

A typical SE setup includes a broad-spectrum light source, polarizers, an analyzer, and a detector (Fig. 3.1.1). Polarizers control the polarization state of the incident light, which is essential for measuring changes in polarization upon reflection. Analyzers are used to measure the polarization state of the reflected light, providing information about the optical properties of the

sample. The combination of polarizers and analyzers allows for precise determination of the ellipsometric parameters Psi (Ψ) and Delta (Δ), which are related to the film's refractive index and thickness. In TIRE, total internal reflection enhances surface sensitivity, making the accurate control and measurement of light's polarization state critical for reliable results. [112].

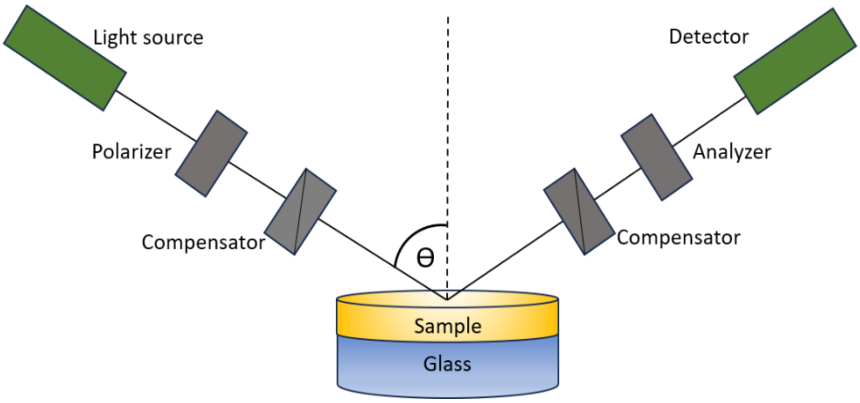

Figure 3.1.1. A typical spectroscopic ellipsometry setup components: a white light source used to illuminate the sample, a polarizer, a compensator that can be placed in the path of the incident or reflected light beam, a second polarizer called analyzer, and the detector.

The measured data is compared to theoretical models to extract the material's properties. This often involves fitting the data to a model that describes the sample structure using advanced software tools [115]. For multilayer films, the total reflection coefficient can be modeled using a transfer matrix approach, accounting for multiple reflections within the film. The complex dielectric function ε is related to the refractive index n and the extinction coefficient k by,

$$\varepsilon = (\tilde{n})^2 = (n + ik)^2 \,. \tag{3.4}$$

For a thin film with thickness d on a substrate, the total reflection coefficient can be expressed as,

$$\rho = \frac{r_{12} + r_{23}e^{2i\delta}}{1 + r_{12}r_{23}e^{2i\delta}}\,, \tag{3.5}$$

where r_{12} and r_{23} are the reflection coefficients at the air-film and film-substrate interfaces, and δ is the phase thickness,

$$\delta = \frac{2\pi}{\lambda} n_2 d\cos(\theta_t). \tag{3.6}$$

3.2. Total Internal Reflection Ellipsometry

TIRE is an advanced optical technique that combines the principles of ellipsometry and TIR to analyze thin films and surface properties with high sensitivity. This method leverages the evanescent wave generated during TIR to probe the sample.

In TIRE, light undergoes TIR at the interface between a high-refractive-index prism and a lower-refractive-index medium. This creates an evanescent wave that penetrates a short distance into the sample. The change in polarization state of this evanescent wave is measured to extract information about the sample's properties. When light hits the interface at an angle greater than the critical angle (Eq. 3.7), it undergoes TIR and evanescent wave is generated. The evanescent wave electric field decays exponentially with distance from the interface, allowing for sensitive surface and thin film measurements. Similar to traditional ellipsometry, the TIRE measures the changes in the ellipsometric parameters Ψ and Δ. These parameters are affected by the optical properties of the thin film or surface layer interacting with the evanescent wave. The critical angle θ_c is given by,

$$\theta_c = arcsin\left(\frac{n_1}{n_2}\right). \tag{3.7}$$

where n_1 and n_2 are the refractive indices of the prism and the medium, respectively. The penetration depth d_p of the evanescent wave into the lower refractive index medium is,

$$d_p = \frac{\lambda}{2\pi\sqrt{n_1^2 sin^2\theta - n_2^2}}, \tag{3.8}$$

where λ is the wavelength of the incident light.

Employing configuration of TIR when $\theta_i > \theta_c$ the behavior of ellipsometric parameters Ψ and Δ is different from the conventional external incidence of polarized light in SE. This means that θ_t has lost its physical interpretation as

the angle of transmission and becomes a complex-valued angle (θ_1), were θ_0 is AOI,

$$cos\theta_1 = -i\sqrt{\left(\frac{sin\theta_0}{sin\theta_c}\right)^2 - 1}\,. \tag{3.9}$$

Thus, for purely dielectric media (n_0 and n_1 represent refractive indices of the media), Fresnel expressions would be,

$$r_s = \frac{n_0 cos\theta_0 + in_1\sqrt{\left(\frac{sin\theta_0}{sin\theta_c}\right)^2 - 1}}{n_0 cos\theta_0 - in_1\sqrt{\left(\frac{sin\theta_0}{sin\theta_c}\right)^2 - 1}}, \tag{3.10}$$

$$r_p = \frac{n_1 cos\theta_0 + in_0\sqrt{\left(\frac{sin\theta_0}{sin\theta_c}\right)^2 - 1}}{n_1 cos\theta_0 - in_0\sqrt{\left(\frac{sin\theta_0}{sin\theta_c}\right)^2 - 1}}. \tag{3.11}$$

From this it can be seen that reflection coefficients are complex numbers with unit modulus $|r_p|=|r_s|=1$ and with phases δ_p and δ_s given by,

$$\delta_s = 2\arctan\left(\frac{sin^2\theta_0 - sin^2\theta_c}{1 - sin^2\theta_0}\right)^{1/2}, \tag{3.12}$$

$$\delta_p = 2\arctan\left[\left(\frac{sin^2\theta_0 - sin^2\theta_c}{1 - sin^2\theta_0}\right)^{1/2}\left(\frac{1}{sin\theta_c}\right)^2\right]. \tag{3.13}$$

If we look to the variation of ellipsometric parameters Ψ and Δ for the case $\theta_i > \theta_c$ it gives further expressions for $\theta = 45°$,

$$\Delta = \delta_p - \delta_s = 2arcsin\frac{\sqrt{sin^2\theta_0 - sin^2\theta_c}}{sin\theta_0 tan\,\theta_0}. \tag{3.14}$$

The value of Ψ=45° is simply due to TIR of *p*- and *s*- polarized components where they have equal values at AOI $\geq \theta_c$. However the non-zero value of Δ and it's angle dependence is caused by the difference in phase shifts between r_p and r_s [117]. Generally, the complexed valued critical angle associated with evanescent field surface wave propagated at the interface between two medias with different refractive index. Such optical configuration is very similar with those are used for surface plasmon resonance excitation, however the combination of ellipsometry with TIR gives advanced possibilities to analyze in detail the polarization properties of reflected, absorbed and emitted light from the plasmon-exciton polaritonic states.

Moreover, TIRE is particularly useful for studying thin films, surface coatings, and biological layers, providing high sensitivity to changes at the interface. It is widely used in biosensing, surface chemistry, nanotechnology [118,119]. Compared to spectroscopic ellipsometry the TIRE method has enhanced sensitivity of ellipsometric parameters Ψ and Δ [117]. A typical TIRE setup involves a glass prism, a polarizer, an analyzer, and a detector. The light source provides a collimated beam that undergoes TIR at the prism-sample interface. The reflected beam is analyzed to determine the ellipsometric parameters.

3.2.1.Spectroscopic Ellipsometer J.A. Woollam RC2

In this study, the J.A. Woollam RC2 ellipsometer has been employed (Fig. 3.2.1) to characterize the thin films refractive index dispersion and thickness.

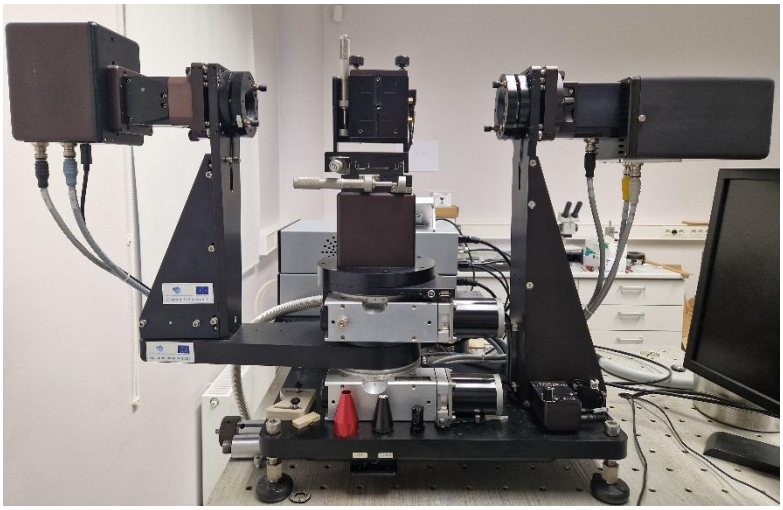

Figure 3.2.1. The J. A. Woollam RC2 ellipsometer.

The RC2 model, a dual-rotating compensator ellipsometer manufactured by J.A. Woollam, is renowned for its ability to measure the full Mueller matrix, providing comprehensive data for advanced material characterization. The measurements were conducted over a broad spectral range from 210 nm to 1700 nm, utilizing incident angles specifically set at 45° and 70° to optimize data accuracy for different sample types. Additionally, the wide AOI range from 20° to 90° facilitated versatile experimental setups, and the use of 45° (Fig. 3.2.2) and 70° BK7 glass prisms ensured the ability to achieve TIRE.

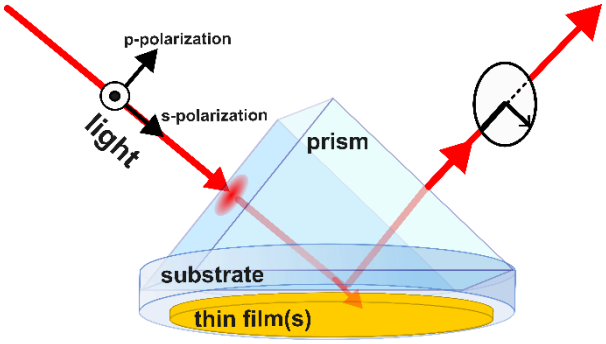

Figure 3.2.2. The scheme of TIRE with ellipsometer J. A. Woollam RC2.

To ensure accuracy, calibration was performed using a standard sample with known properties (Si wafer coated with ~25 nm SiO_2 layer) before each set of measurements. The data acquisition process involved running measurement scans and recording Ψ and Δ values at different wavelengths within the specified spectral range. Multiple measurements were taken to ensure consistency and repeatability. The collected data were then analyzed using the CompleteEASE v6.7 software provided by J.A. Woollam, which allowed to fit the experimental data to theoretical models and extract the film thickness and optical constants (*n* and *k*).

Ellipsometry using the J.A. Woollam RC2 proved to be an invaluable tool for precise and comprehensive characterization of thin films and surface effects. Its advanced features and versatile measurement capabilities made it ideal for this research, providing detailed insights into the material properties essential for the success of study.

3.2.2. Polaritonic Emission in Total Internal Reflection Configuration

The light emitter with high oscillator strength is placed in the vicinity to metallic layer, the strong coupling regime can be achieved between surface plasmon mode and exciton [1]. The plasmon-exciton polariton exhibit the mixed properties of surface plasmon mode and high oscillators strength emitter. Due to their high oscillator strength organic molecules are promising candidates to achieve the strong coupling regime at room temperature. The polaritonic states resulting from the strongly coupled surface plasmon mode and exciton demonstrate the same properties as surface plasmon, they are *p*-polarized and non-radiative. This is because their energy and wavevector is always larger then the wavevector of light. Thus, the polariton and the tangential component of incident light wavevector cannot match, and due to that the polaritonic states cannot couple to radiative modes. In order to generate and detect polaritonic emission it is necessary to use additional coupler (in this case glass prism), the so called TIR configuration.

When TIR is used with thin metal layer on the base of the glass prism it is usually called the Kretschmann configuration which relies on the principle of TIR (Fig 2.3.4 b) [58,120,121]. When light transitions from a denser optical medium with refractive index n_1 to a rarer medium with refractive index n_2, at a certain angle called the critical angle θ_c, light is totally reflected at the interface (Eq. 3.7). By changing the refractive index the critical angle is also changed, the wave vector of the incident light can be aligned with the surface plasmon (SP) wave vector at the metal-dielectric (air) interface [58]. At a certain angle, which is greater than the critical angle (TIR), a sharp minimum of the reflection coefficient is observed due matching incident light wavevector tangential component with the plasmon. The tangential component k_x of the incident light wave vector corresponding to TIR is close to the SPP wave vector, which propagates parallel to the surface of the metal layer (Eq. 2.21) [58,122].

3.3. Total Internal Reflection Fluorescence Lifetime Microscopy and Spectroscopy

Fluorescence microscopy has evolved significantly since its inception, becoming a fundamental tool in biomedical imaging. Initially coined by Stokes in 1852 to describe light emitted at different colors than the absorbed light [122], fluorescence was redefined in the 20th century as the short-lived emission of photons following the absorption of higher energy photons. This

redefinition propelled its use in studying molecular dynamics. Mid-20th century advances by Weber, who used fluorescence properties to study molecular dynamics and enzyme binding [123], cemented fluorescence's role in biophysical and biochemical investigations. By the late 20th century, numerous fluorescent molecules were identified and repurposed as molecular markers, greatly enhancing the specificity and resolution of fluorescence microscopy. The discovery of tetramethyl-rhodamine-ethyl-ester for targeting mitochondria [124] and the identification of endogenous fluorescence, or autofluorescence, further expanded the technique's applications.

The 1980s saw the cloning and expression of green fluorescent protein from jellyfish, revolutionizing in vivo imaging [125]. FLIM exploiting the fluorescence lifetime property, emerged as a highly sensitive technique for studying cellular metabolism and molecular interactions. FLIM can utilize both endogenous and exogenous fluorophores to monitor various cellular processes, disease progression, and drug efficacy [127,128]. This review highlights the principles of FLIM, its advantages over intensity-based methods, instrumentation, analysis techniques, and diverse applications in biomedical research.

FLIM is an advanced imaging technique that measures the decay time of fluorescence from a sample, providing detailed insights into molecular environments and interactions. When a molecule in the ground state (S0) absorbs light with energy equal to or greater than its higher energy levels (S1, S2, ... Sn), an electron is excited to a higher energy state. This excited electron undergoes vibrational relaxation to the lowest vibrational level of the excited state (S1) through a nonradiative process called internal conversion. The electron then returns to the ground state either by emitting photons (a radiative process known as fluorescence) or by nonradiative means.

Fluorescence occurs when molecules decay from the lowest excited electronic level (S1) by emitting detectable photons within nanoseconds (10^{-9} seconds). This emission is characterized by the Stokes shift, where the emitted light has a longer wavelength than the absorbed light due to energy loss in vibrational relaxation and internal conversions. Another luminescence process, phosphorescence, involves the transition of electrons to a triplet state (T1) via intersystem crossing (ISC), resulting in a slower emission of photons over milliseconds to seconds.

FLIM specifically measures the fluorescence lifetime (τ), the average time a fluorophore remains in its excited state. This lifetime is independent of the fluorophore concentration and sensitive to the local molecular environment.

The decay of fluorescence intensity over time follows an exponential function, which can be analyzed to extract the fluorescence lifetime. There are

two main techniques for measuring fluorescence lifetime in FLIM: time-domain and frequency-domain methods. In time-domain FLIM, the sample is excited by a short light pulse, and the decay time of emitted photons is recorded using methods such as time-correlated single-photon counting (TCSPC). In frequency-domain FLIM, the excitation light is modulated, and the phase shift of the emitted light are measured, providing information about the fluorescence lifetime.

An in-house built system was used for FLIM and spectral reflection intensity measurements (Fig. 3.3.1). The system consists of a BK7 Dove-prism, a microscope focus body (not shown in Fig. 3.3.1), and an illumination/detection arm used in total internal reflection fluorescence (TIRF) measurement method. The illumination arm can rotate/translate independently of the microscope objective (NIKON 20x 0.75NA) and the dove prism. This means that for small angles used in this work, only one collection arm is necessary when spectral measurements are required (in contrast to two arms in ellipsometry systems, for example). Spectral measurements were performed using OceanOptics USB4000-UV-VIS spectrometer, with Thorlabs SLS201L/M Stabilized Tungsten-Halogen Light Source.

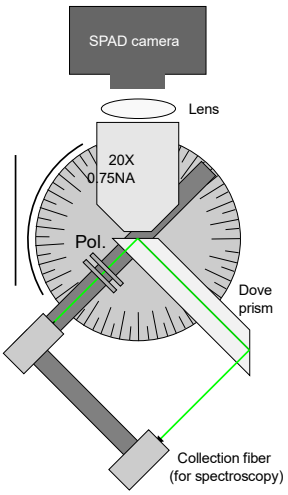

Figure 3.3.1. Schematic of the Dove-prism TIRF system with illumination/detection arm that is attached to a rotation and translation stage. This arm is independent of the dove prism, and the microscope objective.

FLIM measurements were carried out using SuperK EXR-20 picosecond pulsed supercontinuum source filtered with 520-10 nm filter (Thorlabs FBH520-10) and coupled into a single-mode fiber. The fluorescence (filtered with a 550 long-pass filter) was imaged using Horiba FLIMera Single Photon Avalanche Diode array. The sample was coupled to the prism using immersion oil ($n \approx 1.51$). Exposure was set to 30 seconds, and the sample was continuously illuminated between acquisitions (spaced 1 minute apart). The average power density used was ~0.4 mW/mm^2. The instrument response function (IRF) of the system was measured using light reflected from a bare coverslip, with the long-pass filter removed. Because each single-photon avalanche diode (SPAD) in the array has a slight temporal offset, the recovered data were temporally aligned in post-processing to allow averaging the data across all pixels.

3.4. Sample Production Methods

3.4.1. Structures Supporting Tamm Plasmon Polaritons States

TPPs are optical modes formed at the interface between a metal and PC. These hybrid modes arise from the coupling between SPP and the PBG of the PC. Achieving the desired optical properties requires precise design and fabrication of these structures. The PC in this study consists of alternating layers of titanium dioxide (TiO_2) and silicon dioxide (SiO_2) deposited on a BK-7 glass substrate using IBS. The parameters of PC's layers are chosen to create a PBG in the visible range, where the SPP component of the hybrid mode is generated. The PC comprises five alternating TiO_2 and SiO_2 bilayers. The thicknesses ensure the formation of a PBG in the visible spectrum. The total thickness of the Bragg mirror dictates the PBG position, with thicker layers shifting the PBG towards the infrared region. The refractive index contrast between TiO_2 ($n = 2.6142$) and SiO_2 ($n = 1.4585$) influences the PBG width, with a higher contrast resulting in a broader PBG. More bilayers result in a more defined stop band and enhanced reflectivity for wavelengths within the PBG. Constructive interference occurs for wavelengths close to four times the optical thickness of the bilayers, making the multilayer structure a highly reflective mirror for these wavelengths.

The primary fabrication method is IBS. The IBS chamber is evacuated to approximately 7×10^{-6} mbar and filled with high-purity argon and oxygen gases. For TiO_2 and SiO_2, the deposition rates are 0.09 nm/s and 0.14 nm/s, respectively. The PCs for the samples present in sections 4.2 and 4.3 consisted of five TiO_2 (99.95% purity) and SiO_2 (99.99% purity) bilayers (110 nm/200

nm) deposited on a BK-7 glass substrate with an additional 30 nm TiO_2 layer on top. Magnetron sputtering is also employed to deposit the thin metal layers necessary for supporting TPP modes, ensuring uniform and high-quality metal films critical for effective plasmonic mode coupling.

Supporting TPP states necessitates precise design and fabrication of PCs and metal layers. By controlling the thickness, refractive index contrast, and number of bilayers, and using accurate deposition techniques such as IBS and magnetron sputtering, the desired optical properties can be achieved for various applications. Future sections will detail the specific structures and their optical characteristics, demonstrating the practical realization of these hybrid modes.

3.4.2.Thin Metal Layer Fabrication

The sample used for the hybrid surface plasmon-exciton polariton and hybrid TPP-SPP modes excitation consisted of thin metal layers: silver (thickness 35 nm in section 4.1) and gold (thickness 9 nm in section 4.1 and 50 nm in section 4.2 and 4.3). The Ag and Au films were deposited on a BK-7 glass substrate using magnetron sputtering method (Kurt J. Lesker PVD 225). Magnetron sputtering is a PVD technique widely employed for thin-film coating. In this method, a target material, which serves as the source, is bombarded by energetic ions generated in a plasma (Fig. 3.4.1). The plasma is sustained by an applied magnetic field that confines the electrons near the target surface, enhancing ionization efficiency [128]. As the ions strike the target, atoms are ejected through a process called sputtering. These atoms then travel through the vacuum chamber and deposit onto a substrate, forming a

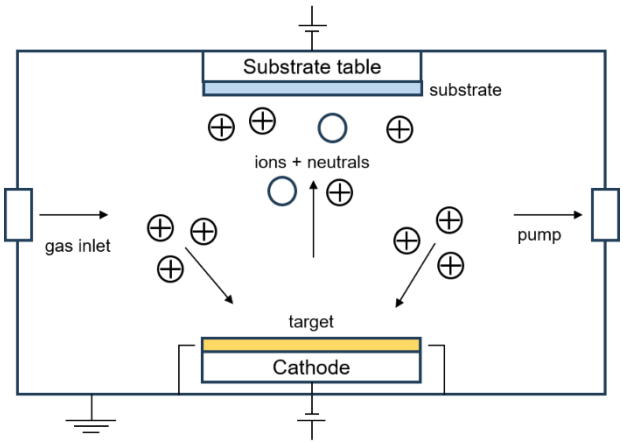

Figure 3.4.1. Scheme of the magnetron sputtering method.

thin film [129]. Magnetron sputtering allows for precise control over the film's thickness, composition, and microstructure, making it ideal for applications requiring high-quality coatings, such as in electronics, optics, and material science [130].

3.4.3. Hybrid Lattice Plasmon Polaritons Formed by DLW

HLPP modes offer significant advantages for plasmonic bio-sensors, allowing excitation without a glass prism and enhancing sensitivity through electric field localization on gold microbumps [75,132]. The resonance frequency of a noble metal nanoparticle depends on the size, shape, composition and the dielectric environment surrounding the particle. For precious metal nanostructures (Au, Ag, Cu) it is typically in the visible or near-infrared part of the spectrum. LSPs have emerged as an alternative to propagating surface plasmons in applications ranging from optical sensors to structures capable of generating coherent radiation, in particular because they do not require wavevector matching to excite the LSP [17]. Metallic nanoparticles can be produced by several popular fabrication methods (e.g. colloidal chemistry based on the reduction of metal salts), and arrays of nanoparticles (arrays) (e.g. using nanosphere lithography).

Another method to produce arrays is Direct laser writing (DLW) technologies currently being explored for the fabrication of periodic nanostructures to replace traditional lithography techniques. In this context, the DLW technique is being used for the formation of plasmonic nanostructures, with subsequent applications in the development of nano-lasers. In order to reduce the cost of fabrication of nanophotonic structures and to provide new functionalities, direct laser inscription technology has been introduced. One of the most common applications of DLW is the formation of periodic nano/micro structures in polymers using multi-photon polymerisation (MPP) [132]. It was introduced in the 1980s for the development of large-scale integrated circuits. Since the 1990s, DLW technology has evolved rapidly and the direct writing process has been refined and extended to a wide range of processing materials and applications. Over almost three decades, in response to the increased demand for micro/nano structures in photonics, optoelectronics, biomedicine and photochemistry, femtosecond (fs) DLW technology has been used as a promising device fabrication technology due to its three-dimensional (3D) processing capabilities [133]. Metallic nanostructures formed by laser writing are suitable for integrated micro/nanoparticle 3D diffractive optics because it is easy enough to fabricate and control the size, shape and periodicity of the elements [134]. Fabrication

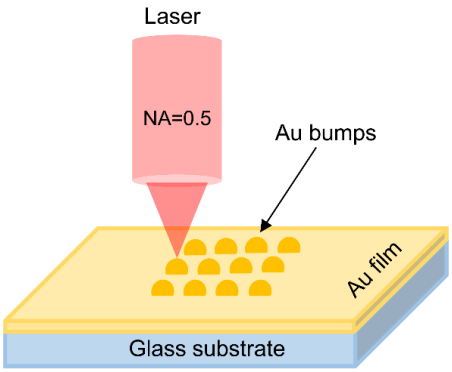

Figure 3.4.2. Illustration of Au bumps formation in a thin gold film using DLW technique.

of nanophotonic structures does not require expensive photolithography and etching processes and is therefore suitable for the production of a small number of special waveguide circuits when DLW is used.

Although progress has been made in fabricating complex plasmonic systems, creating structures with extremely small periodic surface irregularities remains challenging and costly. Lithography-based techniques are common but limited in producing large-area arrays necessary for plasmonic lattice surface resonance [135]. To address these limitations, a cost-effective DLW technique for fabricating large-scale gold microbump arrays in a gold film is used. These arrays support HLPP modes with reduced losses and tunable dispersion properties in the visible to near-infrared (Vis–NIR) range, comparable to structures fabricated by lithography-based techniques [134,135].

Large-scale arrays in thin gold films (thickness ≈ 50 nm) were produced using the DLW technique with the second-harmonic (515 nm) of 300-fs laser pulses generated by an Yb:KGW based fs-laser (Pharos, Light Conversion Ltd.). The femtosecond laser beam was tightly focused into a ≈1 μm spot with an objective having a numerical aperture (NA) of 0.5. Each gold micro bump, a key element of the fabricated grating, was created using a single laser pulse with 1.5 nJ energy (Fig. 3.4.2).

The sample translation speed and pulse repetition rate were set to 2.8 mm/s and 4 kHz, respectively, maintaining a 0.7 μm distance between bumps in the scanning direction (x-axis). The distance between bumps in the y-axis direction was also set to 0.7 μm. The moving of translation stage significantly increases the fabrication speed of the gold bumps array (5 × 5 mm²) compared

to the point-by-point approach. Gold bump formation is driven by thermal stresses from laser pulses below the melting threshold, resulting in film deformations and bump formation. The Gaussian intensity distribution of the laser beam ensures that the main energy is concentrated centrally, producing gold bumps smaller than the laser beam spot.

3.4.4.Spin-Coating

Spin-coating is the formation of a uniform thin film on a rotating base with the material under investigation [138]. Spin deposition is one of the effective methods for thin film fabrication due to its low cost, uniformity, easy reproducibility, and scalability. A typical process involves depositing a small amount of liquid onto the center of the substrate and rotating the tray at required (few hundred to few thousand rpm/min) speed. The spin-coating method is a fast and simple way to deposit thin films on a substrate, the main advantage of which is the formation of a uniform layer. A solution of a specific material is rotated at required speed, and the centrifugal force and surface tension of the liquid combine to create a uniform coating on the substrate. The excess solvent is evaporated and spin coating results in a thin film ranging in thickness from a few nanometers to a few microns [139].

This method is explained in four phases. These include solution precipitation, spinning, separation and solvent evaporation. The first phase involves dosing the solution onto the surface of the substrate. Centrifugal force pulls the solution across the tray surface if the tray is already rotating (dynamic spin deposition) or is set to rotate after deposition (static spin deposition). In

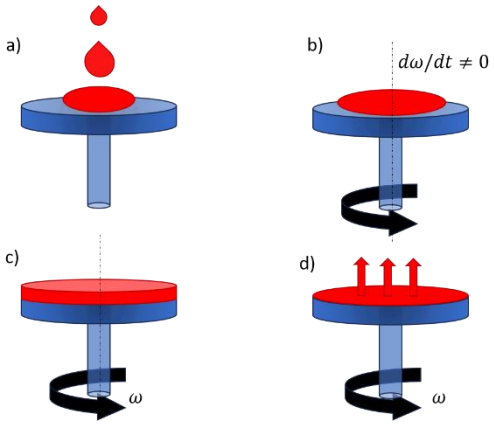

Figure 3.4.3. The four main steps in the spin-coating method are: (a) deposition, (b) acceleration, (c) flow dominance, and (d) evaporation. ω is the rotation speed.

the second phase, when the solution covers the surface of the substrate, the rotating disc is immediately or gradually accelerated to the required rotation speed. In this phase, the solution initially rotates at a different speed than the speed of the tray, but eventually the two rotation speeds coincide when the drag force balances the rotational accelerations, resulting in a thin layer of liquid. In the third phase: the speed is kept constant during the separation stage, the solution begins to transform into a thin film dominated by viscous forces. Fourth stage: solvent evaporation. The rate of solvent evaporation depends on the solvent vapor pressure, volatility and ambient temperature [139] (Fig. 3.4.3).

All the above processes are repeated several times to investigate the desired film thickness. The solution casting and drying steps are an integral and essential part of the spin coating process, contributing to the main process such as stacking/crystallization, phase separation and aggregation. It is very important to precisely control these processes, because the properties of the deposited thin films depend not only on the morphology (thickness, uniformity), but also on the deposition treatment. In general, a rotation speed >1000 rpm is recommended for industrial processing to ensure high uniformity. However, the drilling speed up to 200 rpm. can be used in laboratory-scale deposition, which can slow down the drying process but give more time for self-assembly.

The spin-coating method is widely used in microfabrication, where thin layers with a thickness of less than 10 nm are required. It is used extensively in photolithography to deposit photoresist layers approximately 1 micrometer thick. In the structure of the plasmon laser, the spin-coating method is used to form the active medium layer.

In this work (chapter 4.1) the poly(methyl methacrylate) (PMMA)-R6G was deposited on the top of the metal layers using the spin-coating method (at 3000 rpm, 30 seconds). For obtaining solid state matrix of R6G dye PMMA was used, both of which were dissolved in ethanol. The concentration of PMMA was 1 x 10^{-5} mol/L and concentration of R6G was 25 x 10^{-3} mol/L. The samples were prepared by mixing the PMMA with the dye dissolved in ethyl alcohol with a ratio of 3:1. The thickness of R6G doped PMMA layer formed by spin-coating was ~20 nm thick.

3.4.5.R6G in Hybrid Plasmon-Exciton Structures

R6G is a xanthene dye widely used in various applications, including laser technologies, fluorescence microscopy, and dye-sensitized solar cells. It is renowned for its excellent photophysical properties, such as high quantum

yield, photostability, and strong absorption in the visible region, making it an ideal candidate for use in hybrid plasmon-exciton systems.

R6G exhibits several key photophysical properties that make it suitable for use as a gain material and in hybrid plasmon-exciton structures. R6G has a high quantum yield (~0.95 in ethanol), which means it can efficiently convert absorbed light into emitted light [140]. It has strong absorption in the visible region, with a peak around 530 nm, which overlaps well with the plasmonic resonance of many metallic nanoparticles [90]. Also R6G is highly photostable, which is essential for maintaining performance over extended periods of excitation [141].

Gain materials are substances that can amplify light through stimulated emission. R6G is widely used as a gain material in dye lasers due to its ability to provide optical gain in the visible spectrum. R6G exhibits strong stimulated emission, making it effective in amplifying light in laser applications [142]. The broad emission spectrum of R6G (550-600 nm) enables it to cover a wide range of applications, including sensing and imaging [143]. Efficient energy transfer between R6G molecules and other materials in hybrid structures can enhance the overall optical performances [141]. Hybrid structures that combine plasmons (coherent electron oscillations at the surface of metallic nanoparticles) and excitons (bound electron-hole pairs in semiconductors or organic materials) have garnered significant interest due to their potential to enhance light-matter interactions. When R6G is combined with plasmonic materials, such as gold or silver nanoparticles, the system can enter the strong coupling regime. This regime is characterized by the formation of hybrid modes (polaritons) with properties derived from both the plasmon and exciton components [1]. The interaction between plasmons and excitons can lead to Rabi splitting, where the hybrid modes exhibit an energy gap proportional to the coupling strength. For R6G, this can result in enhanced optical properties and new functionalities [144].

R6G is particularly advantageous in hybrid plasmon-exciton structures for several reasons: the spectral overlap between the absorption/emission of R6G and the plasmon resonance of metallic nanoparticles facilitates efficient coupling [143]. Plasmon-exciton interactions can enhance the emission intensity and modify the emission spectrum of R6G, leading to improved performance in applications such as sensors and lasers [90]. By adjusting the plasmonic material or the environment around R6G, the optical properties of the hybrid structure can be finely tuned, offering flexibility for various applications [1]. The unique properties of R6G in hybrid plasmon-exciton structures make it suitable for a wide range of applications: enhanced fluorescence and sensitivity in plasmonic sensors [141], improved efficiency

and tunability in dye lasers [142], development of advanced photonic devices with enhanced light-matter interactions [144]. R6G is a versatile dye with exceptional photophysical properties, making it an ideal gain material and component in hybrid plasmon-exciton structures. Its ability to strongly interact with plasmons, combined with its high fluorescence quantum yield and photostability, enables the development of advanced optical devices with enhanced performance and new functionalities.

3.5. Scanning Electron Microscopy

The morphology of the structure gold nano-bumps and thin gold layer was evaluated from scanning electron microscopy (SEM) micrographs. In Fig. 3.5.1 are presented the SEM micrographs of two samples: uniform Au layer (50 nm) and nano-bumps lattice array on the same gold layer. The size of the nano-bumps and period of the lattice was evaluated based on SEM micrographs, where the gold nano-bumps diameter was ~370 nm and the structure period in laser scanning direction of the gold nano-bumps lattice was ~650 nm.

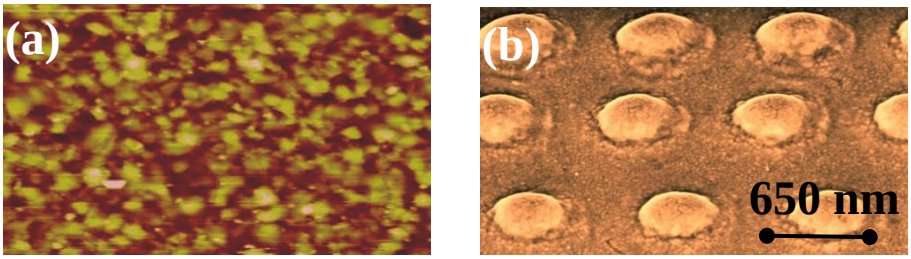

Figure 3.5.1. SEM micrograph of (a) a uniform (50 nm) Au layer and (b) a nano bumps lattice array on the same thin gold layer.

4. RESULTS

4.1. Strongly Coupled Plasmon-Exciton Polaritons for Photobleaching Suppression

Recently, there has been an increase in the use of plasmonic nanocavities to achieve strong coupling due to their ability to highly localize electromagnetic fields at the metal-dielectric boundary and the potential to surpass the diffraction limit due to the small cavity volume [74]. This leads to a small cavity volume which is desirable despite the fact that metals have high Ohmic losses and the Q-factors rather low compared with purely photonic cavities [76]. The important feature of strong coupling between cavity and organic emitter is that this interaction regime significantly changes the chemical reaction rates of molecules participating in the strong coupling at room temperature [11,149]. One of the fundamental phenomena appearing in many organic molecules is the photobleaching effect, which can suppress the fluorescence of the dye molecule due to the transition of singlet excited state electrons to the triplet state. Furthermore, the fluorescent molecule can suffer from irreversible photo damage, which reduces the number of emitters over time. Plasmonic cavities strongly coupled to organic molecule excitons modify the dynamics of excited states, thus, altering the photochemical reactivity. As polaritonic states are coherent and shares properties of plasmon and exciton, their typical lifetimes are very short (~ 10 fs) due to plasmonic component. Meanwhile the ISC rate is orders of magnitude longer (μm- mili seconds), thus probability to efficiently populate triplet state for plasmon-exciton polariton is very low. It was shown that strong coupling between localized plasmons of gold nanoparticles and organic dye molecules can significantly suppress photobleaching [21,150]. One of the first theoretical investigations on how strong coupling influences photobleaching in organic molecules were performed by L. Galego et al. [146]. They found that in the strong coupling regime, many-particle systems suppress photobleaching more efficiently than single strongly coupled organic molecule systems. Later it was experimentally shown by Munkbhat et al. [21] that LSP polaritons in Ag nanoparticles with J-aggregates under different coupling strengths influence the photobleaching, they have found that a larger Rabi gap suppresses photobleaching more efficiently. In contrast to these two papers, we perform experimental studies of photobleaching suppression and fluorescence lifetime measurements on planar nanostructures consisting of thin organic dye molecule layer and metallic film. Optical excitation can create singlet excitons, but subsequent transition from the singlet to the triplet dark state can

occur due to weak spin-orbit coupling and undergo the ISC. The lifetime of the triplet state is longer than that of the singlet, therefore the probability to interact with environmental oxygen is high. The interaction of environmental oxygen with triplet exciton occurs via charge transfer mechanism and as a result creates reactive oxygen species which chemically destroy the fluorophores. Photobleaching in turn influences many physical-chemical processes and can have a negative impact on the investigation of various systems in which PL effect may occur [147]. The decrease of fluorescence emission intensity due to photobleaching is commonly reported and thin metal layers or metallic nanostructures have been widely used to enhance the emission [148] due to plasmonic effect that induces strongly localized electric field. The luminescence enhancement can be achieved by two mechanisms – the light excitation and emission. The incident light is absorbed by the molecule (e. g. fluorescent organic molecule), however, when a metal nanoparticle is in the vicinity of the molecule, the light is coupled to the confined LSP field and the energy is then absorbed by the molecule. Indeed, optical energy is coupled to the tightly confined plasmonic field in the vicinity of organic molecule enhancing the absorption rate of the molecule. The process depends on the absorption cross section, and the relaxation of the excited molecule radiative and nonradiative decay path-ways, where the radiative decay outcome is the relaxation by emission at plasmon frequency (ω_{sp}). The PL is enhanced when the emission and excitation frequencies are close to the plasmon resonance and the nonradiative decay rate is smaller than the radiative decay. Furthermore, such absorbed energy can be emitted with enhanced spontaneous emission of excited molecules through the Purcell effect [8] (weak coupling regime). The rate of photochemical reactions can be modified by the weak coupling in plasmonic systems. However, the relaxation pathways are considerably smaller in weak coupling compared to the strong coupling regime. However, we underline that weak coupling with plasmonic modes does not inhibit the photobleaching effect.

In this work we investigate the influence of strong coupling on photobleaching and fluorescence lifetimes of R6G dye in nanostructures that support plasmon-exciton polaritons states. The plasmonic-photonic nanostructures used in this research consisted of thin silver-gold films (Ag-Au) with R6G dye in nanometer thickness layers. TIRE was used for the plasmon-exciton polariton system by selectively filtering out the incident light responsible for exciton component generation in the hybrid polaritonic mode and thus prove the strong coupling. We then use FLIM to demonstrate that the strong coupling between SPP and dye excitons plays a pivotal role in suppressing photobleaching.

The results presented in the following Chapter were originally published in: J. Anulytė, V. Žičkus, E. Bužavaitė-Vertelienė, D. Faccio and Z. Balevičius. “Strongly coupled plasmon-exciton polaritons for photobleaching suppression”, *Nanophotonics* (2024), 13(22), 4091-4099. https://doi.org/10.1515/nanoph-2024-0259.

Author contributions: The concept for the work was developed by J.Anulytė, V.Žičkus and Z.Balevičius. Experimental work and methodology was undertaken by J.Anulytė and V.Žičkus. Original draft preparation J.Anulytė, V.Žičkus, E.Bužavaitė-Vertelienė, D.Faccio and Z.Balevičius. D.Faccio provided valuable insights for fluorescence lifetime analysis as well as fruitful discussions. All authors analyzed the results and contributed to the writing of the manuscript. The project was supervised by Z.Balevičius and D.Faccio.

4.1.1.Experimental Measurements

In this work four different ellipsometric spectra were measured. Firstly, the ellipsometric spectra of Rhodamine embedded in PMMA matrix measurements (schematic 4.1.1 (b) were performed from which the absorption lines of R6G were determined (Fig. 4.1.2 (b)), dark blue dotted line). The second measurement was performed in TIRE configuration with Ag-Au layer on the glass plate attached through the immersion oil (BK7 matched) to the BK7 glass prism for investigation of optical dispersion of excited SPP (Fig. 4.1.1 (c)). Next, TIRE spectra of Ag-Au/PMMA-R6G were measured (Fig. 4.1.1 (a)), where both components (exciton and SPP) manifested themselves at the 470-730 nm range of wavelengths, respectively. In order to prove that the anti-crossing of dispersion curves of SPP and R6G dye exciton is caused by strong coupling, an optical filter (Fig. 4.1.1 (d)) was used to excite only one of the resonance components. To achieve this an optical filter Schott OG-590 long pass was used to cut a part of the white light in order to leave only the SPP resonance.

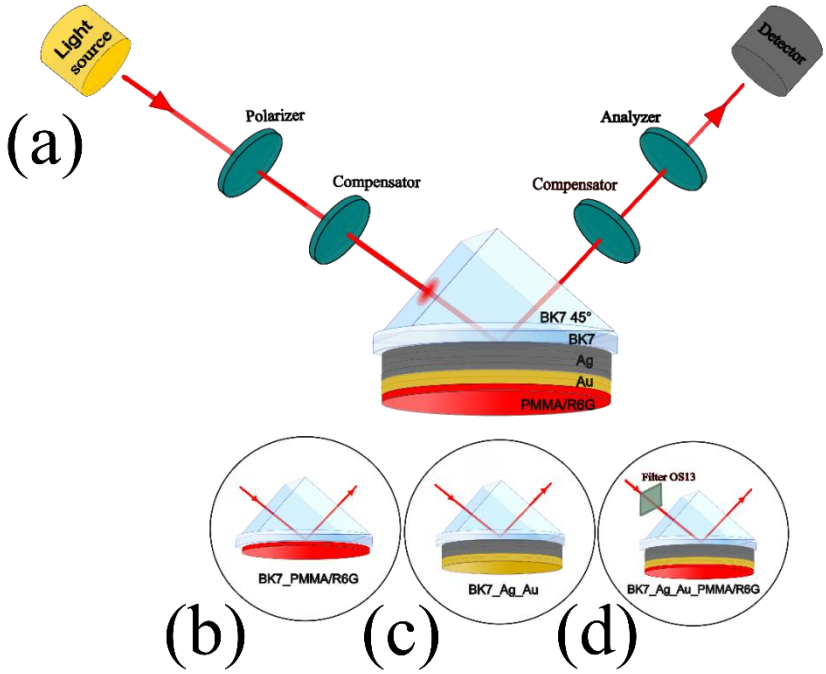

Figure 4.1.1. TIRE scheme of excitation configurations for the (a) hybrid exciton–SPP mode, (b) R6G absorption lines, (c) single SPP mode and (d) the hybrid exciton-SPP mode with an optical filter OG-590.

To achieve the strong coupling regime the interaction between emitter and optical environment should be strong enough to modify the energy levels responsible for emission. SPPs are able to confine energy into small volumes at the metal-dielectric interface, thus, the enhanced electric field can interact with emitter strongly enough. The near field character of SPP is related with the fact that such modes are bound to the inter-face. The confinement of the optical field in the vicinity of the interface arises from the evanescent nature of SPP. The near-field character determines the propagation and localization properties of the SPP's, as well as, increased possibilities for strong coupling between emitters and SPP's. In order to compare the electric field strength of SPP (metal/air) and evanescent wave at dielectric/air interface two structures were modelled, where either Au (45 nm) or PMMA (45 nm) were embedded between two semi-infinite materials – BK7 glass and air. Both of the samples were investigated under TIR, where AOI was equal to 45 degrees. As can be seen from Fig. 4.1.2 a, there is a peak field enhancement in the metal film (green line) case that is approximately 2.9 times stronger compared to the

bare film sample (blue line). In case of a thin metal film the excitation of SPP works as an open cavity in which organic dye emitter is placed.

The TIRE method was used for analysis of the dispersion and optical properties of single SPP for structure consisting of BK7 glass substrate and thin Ag-Au layer. The single SPP dispersion is shown in Fig. 4.1.2 b marked by white dotted curve. In order to determine the absorption lines of the dye, the PMMA-R6G layer was deposited on BK7 glass substrate and measured by SE. From the measured ellipsometric spectra the absorption lines of the PMMA-R6G were determined ($\lambda_1 = 482$ nm, $\lambda_2 = 551$ nm) and are represented by the grey dashed in Fig. 4.1.2 b.

In order to analyze the influence of the dye exciton on the optical response of the Ag-Au/PMMA-R6G structure the sample was attached to the BK7 glass prism via refractive index matching liquid and measured in TIRE configuration. First, the TIRE spectra of Ψ and Δ ellipsometric parameters for hybrid surface plasmon-exciton polariton structure were measured. The results are presented in Fig. 4.1.2 b as reflection intensity maps of the p-polarized light vs. energy in the range of AOI θ = [43-48°]. As can be seen from Fig. 4.1.2 b the hybrid exciton-SPP mode (marked by dark blue and light blue dashed lines) shifts and bends from the initial values of the single exciton (grey dashed lines) and single SPP (white dotted curve) modes.

In order to prove that the SPP resonance and dye excitons are strongly coupled, the TIRE method with spectral filtering where was used to filter out one of the hybrid mode components. This method was previously used to

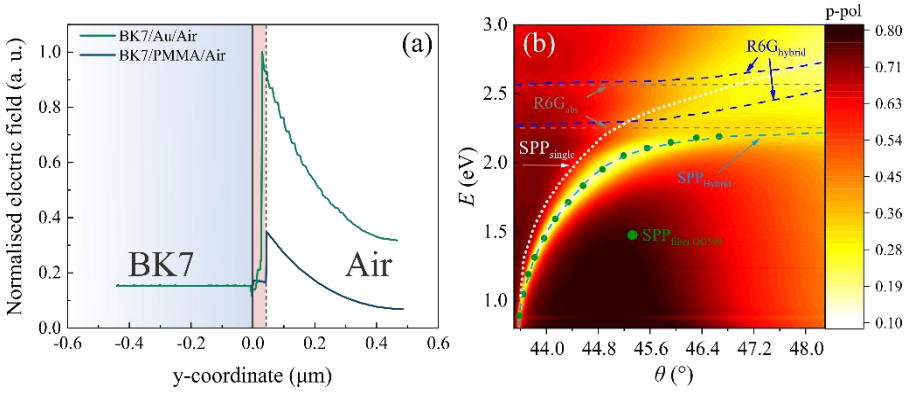

Figure 4.1.2. (a) The modelled normalised electric field distribution of metal/air (green) and PMMA/air (blue) structures. (b) The dispersive relationship of hybrid mode (dark blue (R6G) and light blue (SPP) dashed curves) and single SPP (white dotted curve) and excitons R6G (grey dashed lines) by total internal reflection ellipsometry method. The measurements with filter OG-590 are marked as green dots.

prove strong coupling between the two components of a hybrid mode of strongly coupled plasmonic resonances [66]. Here we use this method to identify the strong coupling between plasmonic resonance and R6G dye excitons.

The ellipsometric parameters of the sample in TIRE configuration (Ag-Au/ PMMA-R6G) were measured without an optical filter (Fig. 4.1.2 b dark blue and light blue dashed lines) and with an OG-590 filter (Fig. 4.1.2 b green dots) in order to determine if the exciton and SPP mode is in strong coupling. The spectra measured with optical filter OG-590 are indicated as green dots in Fig. 4.1.2 b, where the filter cuts out a part of light incident onto sample leaving only the SPP component of the hybrid mode. The use of filters allows to distinguish if the system is in strong coupling or interference of two excitations. The interference can lead to a significant contribution in the optical response as a result leading to a distorted optical response, for example

Fano resonance [12]. Since the experimentally measured dispersion of the SPP with the filter in place follows the unfiltered dispersion of SPP component, it indicates that the system is indeed in strong coupling.

It was shown that the strong coupling between J-aggregates of dye molecules and gold nanoparticles can suppress photo-bleaching [21]. A fluorophore with a high ISC quantum yield can transfer a significant amount of its population to the long-lasting triplet state. This is because the molecules interact with the environment in the triplet state, which in turn leads to photobleaching. FLIM method is independent of the concentration of the fluorescent species. However, typical FLIM samples can have a number of different fluorophores that can be photobleached at different rates, thus, the shape of decay signal changes [153,154]. Moreover, the effect of photobleaching in FLIM can be enhanced due to high optical energy in the light pulses which are necessary for the required large number of photons in order to ensure acceptable signal to noise ratio. Thus, FLIM can create reactive oxygen species that can result in an increased number of damaged fluorophores. In this research, FLIM was used for the investigation of influence of light-matter strong coupling to the suppression of photobleaching in R6G dye exciton. FLIM signal detects all types of emitting fluorophores (various types of fluorophores with different lifetimes that interact differently with the environment) so the photo-bleaching rates are different and the fluorescence decay changes. However, when strong light-matter interaction takes place the singlet probability to interact with environmental oxygen is strongly suppressed, therefore this process influences the fluorescence lifetime decay.

In order to demonstrate the influence of photobleaching on the fluorescence lifetime two samples were used: (i) a fluorescent molecule layer and (ii) a plasmonic structure with fluorescent molecule layer. Firstly, a conventional sample of BK7 glass substrate with PMMA-R6G layer on top was measured (Fig. 4.1.3 a dashed lines). As the bare PMMA-R6G layer absorption lines are determined by the organic fluorescent molecules which absorb at 482 nm and 551 nm and they are non-dispersive at different AOI, these samples were measured at the 45° AOI in the Kretschmann configuration (with glass prism coupled with immersion oil). It can be seen that the fluorescence lifetime intensity peak decreases with increasing laser exposure time. For the second sample Ag-Au/ PMMA-R6G was illuminated in the Θ = 44-46° AOI range to optically excite the strongly coupled states between SPP and R6G dye exciton (Fig. 4.1.3 a solid lines). As can be seen from Fig. 4.1.3 a (44°), the R6G intensity peak now experiences significantly less photobleaching in time compared to the sample with only the PMMA-R6G layer. In order to evaluate the photobleaching effect on the fluorescence lifetime peak intensity, the change of the photo-bleaching effect over time was analyzed by altering the angle of light incidence (Fig. 4.1.3 b). The intensity

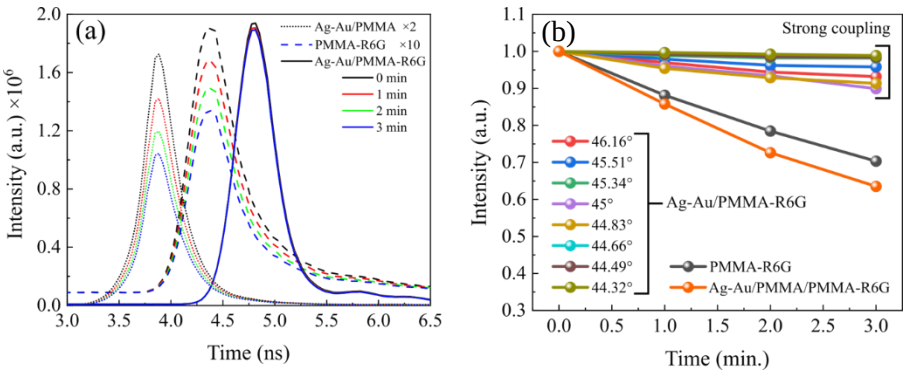

Figure 4.1.3. (a) Fluorescence lifetime and intensity changes in time (from 0 to 3 minutes) due to photobleaching effect of R6G in plasmonic-nanophotonic structure (solid curves) structure with spacer between Ag-Au and PMMA-R6G (dotted lines) and of reference (dashed curves) samples. The AOI for plasmonic structure shown is 44°. FLIM curves of PMMA-R6G on the coverslip (AOI = 45°) are multiplied by a factor of 10 and structure with spacer by factor of 2 in order to show the counts at the same scale as the plasmonic-nanophotonic structures. (b) Photobleaching evolution in time of BK7/Ag-Au/PMMA-R6G structure at different incident angles, and a glass substrate with single R6G dye layer of (black) at 45° AOI.

of the curves of the Ag-Au/ PMMA-R6G structure decrease much slower than intensity of PMMA-R6G sample (Fig. 4.1.3 b black circles). The fluorescence lifetime intensity of Ag-Au/PMMA-R6G sample drops only by approximately 5% in 3 min, compared with 30% of single PMMA-R6G layer.

In order to prove the influence of the strong coupling effect to the suppression of photobleaching, we performed measurements with the sample where a 20 nm PMMA spacer is embedded between metal and PMMA-R6G layers (Ag-Au/PMMA/PMMA-R6G structure in Fig. 4.1.3 a and b). The fluorescence lifetime intensity of sample with PMMA spacer in 3 min period decreases by similar amount as in single PMMA-R6G case. This clearly shows the influence of the strongly coupled plasmon and exciton on the reduction of photobleaching effect (6-fold reduction) at the zero detuning point and dependence on the AOI. These results indicate that strong coupling interactions play a crucial role in stabilizing photo-bleaching mechanisms and open possibilities for creating nanophotonic devices with organic molecules. Additionally, the improvement FLIM signal using nanostructures in the strong coupling regime provides the opportunity to investigate molecular relaxation processes without the influence of photobleaching.

Note that the IRF of the system is limited to ~150ps. The data is fitted using least-squares approach, where the model function is a convolution between the IRF data, and a bi-exponential decay equation [151],

$$I = a_1 \, exp\left(-\frac{t - t_0}{\tau_1}\right) + (1 - a_1) \, exp\left(-\frac{t - t_0}{\tau_2}\right), \qquad (4.1)$$

where I is intensity, τ_1 and τ_2 are the two distinct lifetimes, a_1 is the decay amplitude of the first lifetime, t and t_0 are the time and temporal offset of the laser pulse that is misaligned with fluorescence pulse, respectively.

While FLIM literature suggests that lifetimes that are ~10x shorter than the IRF can be recovered, the recovered values must be interpreted with care. Nonetheless, there is a clear difference between the decay curves with strongly coupled plasmon-exciton polaritons and pure exciton on the sample without metal. Due to the use of TIR configuration, that is required to achieve SPP, the surface plasmon electric field is localized at the metal/PMMA-R6G interface. It is reasonable to assume that the main contribution to lifetimes comes from the molecules near the interface strongly coupled to the surface plasmon electric field. The enhancement of fluorescence lifetime intensity arises due to the suppression of the photo-bleaching effect, caused by the strong interaction between the plasmon and exciton, which influence the shortening of the fluorescence lifetime of R6G molecules. This is also

confirmed by the lifetime's fitting procedure for the sample with a metal layer (strongly coupled) where the obtained values of amplitude a_1 were close to 1 along with the lifetime τ_1 being significantly shorter than τ_2 (Table 1). Meanwhile, for the sample without a metal layer the fitting parameter a1 was considerably lower.

Tab. 1: Components of lifetime decay from bi-exponential fits of data shown in Figure. 4.1.4.

Fit	**a_1**	**τ_1 (ns)**	**τ_2 (ns)**	**R-squared**
Ag-Au/PMMA-R6G 44°	0.972±0.0058	0.079±0.0035	0.732±0.1298	0.98
Ag-Au/PMMA-R6G 47°	0.995±0.0008	0.037±0.0009	1.701±0.3209	0.994
CS/PMMA-R6G 45°	0.899±0.0104	0.077±0.0038	0.585±0.0498	0.983

Each of the obtained fluorescence decay curves (Fig. 4.1.4) corresponds to a certain p-polarized reflectance spectra taken from ellipsometric measurements (Fig. 4.1.5). While the fluorescence decay can be easily determined from fluorescence lifetime measurements, the influence of strong interaction between SPP and dye exciton components can be inspected in the frequency domain measurements. SE measurements in TIRE seen in Fig. 4.1.5 were performed at the AOI between 44 - 46 degrees. The corresponding hybrid SPP-exciton resonances appear, in the vicinity of the zero-detuning point, where strong interaction between SPP and R6G dye was achieved. From the graph (Fig. 4.1.5), it is evident that as the incident angle increases, the lower polariton branch (LP) shifts towards the blue side of the spectra.

Together with LP component the upper polariton branches (UP), also shift towards shorter wavelengths and bend (black dashed lines), contrary to R6G dye absorption lines (marked with dotted black lines in Fig. 4.1.5 inset). The inset in Fig. 4.1.5 shows the p-polarized reflectance spectra of a single dye layer (PMMA-R6G) on microscopic glass substrate.

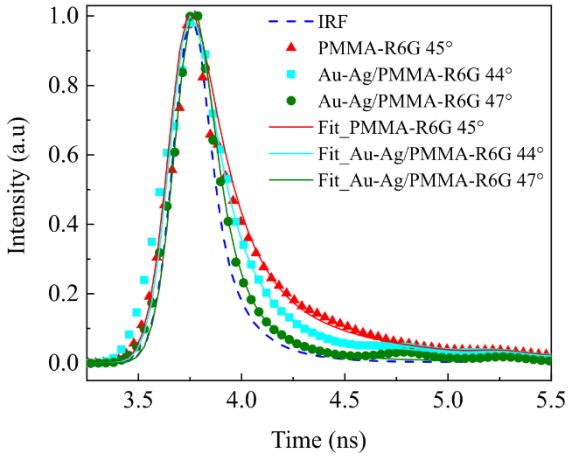

Fig. 4.1.4. Fitted normalized fluorescence lifetime decay curves for different samples (solid lines), as well as the IRF. Nanostructures (Ag-Au) with a layer of spin-coated PMMA-R6G on have a significantly larger fraction of short lifetime component compared to the control sample (CS_PMMA-R6G 45°). In fact, nanostructure samples show a significant contribution from very short lifetimes (limited by the IRF of the system).

The spectral measurements have shown that the R6G dye absorption lines do not depend on the AOI, i.e. the absorption lines of the single dye layer are fixed at 485 nm and 520 nm wavelengths. The gap (or Rabi splitting) between LP and UP dispersion lines depends on the product of the dipole moments sum associated with organic dye exciton and the electric field of the plasmonic resonance per one vacuum oscillation. To accurately determine the interaction strength and its variation with the incident light angle, it is necessary to establish the dependence on optical dispersion. This involves determining the relationship of dispersion curves, the function of wave vector vs. energy broadening (Fig. 4.1.5).

When dye molecules strongly interact with plasmons, absorption lines shift to higher energy. This clearly shows the hybridization of dispersion lines and indicates a strong coupling regime and vacuum Rabi oscillations. The exact Rabi splitting for the hybrid plasmon-exciton polariton modes can be seen in Fig. 4.1.6 and was determined to be about 90 meV. The strong coupling regime in plasmonic-photonic structures is reached when the splitting of the modes (strong coupling parameter g) exceeds the energy losses (damping) [12] and the g parameter can be obtained only by the fitting of the whole spectra [66]. Yet the strong coupling regime can be easily distinguished from the weak coupling by observing the measured dispersion, where it can be

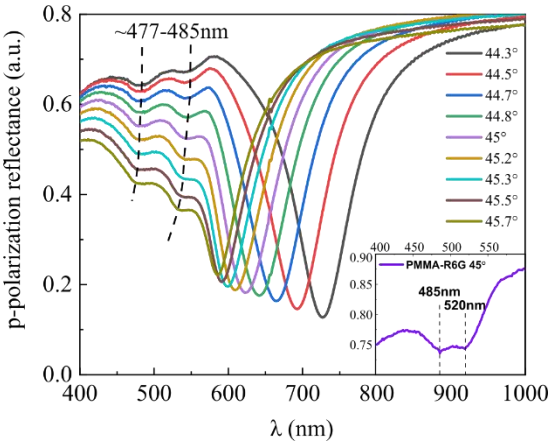

Figure 4.1.5. The experimental p-polarization reflectance (at 44-46 degrees AOI) spectra of a hybrid SPP-exciton mode (black dashed lines show the R6G absorption lines variation with AOI). The inset on the bottom right shows the R6G absorption lines (at 45 degrees AOI). The dashed lines correspond to the hybrid SPP-exciton mode component of PMMA-R6G absorption.

defined by the splitting being large enough compared to the linewidths [6]. The wave vector value at the anti-crossing point (k_x) was equal to 12.3 μm (taken from dispersion lines in Fig. 4.1.2 b). At this wave vector value, the corresponding energies of the upper (UP) and lower polariton (LP) branches were equal to 2.28 eV and 2.19 eV. From these energies and wave vector k_x the corresponding AOI were calculated to reveal at what values the full width at half maximum (FWHM) for each UP and LP branch has to be evaluated in the experimental dispersion (Fig. 4.1.2 b).

It was determined that the FWHM (damping γ) was equal to 120 meV (at 46.9° AOI and ELP = 2.19 eV) and 90 meV (at 44.8° AOI and E_{UP} = 2.28 eV) for the LP and UP branches, respectively. Yet, to distinguish whether the strong coupling regime is reached, the coupling strength should exceed the linewidths of the coupled system, that is described by equation [12],

$$g > \frac{1}{4}(\gamma_{pl} + \gamma_{em}), \qquad (4.2)$$

where the right-hand side of this equation (damping) is equal to ~52 meV. While in the weak coupling regime the mode damping prevails the light-matter interaction, the strongly coupled mode damping should be less than the

Rabi gap [152]. This therefore shows the Rabi gap obtained in this research (90 meV) is larger than the damping (~52 meV) of the hybrid mode, confirming that the system is in the strong coupling regime.

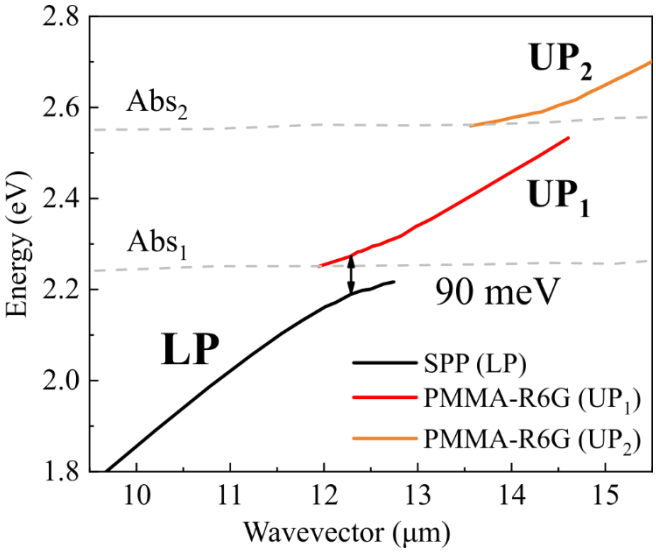

Figure 4.1.6. Dispersion relation showing the hybrid polariton modes (UP and LP) resulting from the strong coupling between surface plasmon polaritons (SPP) and the organic dye excitons (the absorption (Abs) lines of PMMA-R6G layer - grey dashed lines). The Rabi splitting of 90 meV is indicated. The observed states are hybrid excitations, not the parent SPP or exciton states.

The strong coupling between SP mode and R6G dye exciton exhibits the polaritonic emission which is different from the conventional spontaneous fluorescence emission of pure organic R6G. The polaritonic emission of sample consisted from PMMA/R6G_Au/Ag studied in Kretschmann configuration. Emission was excited on the PMMA/R6G layer using 480 nm laser (EKSPLA NT: Nd:YAG laser, with parametric generator: max output 1mJ, pulse duration 3-6 ns, wavelength 210-2600 nm, excitation power of 132 μW at 480 nm). The emission at various angles was detected through the prism using CCD detector incorporated in spectrometer (Hamamatsu) (Fig. 4.1.7). Figure 4.1.8 presents the TIRE p-polarized reflectance intensity map and polaritonic emission (white dots) spectra recorded from 40 to 50 degree. The Figure 4.1.9 a emission spectra shows angular dependence and follows

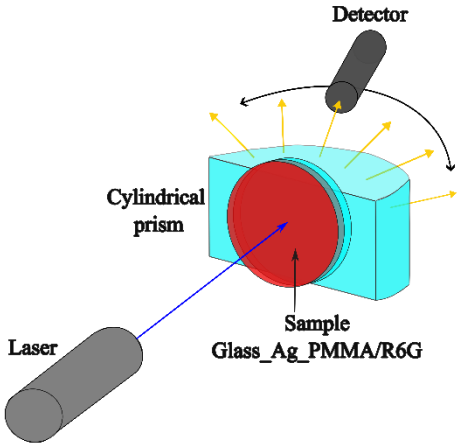

Figure 4.1.7. Setup for angular fluorescence dependence measurements of R6G dye in inverse Kretschmann configuration of excitation.

the dispersion curve of the reflectance map of lower polariton (LP) (Fig. 4.1.8) meanwhile smaller peak at the 534 nm attributed to exciton like upper polariton (UP) which shifted to the lower wavelengths by about 2 nm compared with pure R6G/PMMA layer fluorescence emission (Fig. 4.1.9 b). The exciton like upper polariton at 534 nm weakly depends on the angle, meanwhile the intensity peak of lower polariton strongly depends on the angle. The first peak is from upper polaritonic branch associated with excitonic part of hybrid plasmon-exciton polariton state, meanwhile the second is related with SPP polaritonic branch and this peak is about 3 times more intense than excitonic part and then pure R6G exciton luminescence in the same PMMA matrix. Indeed, the intensity peak position in spectra for SPP polaritonic branch follows the lower branch of polariton-dispersion curve obtained by TIRE in p-polarized reflectance map (Fig. 4.1.8). In polaritonic state when organic molecules are pumped into an excited state, instead of emitting light, exciton can transfer energy coherently to the plasmonic resonance. Plasmon oscillations can emit accumulated energy into free space, resulting in a coherent emission. This implies that due to coherent energy exchange between organic dye exciton and SPP excitonic emission radiates through the lower SP polaritonic branch and is no longer purely excitonic, becoming hybrid with mixed plasmon-exciton properties. This results clearly shows that polaritonic states can significantly modify the emitters properties.

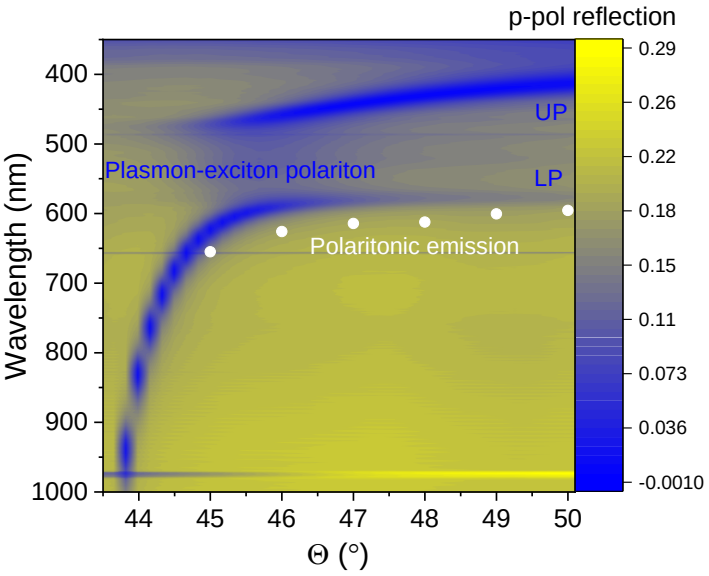

Figure 4.1.8. The optical dispersion relationship polarised intensity map of hybrid polaritonic mode (excitonic upper dispersion branch (R6G) and plasmonic (SPP) lower branch) measured by total internal reflection ellipsometry method and polaritonic emission from the lower branch (white dots)

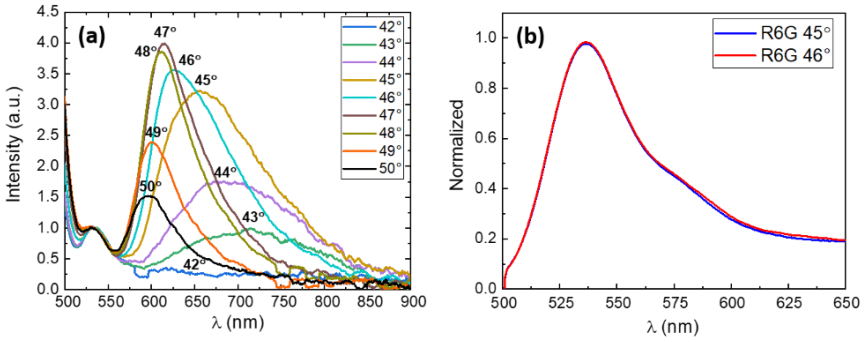

Figure 4.1.9. (a) Polaritonic emission from the lower polariton (LP) branch related with plasmonic resonance. (b) Coherent emission from strongly coupled plasmon- R6G emitter sample.

4.1.2.Summary

This study employed TIRE to investigate the room temperature strong coupling between SPP and excitons within plasmonic-photonic nanostructures. Notably, the “filtered TIRE method” was applied for the first time in plasmon-exciton polariton system to experimentally verify strong coupling by selectively filtering exciton component in the hybrid polaritonic mode. The Rabi splitting, determined from the optical dispersion E(k) at the zero-detuning point, was measured to be 90 meV, the comparison of Rabi gap with the linewidths (γ) of the plasmonic and excitonic resonances, confirms the presence of strong coupling regime.

FLIM has demonstrated that using polaritonic nanostructures where plasmons and excitons are in a strong coupling regime, reduces the fluorescence intensity by approximately 5%, over the course of the 3 minutes measurement and the strongly coupled sample is photobleached approximately 6 times less. While fluorescence lifetime is in general independent of intensity, recovering accurate lifetimes (which in real systems are often bi-exponential in nature) requires a large number of photons [153]. Therefore, suppressing photobleaching could enhance FLIM measurements. The photobleaching can be suppressed by using plasmonic-photonic nanostructures supporting strong coupling and combining it with oxygen scavenging media. It was observed that the strong coupling between SPP and dye excitons plays a pivotal role in suppressing photobleaching, a phenomenon that often impedes fluorescence-based studies. The hybrid plasmonic-nanophotonic structures exhibit a remarkable ability to stabilize photo-bleaching mechanisms, thereby offering a promising avenue for the development of quantum multiparticle nanophotonic devices with organic molecules. Findings presented in this study offer possibilities for fundamental understanding of strongly coupled quantum dynamical systems, thus hold significant implications for various fields, including coherent light nanosources research, macroscopic quantum coherence, quantum biosensing and information processing.

4.2. Influence of Gold Nano-Bumps Surface Lattice Array on The Propagation Length of Strongly Coupled Tamm and Surface Plasmon Polaritons

In order to optimize and achieve higher efficiency of plasmon-exciton polaritonic coupling ordered metallic nanostructures should be used instead of planar structures studied in the chapter 4.1. Localized surface plasmons on metallic nanoparticles exhibits very high electric field enhancement in extremely small volumes. When metal nanoparticles are arranged in an ordered array, the part of scattered light propagate in plane of lattice and coupled with LSP, this leading to strong narrowing of surface plasmon lattice resonances. Such well-ordered surface lattices with extremely small volumes around the nano-bumps, as a „hot-spots“ are promising nanostructures to achieve efficient photobleaching suppression, high fidelity coherence lasing, extremely sensitive quantum optical sensing, Bose-Einstein condensation states. The enhancement of local electromagnetic field at the metal dielectric interfaces is widely studied for various purposes such as sensing [64,69,160, 161,162], absorbers [163], fast switching [164] or novel lasing [83,165] structures. The crucial role in field enhancement lies on plasmonic effect, first of all due to ability to focus optical fields to volumes below the diffraction limit [10]. The plasmonic effects manifested themselves on the metallic nanoparticles [12], thin metal layers [166] or metallic nanostructures [167] under certain conditions. Metallic nanoparticles have shown very high electromagnetic field confinement [67], meanwhile propagating surface plasmon resonance can be excited on the thin metal layer (≈ 50 nm) and have been widely applied for biosensing applications. Also, Tamm plasmons in the nanostructures of 1D PCs with metal layer on the top applied for narrow band tunable filters [168]. Recently various metallic nanostructures (grating arrays) have been starting to employ in order to minimize losses in the metals. Such metallic lattices exhibit narrow plasmonic resonances compared with randomly distributed metal nanoparticles or propagated surface plasmon resonance [169]. SPPs are collective charge oscillations coupled to an external electromagnetic field that propagate along an interface between a metal and a dielectric. Meanwhile, the TPPs which exist between the metal and PC are non-propagating optical states. The TPPs have in-plane wavevector smaller than the wave vector of light in vacuum, thus excited directly with incident light [46], contrary to the SPPs, which wave vector is always larger than the incident light and prism or grating coupler is needed for excitation [67]. However, when the conditions for both plasmonic excitations are fulfilled the new state of hybrid TPP-SPP mode arises [66]. This situation can be realized

whenever the glass prism is optically connected with PC with thin metal layer on the top. Such light-matter interaction leads to a strong coupling between TPP and SPP components and they become inextricably linked with each other [6]. When strong coupling regime is achieved the energy exchange between the TPP and SPP occurs during the coherence time [170], which are about tens of femtoseconds. This means that in such coupled systems, the coupling strength between the TPP and the SPP exceeds the damping rate [164]. Such polaritonic hybrid modes can be achieved when the interactions are sufficiently strong, then the energy spectrum is modified, and losses in the metal layer decreasing [64].

Another way to obtain the narrow plasmonic resonances with lower losses have been demonstrated by using metallic grating arrays [167]. The current lithography methods [171] or DLW [75] enables the creation of complex plasmonic systems supporting multiple plasmon modes. The most popular nanostructures of complex plasmonic systems are metallic nanoparticle arrays whose period is comparable with the incident light wavelength [172]. Such nanostructures exhibit the plasmon hybridization effect where LSPs interact with each other. The ordered array of metal nanoparticles acts as a diffractive grating for incident light which diffraction effect depends on the size, shape, and period of the array. If one of the scattered waves propagates in the plane of the array it can couple with localized plasmon resonance of these nanoparticles. When nanoparticles are arranged by an appropriate period, the scattered light field is in phase with local plasmon resonance to the nearby nanoparticle thus enhancing the plasmonic excitation in the neighbor particle. This leads to a significant narrowing and increase coherence of the plasmonic resonances due to compensation the damping of localized plasmon resonance of the individual particles by the scattered field of light [64]. The strong coupling between metal nanoparticles, which leads to the generation of surface lattice resonances, was predicted and provided design rules for the optimization of ultra-narrow resonances [73,173,174,175]. In order to achieve lattice resonances with a high-Q, bipartite nanoparticle arrays have been used and it was shown that it is possible to obtain lattice resonances with bright or dark modes, depending on the relative position of the two particles within the unit cell [17,70].

The coherent nature of various microcavities [158,176], surface lattice plasmonic resonances [177] have attracted a lot of attention due to the ability of light and electronic excitations to strongly interact. The coherence properties of polaritonic hybrid modes also have been studied by using interference experiments where direct information about mode coherence was explained [178]. Comprehensive analysis of hybrid exciton-plasmonic surface

lattice resonances from weak to strong coupling was made and the weight of mater-like (exciton) and light-like (plasmon) was evaluated [177].

In this study the nanostructure of gold nano-bumps lattice array produced by DLW on thin gold film and 1D PC from periodic five TiO_2/SiO_2 bilayers were used as the coherent energy transfer channels between Tamm plasmons and hybrid propagated lattice plasmon resonances in the strong coupling regime. In TIR configuration by using glass prism the uniform gold layer with 1D PC supports hybrid TPP-SPP mode with strong coupling meanwhile, the area of the metal film with gold nano-bumps lattice induced additional in-plane Bragg mode (BM) and modifies the propagation length of such hybrid plasmonic mode. The optical dispersion and surface waves propagation features of 1D PC with uniform gold layer and the lattice of gold nano-bumps array were analyzed by two coupled oscillator model and wavevector vs. energy broadening. Attention to the nanophotonic – plasmonic structures which are able to support extended coherence properties under strong coupling arises from their promising applications to the plasmonic lasing [3], information processing [179], and using such polaritonic structures for new generation of optical sensing [68]. Aditionally, the optical dispersion of surface plasmon lattice resonances on such gold nano-bumps arrays and their strong coupling with excitons of R6G dye organic molecules layer in PMMA matrix was analyzed.

The results presented in the following Chapter were originally published in: J. Anulytė, E. Bužavaitė-Vertelienė, V. Vertelis, E. Stankevičius, K. Vilkevičius, and Z. Balevičius, “Influence of a gold nano-bumps surface lattice array on the propagation length of strongly coupled Tamm and surface plasmon polaritons,” J. Mater. Chem. C, vol. 10, no. 36, pp. 13234–13241, 2022, doi: 10.1039/D2TC02174A.

Author contributions: The manuscript was written through the contributions of all authors. All authors have approved the final version of the manuscript. Contributions: conceptualization, J. Anulytė, Z. Balevičius; methodology, J. Anulytė, E. Bužavaitė-Vertelienė, E. Stankevičius, K. Vilkevičius; formal analysis, Z. Balevičius, J. Anulytė, E. Bužavaitė-Vertelienė, V. Vertelis, E. Stankevičius; writing—original draft preparation, Z. Balevičius, J. Anulytė, E. Bužavaitė-Vertelienė; writing—review and editing, Z. Balevičius, J. Anulytė, E. Bužavaitė-Vertelienė. All authors have read and agreed to the published version of the manuscript equally (J. Anulytė, E. Bužavaitė-Vertelienė, V. Vertelis, E. Stankevičius, K. Vilkevičius, Z. Balevičius).

4.2.1.Experimental Measurements

In this chapter studied the optical properties of surface plasmon polariton coupled with a TPP, and the additional influence of parallel Bragg reflections which arise due to the lattice array of gold nano-bumps. It was shown [154] that coupled plasmon polaritons on gold films can generate a lower energy symmetric mode and a higher energy antisymmetric mode, which corresponds to the SPP and TPP, respectively. When light is incident on the lattice array of gold nano-bumps with a subwavelength lattice period, the wave vector of photons can vary, and, due to this, a hybrid BM–SPP mode is generated under the Bragg coupling conditions. This mode exists at the outer metal–ethanol interface. Meanwhile, at the inner interface of the 1D PC and the Au layer, the optical Tamm state is generated. However, the inverse system under TIR does not generate the lattice plasmon resonances which have been widely reported on various metallic subwavelength structures under traditional reflection [74], [76]. Another optical phenomenon which is related to gratings is the Rayleigh anomaly (RA), which sometimes leads to a narrower spectral width [154], however, it was demonstrated that the coupling between the RA and SPPs can occur only for a specific range of the metal film thickness [155].

The TIRE method was used for the analysis of the dispersions and optical properties of the TPP-SPP hybrid modes. Firstly, the TIRE spectra of Ψ and Δ ellipsometric parameters were measured and presented as reflection intensity maps of the p-polarized light vs. energy in the range of AOI (θ = 66-71°). Figure 4.2.1 a and b show the hybrid TPP-SPP mode excitation which generated in the planar structure with 1D PC and uniform thin gold film on the top (a) and modified with gold nano-bumps (b) in the ethanol as the ambient. As can be seen from the dispersion maps the strong coupling effect

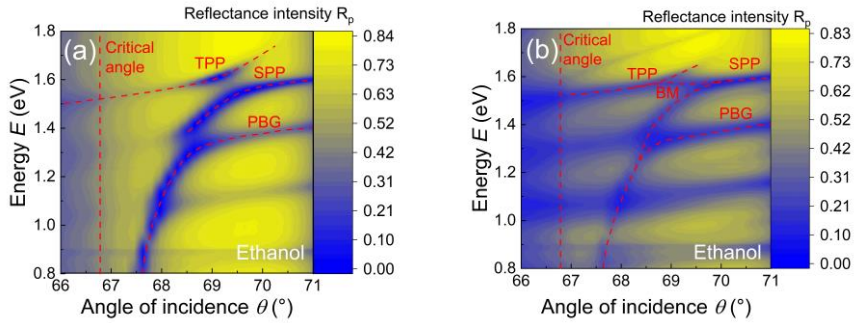

Figure 4.2.1. Reflectance intensity of p-polarized light plotted as a function of energy vs. incident angle: a – for uniform gold layer, b – for lattice array of gold nano-bumps.

between the Tamm plasmons and the surface plasmon exhibits at 1.4-1.6 eV in the energy spectrum. For the hybrid TPP-SPP modes, the SPP component becomes narrower due to the anti-crossing Fig. 4.2.1 a and lies in the 1.45-1.55 eV energy range for the AOI θ = 69-71°. It has been shown that this narrowing of resonances is related with decreased losses of surface plasmonic resonances in the metal layer [156]. In other words, the SPP component is "pushed" more away from the metal layer to the dielectric, compared with the single surface plasmon resonance wave. The lower split of the SPP mode (Fig. 4.2.1. a) was observed at the energies of about 1.3 eV, which corresponds to the coupling of PBG edge with dispersion line of SPP. However, this coupling was weaker than the upper polariton between TPP and SPP excitations.

Secondly, the TIRE spectra of ellipsometric parameters (θ = 66°-71°) were measured in the area modified by DLW method where lattice array of gold

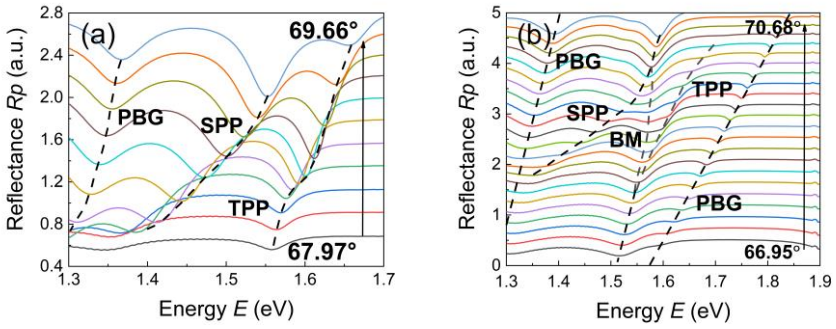

Figure 4.2.2. Reflected intensity as a function of the incident light energy for different angles of incidence for the (a) structure with uniform gold layer and (b) and with lattice array of gold nano-bumps.

nano-bumps was fabricated. From the optical dispersion map the upper anti-crossing Fig. 4.2.1 b effect remains at the same energies as for uniform layer (1.45-1.6 eV) however, additional dispersion line between TPP and SPP components appears around 1.57 eV which is associated with light diffracted parallel to the grating surface [154]. The Tamm plasmon dispersion line in the vicinity of strong coupling splits in to two: one is coupled with SPP component and creates a hybrid plasmonic mode and the other propagate through the energy gap of strong coupling (Fig. 4.2.1 b). In fact, the introduction of surface lattice array of gold nano-bumps generates Bragg reflections along the inside interface of 1D PC and gold. The inspection of dispersion lines of the hybrid TPP-SPP mode clearly showed that both components had the same dispersion lines shape compared with sample area without gold nano-bumps (except Bragg mode), what implies that strong

coupling regime still exist in the structures with array of nano-bumps lattice (Fig. 4.2.2 a, b).

The dependence on angle can be seen more clearly by energy spectra vs reflection intensity (Fig. 4.2.2) than on the dispersion maps in the Fig. 4.2.1. For both areas, the spectra exhibit two dips related with TPP and SPP components whose are angle dependent. For the area with uniform gold layer both components of hybrid mode blue shifted with increasing AOI (Fig. 4.2.2 a). The same behavior was registered for the area with lattice array, however, the dispersion line of the uncoupled Bragg mode slightly red shifted for the higher AOI (Fig. 4.2.2 b). The optical dispersion of the new Bragg mode was related with multiple reflections from the surface lattice array of gold nano-bumps. It is reasonable to assume that generation of Tamm optical state at the 1D PC and gold interface occurs when wave propagates back and forth and simultaneously generates multiple reflections (Bragg mode) which phase is determined by the lattice period. However, due to interference effect from the gold lattice such Bragg mode have distinct energy and thus differs from the Tamm optical state. Such Bragg mode along the interface do not satisfy the condition of coupling in the wave-vectors range 11.2 to 11.4 μm^{-1} (Fig. 4.2.3 b). In other words, some part of incident photons of light are not involved in the strong coupling. It was shown that on the surface lattice arrays the enhancement of the electric field strength occurs in the vicinity of the metallic nanoparticle, a so called “hot spots” [68]. In TIR configuration, the surface lattice array also works as a hot spot which leads to higher electric field intensity at the interface than compared with separated metal particles for surface lattice resonances excited from the grating side [68].

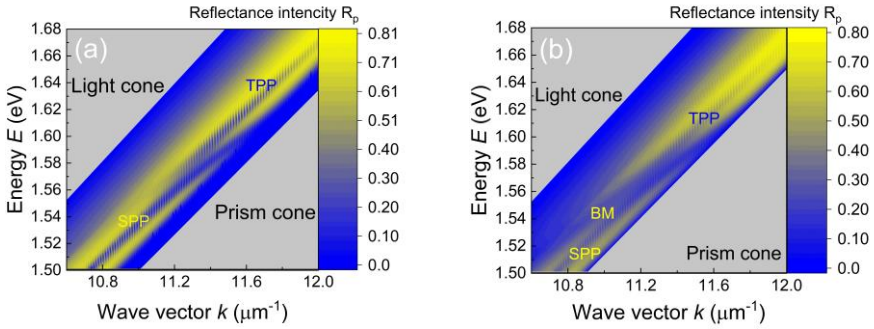

Figure 4.2.3. Reflectance plotted as a function of energy vs in-plane wavevector. The dispersion maps for the uniform gold layer (a) and lattice array of gold nano-bumps (b) areas determine the broadening of the energy and wave vector.

Meanwhile in this case the localized mode with properties of Bragg reflections formed at the outer interface around the gold nano-bumps and ethanol. The light-matter hybrid modes in strong coupling regime distinguished the extended spatial coherence [157] due to their polaritonic nature. Usually the interferometric experiments are performed for direct evidence of existence of the spatial coherence in nanostructures supported hybrid light-matter modes [160,162]. In this case the dispersion maps (Fig. 4.2.3 a, b) for the uniform and lattice areas determine the broadening of the energy and wave vector, which in turn indicates degree of localization of the mode components (TPP and SPP). The uncertainty of wave vector corresponds to higher localization of excited state, this was widely demonstrated for various exciton polaritons [157]. In this study two plasmonic resonances which itself are polaritons and when strong coupling regime is achieved between them, they form new hybrid polaritonic mode. The polaritonic states distinguished high degree of spatial coherence if damping is rather small. To study the polaritonic TPP-SPP mode the uncertainty of wave vector Δk were analysed. The figure 4.2.4 a and b clearly show the evolution of Δk in the vicinity of strong coupling for TPP and SPP components in the uniform layer and lattice of gold nano bumps. The SPP component for lattice $\Delta k_{\text{SPPlattice}}$ had the lowest values of the full width at half minimum (FWHM) from 0.04-0.06 eV meanwhile the SPP component for the uniform layer Δk_{SPP} have slightly wide dispersion line 0.525-0.0725 eV. These differences in Δk cannot be explained without analysis of TPP components for both uniform

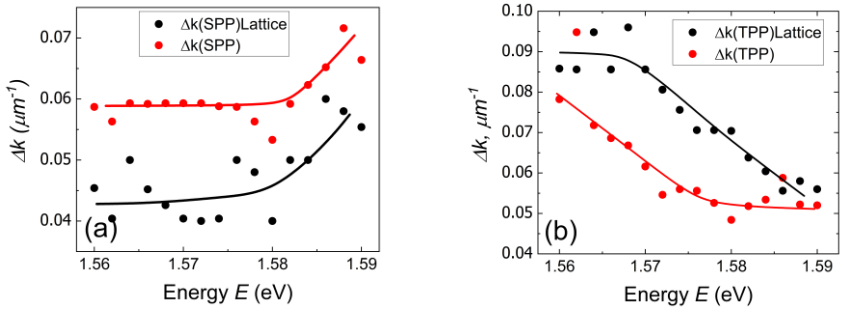

Figure 4.2.4. The evolution of Δk in the vicinity of strong coupling for SPP (a) (red circles – uniform layer; black circles – lattice array) and TPP (b) (red circles – uniform layer; black circles – lattice array) components in the uniform gold layer and lattice array of gold nano bumps. The Δk was evaluated from the dispersion map (Fig. 4.2.3) at FWHM as a function of wavevector vs. energy. The solid black and red lines represent fit to eye curves to represent the evolution of the Δk at the FWHM.

layer and lattice (Fig. 4.2.4 b). In the vicinity of strong coupling registered uncertainty of wavevector for gold lattice was highest and reaches $\Delta k_{\text{TPPlattice}} \approx$ 0.09 eV at 1.564-1.567 eV and monotonically decreasing moving away from zero detuning point. The same trend was observed for the TPP component for the uniform layer however the broadband of Δk_{TPP} values was lower than for $\Delta k_{\text{TPPlattice}}$. The width of Δk in general related with losses in the system and represents the imaginary part of the wave vector.

The evolution of the Δk uncertainties gives information about propagation length δ of the hybrid plasmonic modes $\delta = 1/2\Delta k$, where $\Delta k = k''$, k''-imaginary part of the wave vector. The figure 4.2.5 shows the propagation length δ, the distance over which the intensity of the surface electromagnetic wave decreases to 1/e value from it's initial. The investigation of propagation properties have shown that presence of gold nano-bumps lattice changes the propagation length δ for TPP and SPP compared with the uniform gold layer. For the nanostructures with uniform gold layer the evaluated propagation length was in between $\delta_{\text{SPP}} \approx$ 5.5-6.5 μm and $\delta_{\text{TPP}} \approx$ 6.5-9.5 μm for SPP and TPP component in hybrid polaritonic mode, respectively. Meanwhile the changes induced by periodic gold lattice gives higher values of propagation length for SPP component $\delta_{\text{SPPlattice}} \approx$ 7-10.5 μm and decreasing length for TPP $\delta_{\text{TPPlattice}} \approx$ 5.5-8.5 μm. The obtained values of propagation length clearly indicate that for lattice $\text{SPP}_{\text{lattice}}$ component had longer propagation length than for uniform gold layer (Fig. 4.2.5 a), meanwhile for the TPP component on the lattice $\delta_{\text{TPPlattice}}$ was shorter than for uniform layer (Fig. 4.2.5 b). This fact

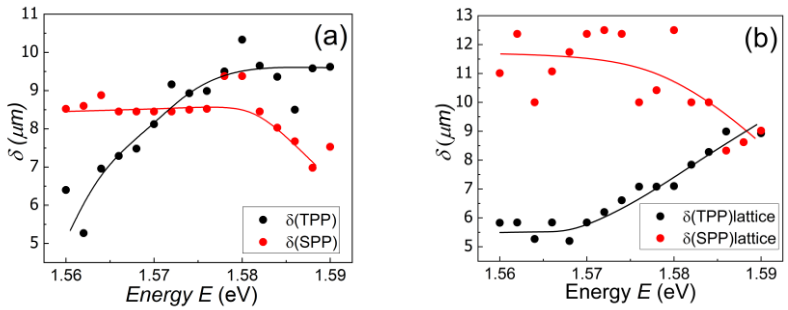

Figure 4.2.5. The propagation length δ, the distance over which the intensity of the surface electromagnetic wave decreases to 1/e value from it's initial. (a) black circles - δ_{TPP}, red circles - δ_{SPP}; (b) black circles – $\delta_{\text{TPP(lattice)}}$, red circles - $\delta_{\text{SPP(lattice)}}$. The solid black and red lines represent fit to eye curves to represent the changes of the propagation length for TPP and SPP components for both areas.

confirms the assumption that part of the wave vector of TPP is lost due to the presence of lattice and Δk is increased. However, this part of energy possibly involved in the $SPP_{lattice}$ component, which $\delta_{SPPlattice}$ increased compared with δ_{SPP} on the uniform layer. The propagation length δ is closely related with coherence properties of the excited states[157], [158] thus it is reasonable to assume that increasing of propagation length leads to extended coherence related with periodic surface lattices.

Moreover, it should be noted that wider full width at half maximum was registered for the SPP excitation in the hybrid mode with uniform gold layer $\delta\lambda_{FWHM(SPP)}$ = 100.78 nm. As a result, the Q-factor in experimental hybrid (uniform film) structure was Q_{SPP}=12.4. Meanwhile, for the hybrid mode with lattice of nano-bumps FWHM was $\delta\lambda_{FWHM(HSPP)}$ = 13.48 nm. The Q-factor in experimental hybrid polaritonic mode for HSPP component was Q_{HSPP}=58.6. As can be seen, the Q-factor was better for the hybrid structure with lattice of gold nano-bumps. This indicates lower losses and confirm longer propagation length for the SPP component in hybrid mode on gold lattice and as a result, changes in coherence properties of such polaritonic mode.

In order to analyse the changes in strong coupling due to presence of the lattice array of gold nano-bumps the coupling strength of uniform gold layer and modified with lattice array were compared taking into account the localized in-plane Bragg mode for modified area. The strong coupling between the TPP and SPP leads to the alteration of their initial frequencies and two plasmonic branches form the gap in frequency spectra called the vacuum Rabi splitting. For plasmonic and photonic nanostructures strong coupling defined as the gap between two resonances which exceeds their linewidths. However, in most cases the essential signature of the strong coupling regime is the experimental observation of Rabi splitting [6]. The distort dispersion and magnitude of the coupling splitting's for the uniform gold layer were modelled by two coupled oscillators: the TPP and SPP. In the model, the dispersions were described by two Lorentz oscillators which influence each other with equal strengths [66]. The splitting frequencies of two coupled harmonic oscillators can be written as

$$\omega_{\pm} = \frac{\sqrt{\omega_{TPP}^2+\omega_{SPP}^2 \pm \sqrt{4g^2+\left(\omega_{TPP}^2-\omega_{SPP}^2\right)^2}}}{\sqrt{2}}, \tag{4.3}$$

where $\omega_{\pm}$ - corresponding resonance frequencies of TPP and SPP resonances, and g- coupling strength. The free Bragg mode frequency ω_{Br} is not involved in the strong coupling, thus it is excluded out of the equation. The ω where

treated as the function of the angle of the incidence $\omega_j=\omega_j(\theta)$. For characterization of the strong coupling regime, we fit separately two pairs of the two coupled oscillator's mode model for TPP-SPP and SPP-PBG edge for the uniform gold layer. It was assumed that these two couples of hybrid modes (TPP-SPP and SPP-PBG) do not interact with each other. Evaluated dispersion lines fit reasonably well with experimental dispersion curves and has splitting of about 13 ± 1 meV for TPP-SPP and 9 ± 1 meV for SPP-PBG, respectively (Fig. 4.2.3 a).

The presence of lattice array from gold nano-bumps generates new Bragg mode in between the strong coupling of TPP-SPP hybrid mode. The contribution of Bragg mode to the optical dispersion was modelled by three Lorentz oscillator model where one oscillator (corresponds to Bragg mode) does not couple with other two and the obtained dispersion curves gives reasonably good fit. However, the Rabi splitting between TPP and SPP slightly decreased to 9 ± 1 meV, indicating weakening of the strong coupling (Fig. 4.1.4 b). Moreover, from the dispersions in the figure 4.2.2. a, b clearly seen that additional Bragg mode appears at the slightly lower energies $E \approx$ 1.51-1.56 eV and wave-vectors values $k \approx$ 10.2-10.9 μm^{-1} than TPP component which involved in the strong coupling. The figure 4.2.3 a determine the strong coupling in the uniform gold layer, meanwhile additional dispersion line at the lower energies and *k* values fig. 4.2.3 b corresponds for Bragg mode on the lattice of gold nano-bumps. This fact validates the application of three oscillator model with one non-coupled oscillator for additional Bragg mode. The coefficient of determination (COD) for the fitting experimental dispersion curves varied from 0.98475 to 0.99782.

4.2.1.1. Surface Lattice Resonances Strong Coupling with R6G Dye Organic Molecules

The delocalized nature of surface lattice plasmonic resonances and it's variations of the gold nano-bumps arrays pave the way for extended polaritonic states based on surface lattice resonances strongly coupled with organic molecules. Such polaritonic states are characterize by strongly delocalized (extended nature), longer propagation lengths and better coherence properties. In this section studies involving strong coupling between surface lattice plasmonic resonances, LSP resonances on single nano-bumps and absorption lines of organic R6G dye molecules are presented. The optical dispersion of pure silver lattice array and with PMMA/R6G layer on the top was measured by SE in p-polarized reflection intensity (Fig. 4.2.6). From the intensity maps is clearly seen the splitting of surface localized

plasmon dispersion line due to two absorption lines of the R6G dye at the 486 nm and 532 nm.

To investigate coupling influence between surface lattice plasmonic resonances and R6G exciton dye molecules angle resolved transmission map was recorded for gold nanobumps array (Fig. 4.2.7), the sample was measured in two position 0° and then rotated 180°. Incident light can couple via diffraction to the surface lattice plasmonic mode where the different scattered SPP modes across the gap is formed due to anti-crossing. Where counter propagating SPP modes are linked to a first-order scattering process the gap is more clearly seen. So, as have been shown before in Kretschmann configuration, the grating also can induce band gaps in the dispersion of plasmonic resonances. This effect leads to increasing the local density of optical states and thus can increase the light-matter interactions between plasmons and organic molecules excitons. Strong coupling between surface lattice plasmonic resonances and R6G can be clearly seen at around 590 nm. Figure 4.2.7 presents measured and modelled transmission spectra of silver nano-bumps lattice array with R6G/PMMA 20 nm thickness layer on the top.

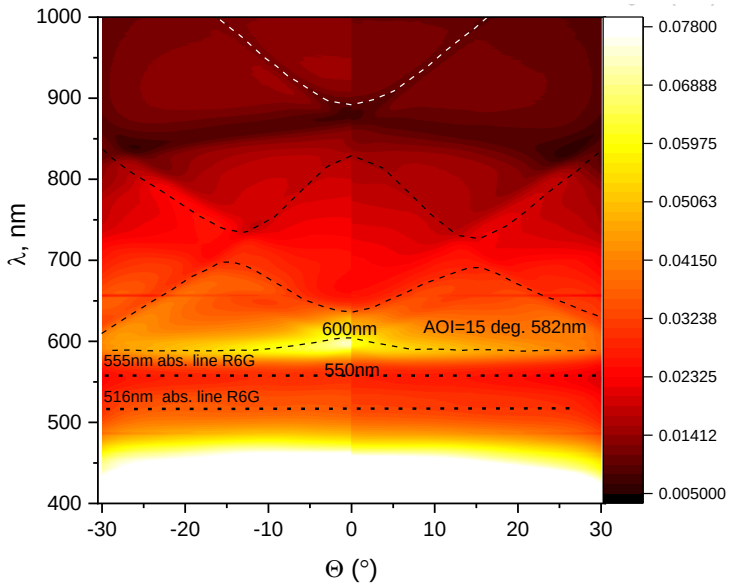

Figure 4.2.6. Surface lattice plasmonic resonance dispersion curve for propagating on the surface of metallic nano-bumps lattice array.

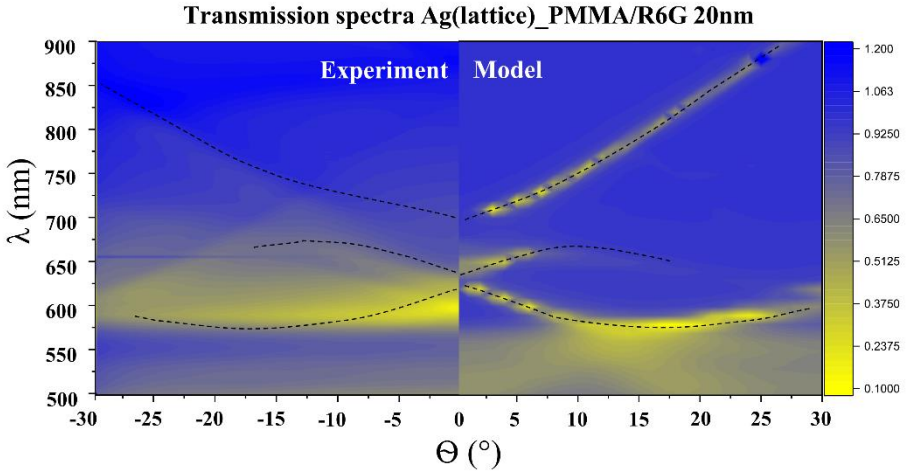

Figure 4.2.7. Measured and modelled transmission spectra of 50 nm silver lattice and 20 nm PMMA/R6G dye organic molecules layer.

Surface lattice plasmonic strong coupling regime with emitter combines long coherence lengths and times (high Q-factor) with local high field intensities on LSP (small mode volumes). The spatial coherence lengths in strongly coupled system are observed even in very excitonic like (matterlike) modes due to long-range extended surface lattice resonances [6].

4.2.2.Summary

The TIRE method was used for the excitation and study of strong coupling between TPP and SPP in nanophotonic structures with 1D PC and lattice of gold nano-bumps on the top. Recent studies have shown that lattice of gold nano-bumps induced the generation of additional Bragg mode related with lattice period which do not involve in the strong coupling of hybrid TPP-SPP polaritonic mode. Despite of this, the changes of propagation length of the TPP and SPP components due to surface lattice were identified. The detail analysis of the uncertainty in the wave-vector Δk has shown that propagation length of SPP on the lattice increased, meanwhile for the TPP component decreased compared with the hybrid plasmonic mode on the uniform gold layer.

The DLW method proved as a suitable optical technique to fabricate plasmonic array lattices with the quality of plasmonic resonances comparable with lithography methods in the VIS-NIR range. Such nanophotonic-plasmonic structures supported extended coherent polaritonic mode in the strong coupling regime gives possibilities to develop more efficient nano-

sources of coherent emission based on plasmonic and coherence properties of such nano systems plays the crucial role. The obtained results demonstrate the potential of DLW method for creating nanophotonic-plasmonic structures with designed properties, in this case changing the propagation length between TPP and SPP components in the hybrid plasmonic mode. The application of surface lattice resonances together with strong coupling regime leads to decreasing losses, resulting in the increasing propagation length and better coherence properties of such plasmonic excitations which in turn promise advanced properties for plasmonic based coherent emission nano sources.

4.3. High Spectral Sensitivity of Strongly Coupled Hybrid Tamm-Plasmonic Resonances for Biosensing Application

Experimental results of hybrid SPP-TPP polaritonic modes presented in this chapter demonstrated an increased sensitivity to refractive index changes. Such approach is used for optical sensors technologies in bio- and gas sensing. Optical bio and gas sensors have advantages as they are non-destructive, real-time and can detect nano objects through the refractive index changes at the sensor interface. More than three decades ago, surface plasmon resonance was successfully applied for optical biosensors studying protein interaction [159]. Later various structures based on plasmonic effects were studied for different possible applications, such as label-free single molecule and optical sensing [163,164], perfect absorbers [162], fast switching [163], as well as novel plasmonic lasing [164] in room temperature. These applications of various plasmonic resonances under certain conditions could be achieved in structures such as metallic nanoparticles [165], thin metal layers [97], or metallic nanostructures [17]. One of the excitations that has been widely used for biosensing applications is the propagating surface plasmon resonance, generated on the thin metal layer (up to 50 nm). The SPR has greater wave-vector than a photon in the free space for the same frequency due to the wave-vector matching optical elements, such as prism or grating [97]. The Kretschmann (prism) configuration is one of the most popular, p-polarized light incidents to a glass prism, which is then reflected from the thin metal layer deposited on the prism base. The surface plasmon polariton wave is excited at the outer side of the metal film for a specific wavelength and AOI. The SPR resonance manifested themselves as dips in the reflection spectra. The LSP are the oscillations of free electrons on the metallic nanoparticles. The resonance frequency of LSP depends on size, shape, and local dielectric function of the media. Such plasmonic resonances mostly occur from visible to near infrared (VIS-NIR) region and do not require wave vector matching couplers (prism, grating, or waveguide) or periodic photonic structures (Bragg reflector). However, LSPR usually has a wider width of the resonances than SPR, which indicates lower losses of the latter.

Another plasmonic excitation generated in a 1D PC structure with a thin metal layer on top is the TPP, which were applied for narrow band tunable filters [166] and biosensors [70,170]. The TPPs are non-propagating optical states that exist at the metal and PC boundary. The confined optical state of TPP in the metal is formed due to the negative dielectric permittivity of the metal that is the same as the SPP; meanwhile, the electric field confinement in the periodic structure of the Bragg mirror is achieved because of the

photonic stop band of the 1D PC. One of the main features of TPP is its in-plane wave-vector, which is smaller than the wave vector of light in a vacuum; thus, the TPPs can be directly excited with incident light without a prism coupler, contrary to the SPPs, which have a wave vector larger than the one of the incident light [48]. However, the plasmonic excitations, such as SPPs or randomly distributed nanoparticles have high energy losses due to metal. In order to minimize the energy losses or in cases when metal surfaces cannot be used, the periodic dielectric structures of Bragg reflectors can be used in TIR configuration for excitation of Bloch surface waves (BSW). The optical dispersion of these surface waves are below the light cone which is similar to the SPP. Thus, BSW share some of the optical features [168] as the SPP, and therefore they are used widely for optical biosensing in TIR configuration as SPR biosensors [169,170]. It has been shown that spectral sensitivity of the BSW biosensors is lower than SPR; however, due to lower losses in periodic dielectric structures the angular sensitivity of reflected polarized intensity or ellipsometric parameters was better than for SPR [169]. Moreover, the energy density of the BSW in dielectric periodic structures were theoretically modelled by applying the zero-admittance approach [171] and further changes in the spatial profile of the reflected laser beam intensity were experimentally measured [172]. The sensitivity of $\Delta n \approx 10^{-5}$ for refractive index measurements was achieved, which is typical for commercially available SPR devices. Recently, it has been shown that using various metallic nanostructures (grating arrays) arranged in a periodic manner allows us to minimize losses in the metals. As a result, such metallic arrays compared with randomly distributed nanoparticles or SPPs exhibit narrow plasmonic resonances [173] with an increased Q. As it was demonstrated in the previous section, the surface lattice arrays influence the strongly coupled hybrid Tamm surface plasmon polaritons mode‘s propagation length [174]. The decreasing losses were also achieved in hybrid TPP modes due to strong coupling between them [66]. By achieving the conditions needed for both plasmonic excitations, a new state of hybrid TPP-SPP mode appears [67]. These hybrid TPP-SPP modes can be realized in structures consisting of PC with a thin metal layer on the top by optically connecting a glass prism to the PC. The light-matter interaction in such structures can lead to strong coupling between the TPP and SPP components in the hybrid mode and the components become inextricably linked with each other [6,12]. If the strong coupling regime is achieved, the energy exchange between the TPP and SPP modes occur during a coherent time that is about tens of fs.

As mentioned above, narrow plasmonic resonances with lower energy losses have been demonstrated on periodically arranged metallic

nanostructure arrays [175]. The current lithography and DLW [76] methods enable the production of complex nanostructures supporting multiple plasmonic modes, which can be analyzed as the interaction of elementary plasmons supported by the nanostructures. The most popular nanostructures of complex plasmonic systems used are the arrays of metallic nanoparticles with a period that is by size comparable with the wavelength of the incident light [68]. Such nanostructures exhibit a hybridization effect of the plasmonic resonances where different LSPs of the nanoparticles interact with each other [176]. The damping of the localized plasmon resonance is compensated by the scattered field of light [17] in the individual particles; as a result, this led to a significant narrowing of the plasmonic resonance. For surface plasmon resonance biosensors the Kretschmann configuration with glass prism was applied for most cases [64,164,181]. The attempts to increase the sensitivity of the SPR sensors led to employing the phase measurements by using ellipsometry [117], where the amplitude (Ψ) and phase (Δ) of ellipsometric parameters for light reflected from the sample can be obtained. The ratio of reflected *p*- and *s*- polarization amplitudes gives ellipsometric parameter Ψ, meanwhile the difference between them is the phase shift Δ. The combination of an ellipsometric optical scheme with a glass prism gives ellipsometric measurements under a TIR [178]. Such TIRE gives more sensitive phase measurements, and ellipsometric parameter Ψ for SPR resonance has a narrower FWHM width compared with conventional intensity measurements, which also give better sensitivity characteristics. It was shown that an abrupt phase jump occurs at the plasmonic resonances when reflection intensity drops to zero (or so-called topological darkness); however, it is difficult to achieve it experimentally due to the surface roughness and other non-idealities of the sample [160]. TIRE method was also widely tested for the study of protein interactions [179,180].

In this study, the sensitivity to the refractive index changes of the ambient was studied on the uniform gold film with 1D PC with periodic five TiO_2/SiO_2 bilayers and gold nano-bumps array produced by DLW on the same sample. The optical signal sensitivity of hybrid plasmonic resonances was compared with traditional surface plasmon resonance (SPR) on a single gold layer. The influence of the strong coupling regime between Tamm and propagated plasmon polaritons in the hybrid plasmonic modes on the sensitivity of the optical sensors was discussed. In addition, the contribution of gold nano-bumps to the Q-factor of plasmonic resonances was estimated.

The results presented in the following Chapter were originally published in: J. Anulytė, E. Bužavaitė-Vertelienė, E. Stankevičius, K. Vilkevičius and Z. Balevičius. “High Spectral Sensitivity of Strongly Coupled Hybrid Tamm-Plasmonic Resonances for Biosensing Application” *Sensors* **22**, 2022, 9453. https://doi.org/10.3390/s22239453.

Author Contributions: Conceptualization, Z. Balevičius and J. Anulytė; methodology, J. Anulytė, E. Stankevičius, K. Vilkevičius, E. Bužavaitė-Vertelienė; formal analysis, J. Anulytė, Z. Balevičius; investigation, J. Anulytė, E. Bužavaitė-Vertelienė, E. Stankevičius, K. Vilkevičius, Z. Balevičius; writing—original draft preparation, J. Anulytė, Z. Balevičius; All authors have read and agreed to the published version of the manuscript.

4.3.1. Experimental Measurements

The TIRE method was used for the analysis of the optical properties and sensitivity features of the TPP-SPP hybrid modes. In this research two different areas of a sample were investigated: one with PC and a uniform gold layer and another with PC and nano-bumps array produced by DLW Fig. 4.3.1. The TIRE spectra of ellipsometric parameters Ψ and Δ were measured on the sample with non-modified thin metal film and maps of these parameters are presented as wavelength dependence on the AOI (θ = 64–72°). Figure 4.3.2 shows the hybrid TPP-SPP mode excitation generated on 1D PC and uniform thin gold film on the top when ambient was deionized water and ethanol. As can be seen from the dispersion maps λ(θ) of ellipsometric parameters Ψ and Δ, the strong coupling effect between the Tamm plasmon and the surface plasmon at the zero detuning point excited at 784 nm and 820

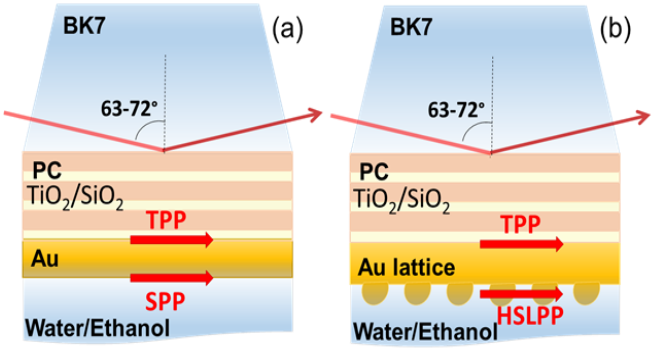

Figure 4.3.1. Scheme of excitation configurations of the PC(TiO_2/SiO_2)/Au structures for excitation of TPP-SPP (a) and TPP-HSLPP (b) modes in TIR configuration of spectroscopic ellipsometry.

nm in water, and 770 nm and 804 nm in ethanol, respectively. For the hybrid TPP-SPP modes, the SPP component of ellipsometric parameter Ψ becomes narrower due to the anti-crossing which lies in the λ = 780–800 nm spectral range for the AOI θ = 67–69°. It has been shown that this narrowing of resonance is related to decreased losses of the hybrid plasmonic modes and strong coupling between Tamm and the propagated SPP, described reasonably well by the simple two coupled oscillators model [66]. The maps of the ellipsometric parameter Δ show sharper dispersion lines of the resonances (Figure 4.3.2 b,d). The hybrid plasmonic excitation of the TPP and SPP at a fixed AOI (θ = 67.6°) (Figure 4.3.4 a) was λ_{TPP} = 783 nm and λ_{SPP} = 843 nm for the deionized water and was λ_{TPP} = 801 nm and λ_{SPP} = 1401 nm for the ethanol at the same AOI. The shifts were $\delta\lambda_{TPP}$ = 18 nm and $\delta\lambda_{SPP}$ = 558 nm in the different ambient. The spectral shift of TPP and SPP resonances was caused by the refractive index change of the ambient $\delta n_{(\lambda=783nm)}$ = 1.3495 – 1.3286 = 0.0209 and $\delta n_{(\lambda=843nm)}$ = 1.3486 – 1.3276 = 0.021, respectively. The refractive index values for deionized water and ethanol were taken for CompleteEase ellipsometric software database [116]. Spectral shift of these resonances gave the corresponding sensitivities to the refractive index unit (RIU) $\delta\lambda_{TPP}/\delta n$ = 18.2/0.0209 ≈ 871nm/RIU and $\delta\lambda_{SPP}/\delta n$ = 559.7/0.021≈ 26 600 nm/RIU. It should be noted that the sensitivity of the conventional SPR sensor with a single thin (~50 nm) gold layer on the glass prism base to refractive index of the ambient was about 19,000 nm/RIU when the ambient was changed from deionized water to ethanol (the results not shown). This number is higher than earlier reported for wavelength investigation (13 800 nm/RIU) [97].

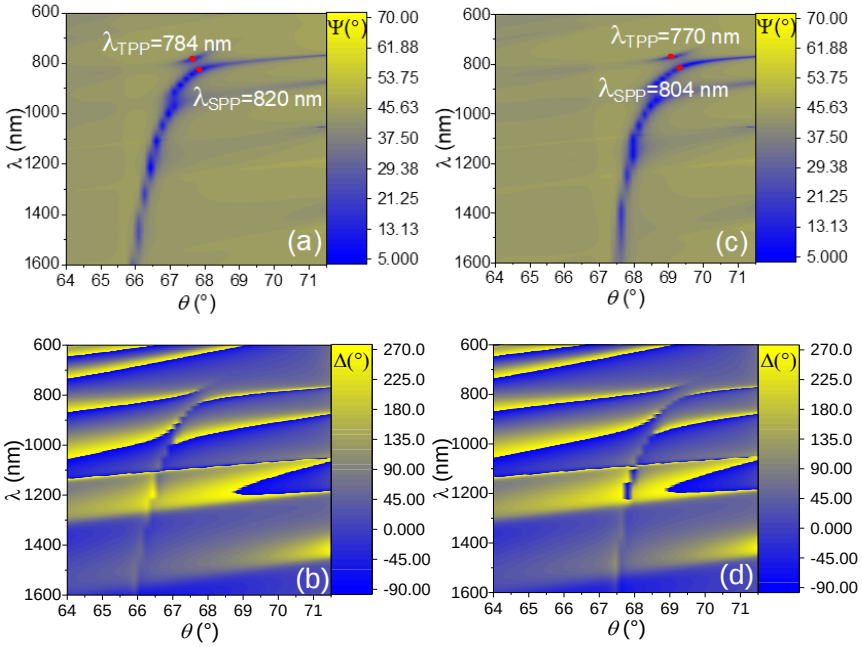

Figure 4.3.2. The dispersion maps λ (θ) of ellipsometric parameters Ψ(°) (a and c) and Δ(°) (b,d) for structure PC (TiO_2/SiO_2 (110nm/200nm)/Au (50nm) in water (left side) and in ethanol (right side). The red points show the strong coupling effect between the Tamm plasmons and the surface plasmon at zero detuning.

The TIRE spectra of ellipsometric parameters Ψ and Δ (θ = 64–72°) were also measured in the area with nano-bumps grating formed by the DLW method. As can be seen from Figure 4.3.3., the ellipsometric parameters Ψ and Δ optical dispersion maps λ(θ), the anti-crossing effect remains at the same energies as the uniform layer, however, an additional dispersion line appears between the TPP and SPP components (λ_{TPP} = 805 nm and λ_{SPP} = 813 nm in water, λ_{TPP} = 778 nm and λ_{SPP} = 798 nm in ethanol, for TPP and SPP, respectively) (Fig. 4.3.3 a,b). These optical dispersion features were related to the presence of a surface lattice array on the gold layer. In fact, the introduction of the surface lattice grating array generates a new hybrid plasmonic mode where the propagated SP from the ambient side are coupled with Bragg reflections on the nano-bumps and simultaneously coupled with Tamm plasmons from the 1D PC side. Compared to the surface lattice resonances excited from the grating side, the internal reflection configuration on the surface lattice array works as hot spots, leading to an increased electric

field intensity at the interface [68]. This periodic surface nanostructure generates a new type of hybrid plasmonic excitation related to propagated SP, localized plasmons and Bragg reflections from the surface grating array-PSLPR.

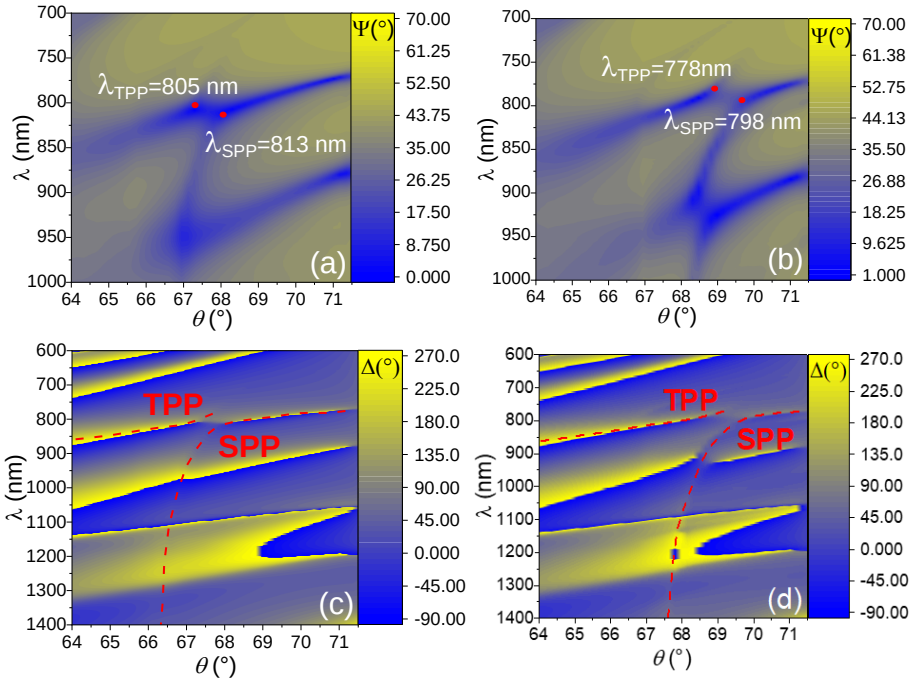

Figure 4.3.3. The dispersion maps $\lambda(\theta)$ of ellipsometric parameters $\Psi(°)$ (a,b) and $\Delta(°)$ (c,d) for structure PC (TiO_2/SiO_2 (110nm/200nm)/with gold nano-bumps (50nm) in water (left side) and in ethanol (right side). The red points show the strong coupling effect between the Tamm plasmons and the surface plasmon at zero detuning.

The same ellipsometric measurements were performed on the area with gold lattice. The TPP and HSLPP components of the hybrid plasmonic excitation was at fixed AOI (θ = 70.5°), where the components lies in λ_{TPP} = 667 nm and λ_{HSLPP} = 783 nm for the deionized water and at λ_{TPP} = 683 nm and λ_{HSLPP} = 787 nm for the ethanol at the same AOI (Fig. 4.3.4 c,d). The shifts were $\delta\lambda_{TPP}$ = 16 nm and $\delta\lambda_{HSLPP}$ = 4 nm in both ambients. For the TPP resonance, such spectral shift corresponds for refractive index change $\delta n_{(\lambda=667nm)}$ = 1.3512 – 1.331 = 0.0202 and for the HSLPP resonance shift corresponds for $\delta n_{(\lambda=783nm)}$ = 1.3494 – 1.3286 = 0.0208 refractive index change. Thus, this leads to the corresponding spectral sensitivity of these resonances

to refractive index unit $\delta\lambda_{TPP}/\delta n$ = 15.5/0.0202 = 767 nm/RIU and $\delta\lambda_{HSLPP}/\delta n$ =4.5/0.0208 = 215 nm/RIU.

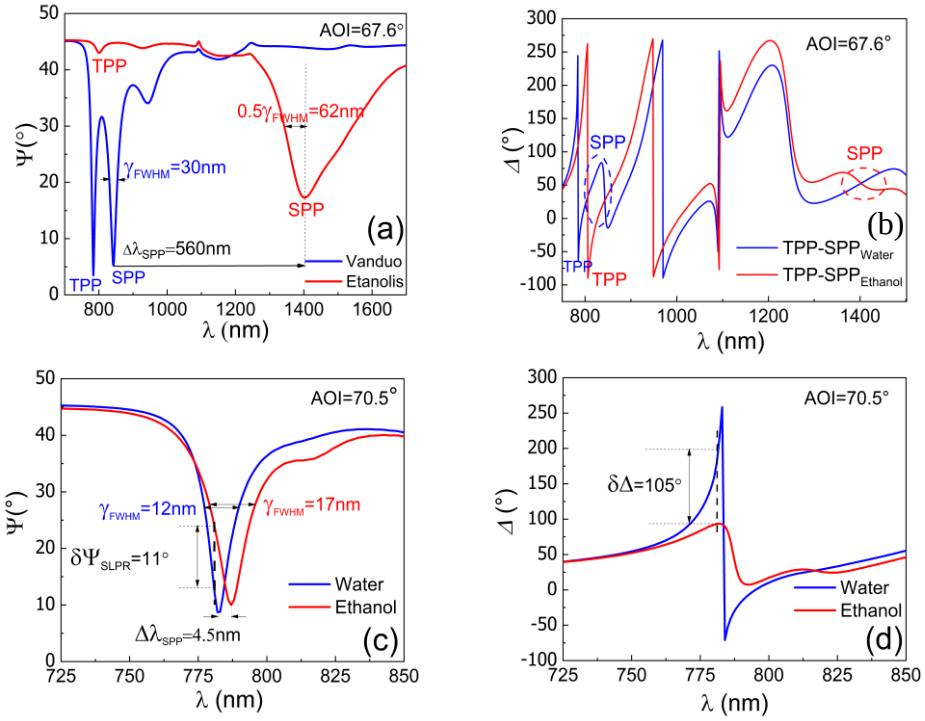

Figure 4.3.4. Spectra of ellipsometric parameters Ψ(λ) (a,c) and Δ(λ) (b,d) in both ambient materials, where blue curve corrsponds to water and the red curve to ethanol. The ellipsometric spectra for structure with thin gold layer (a,b), for structure with gold nano-bumps (c,d). The dashed areas (blue and red) in figure (b) show the ellipsometric parameter Δ at the SPP position and the wavelength shift due refractive index changes in different ambient.

It should be noted that a much wider full width at half maximum (FWHM) was registered for the SPP excitation in the hybrid mode with a uniform gold layer: in the deionized water $\delta\lambda_{FWHM(SPP)}$ = 29.6 nm and in ethanol $\delta\lambda_{FWHM(SPP)}$ = 124.5 nm. As a result, the Q-factor in the experimental hybrid (film) structure were Q_{SPP} = 28.4 in deionized water and Q_{SPP} = 11.3 in ethanol (Figure 4.3.4 c,d). For the hybrid mode with nano bumps array FWHM was registered: $\delta\lambda_{FWHM(HSLPP)}$ = 63.6 nm in the deionized water and $\delta\lambda_{FWHM(HSLPP)}$ = 46.3 nm in ethanol. The Q-factor in the experimental hybrid mode for the lattice SLPR: Q_{HSLPP} = 63.6 deionized water and Q_{HSLPP} = 46.3 in ethanol. As can be seen, the Q-factor was better for the hybrid structure with a lattice of

gold nano-bumps than on the uniform gold layer. It can be explained by the lower losses of such lattice mode in which Bragg reflection compensates the phase changes of SPP on the lattice. The presence of nano-bumps lattice on the gold surface significantly decreased optical signal sensitivity to the changes of the refractive index of the ambient compared with the uniform gold layer. However, at the same time, the Q-factor increased for the sample area with lattice, which indicates decreasing losses in the metal layer for such plasmonic modes. It should be noted that high Q-factors (~150) were achieved with surface lattice plasmonic resonances (SLR) generated on ordered gold nanoparticles also with prism coupler in the deep red spectral range [173]. Even higher Q-factors for SLR were demonstrated on indium tin oxide in the infrared region ($\lambda \sim 5$ μm) [181]. The better Q-factor for plasmonic resonances with gold nano-bumps lattice increases the sensitivity of ellipsometric parameters Ψ and Δ to the refractive index changes. The ellipsometric parameter Ψ changes about ~11° meanwhile Δ changes ~105° for $\delta n = 0.0205$, which gives sensitivity $S_\Psi \approx 537°/RIU$ and $S_\Delta \approx 5122°/RIU$.

4.3.2. Summary

The TIRE method in the Kretschmann configuration was used for the excitation of strong coupling between TPP and SPP in nanophotonic structures with 1D PC and gold layer on the top. The sensitivity properties of the uniform gold layer and modified area forming a lattice of gold nano-bumps by DLW were compared. Recent studies have shown very high hybrid plasmonic mode sensitivity $S_{HSPP} \approx 26{,}000$ nm/RIU to the refractive index on the uniform gold layer; meanwhile, the introduction of gold lattice decreases the spectral signal sensitivity but increases the Q-factor of the plasmonic resonances and also induces the generation of additional Bragg mode related to lattice period, which is not involved in the strong coupling of the hybrid TPP-SPP polaritonic mode. Despite this, the sensitivity to the ellipsometric parameters Ψ and Δ was rather high due to the increased Q-factor of the resonances. The comparison of plasmonic resonance sensitivity to the refractive index changes of hybrid TPP-SPP mode on the uniform gold layer and traditional surface plasmon resonance (SPR) have shown that hybrid plasmonic mode, due to the strong coupling effect, overcomes the SPR by about 27%. The involvement of the strong coupling effect in optical sensing development of plasmonic-based sensors opens new possibilities to the advanced detection of proteins interaction, for instance, a higher sensitivity of the signal, tuning of chemical reaction rates, more than one plasmonic mode monitoring in real-time, and others.

5. CONCLUSIONS

- This study employed TIRE to investigate the room temperature strong coupling between SPP and excitons within plasmonic-photonic nanostructures. The Rabi splitting, determined from the optical dispersion E(k) at the zero-detuning point, was measured to be 90 meV, the comparison of Rabi gap with the linewidths (γ) of the plasmonic and excitonic resonances, confirms the presence of strong coupling regime.
- FLIM has demonstrated that using polaritonic nanostructures where plasmons and excitons are in a strong coupling regime, reduces the fluorescence intensity by approximately 5%, meanwhile in weak coupling regime fluorescense intensity decreases by 25-30%. It was observed that the strong coupling between SPP and dye excitons plays a pivotal role in suppressing photobleaching (about 6 times), a phenomenon that often impedes fluorescence-based studies.
- The TIRE method was used for the excitation and study of strong coupling between TPP and SPP in nanophotonic structures with 1D PC and lattice of gold nano-bumps on the top. The detailed analysis of the uncertainty in the wave-vector Δk has shown that propagation length of SPP in the lattice increased by about 30%, meanwhile the TPP component decreased by $\approx$10% compared with the hybrid plasmonic mode on the uniform gold layer.
- Surface lattice arrays fabricated by DLW on metallic layer supports extended coherent polaritonic modes in strong coupling regime with suppressed losses and thus increases Q-factor. The obtained results demonstrate the potential of DLW method for creating nanophotonic-plasmonic structures with designed properties, for instance, changing the propagation length between TPP and SPP components in the hybrid plasmonic mode.
- Traditional Kretschmann configuration combined with the ellipsometric optical configuration was used for the excitation of strong coupling between TPP and SPP in nanophotonic structures with 1D PC and gold layer on the top. Recent studies have shown very high hybrid plasmonic mode sensitivity SHSPP$\approx$26000 nm/RIU to the refractive index on the uniform gold layer.
- The presence of gold nanolattice on plasmonic-nanophotonic structure increased the Q-factor of the hybrid plasmonic resonances. The sensitivity to the refractive index changes of ellipsometric parameters Ψ and Δ was rather high due to increased Q-factor (Q_{HSLPP}=63.6) of the resonances indicating decreased propagation losses.

- The comparison of hybrid TPP-SPP mode on the uniform gold layer and traditional SPR sensitivity to refractive index changes have shown that hybrid plasmonic mode overcomes the SPR by approximately 27% due to the strong coupling.

6. SANTRAUKA

ĮVADAS

Koherentinių energijos mainų išplėstinėse plazmoninėse būsenose supratimas atveria galimybes taikyti stipriosios sąveikos režimą fotocheminių reakcijų greičio modifikavimui [1], naujos kartos nanolazeriams [2], Bose-Einstein‘o kondensatui pasiskirstyti kambario temperatūroje pasiekti [3], kvantinių optinių nanoprietaisų [4] bei pažangių optinių jutiklių kūrime [5].

Pagrindinė stipriosios sąveikos režimo prielaida yra ta, kad du harmoniniai osciliatoriai tampa stipriai susieti, jei yra būdas, leidžiantis jiems keistis energija greičiau, nei įvyksta energijos nuostoliai [6]. Jei taip atsitinka, hibridinės sistemos energijos lygmenys skiriasi nuo nesąveikaujančio emiterio ir rezonansinės optinės modos. Tokiose susietose sistemose dviejų harmoninių osciliatorių sąveikos stipris viršija nuostolius, todėl sistemos nuosavoji būsena yra poliaritoninė moda [7]. Šios hibridinės būsenos suteikia galimybę tirti šviesos ir medžiagos sąveiką, bei panaudoti įvairius nanotechnologijų gamybos būdus kvantinių optinių prietaisų kūrime [5,8].

Paprastai spinduliavimo proceso greitį galima keisti patalpinant emiterį į struktūrizuotą aplinką (rezonatorių). Tradiciniuose lazeriuose plačiai naudojamas spontaninio spinduliavimo sustiprinimas (Purcell‘io efektas) [9], kuris yra silpnosios sąveikos atvejis, kai spinduliavimo dažnis išlieka nepakitęs. Tačiau jei sąveika yra pakankamai stipri, tuomet energijos lygmenys, lemiantys spinduliavimą pasikeičia. Jie tampa neatsiejamai susiję su lokalios optinės aplinkos modomis, o skirtumas tarp pradinių ir naujų energijų priklauso nuo sąveikos stiprumo. Dažnių išsiskyrimas ties pavienių modų susikirtimo tašku vadinamas nuosavųjų modų skilimu arba Rabi skilimu [10]. Stipriosios sąveikos režimas fotoninėse sistemose paprastai pasiekiamas, kai eksperimentiškai stebimas Rabi skilimas. Stipriosios sąveikos režimas rodo, kad pereinama į būsenas, kuriose pasireiškia geresnės spinduliuotės koherentiškumo savybės. Todėl jis glaudžiai susijęs su tokiais reiškiniais kaip priverstinis spinduliavimas, stiprinimas ir lazerinė spinduliuotė, (pavyzdžiui, lazerinė spinduliuotė be slenksčio).

Įprasto fotoninio rezonatoriaus modos tūris negali būti mažesnis nei difrakcijos riba, kuri riboja sąveikos stiprumą esant stipriosios sąveikos režimui. Tuo tarpu plazmonika leidžia pasiekti sub-banginius matmenis ir įveikti difrakcijos ribą, todėl modų tūrį galima sumažinti dar labiau nei fotoninės modos atveju. Dar vienas privalumas, kad plazmonika kartu su emiteriais suteikia galimybę naudoti vadinamąjį „atvirą rezonatorių“, t. y. leidžia lengvai pasiekti modų tūrį, kuriame emiteris sąveikauja su plazmonine

moda [6]. SPP yra kolektyvinis rezonansinis svyravimas, kurį sukelia laisvieji metalo elektronai, kai jie sąveikauja su krintančiu išoriniu elektromagnetiniu lauku [11]. SPP yra labiausiai koherentiniai kolektyviniai svyravimai žinomi gamtoje. Todėl tokie plazmoniniai sužadinimai potencialiai gali būti panaudoti priverstinio spinduliavimo generavimui [2].

Šios disertacijos tyrimai skirti išplėstinių plazmonų poliaritoninių būsenų esančių stipriosios sąveikos režime, koherentinių savybių tyrimams ir jų taikymui FLIM metode bei optinių jutiklių technologijose. Šiame darbe tiriama stipriosios sąveikos tarp SPP ir eksitonų įtaka fluorescencijos gyvavimo trukmei ir fotoblukimo efektui. Plazmoninė-fotoninė struktūra, sudaryta iš plonų sidabro (Ag) ir aukso (Au) sluoksnių su R6G dažo sluoksniu, parodė plazmonų rezonanso ir R6G sugerties linijų poslinkį ir priklausomybę nuo krintančios šviesos kritimo kampo. Tai yra indikacija, kad sistema yra stipriojoje sąveikoje, o išmatuotas Rabi tarpas yra maždaug 90 meV. Pirmą kartą fluorescencijos gyvavimo trukmės vaizdinimo mikroskopija buvo panaudota siekiant įvertinti fotoblukimo slopinimą ir parodė, kad plazmoninėse-eksitoninėse struktūrose stipriosios sąveikos režime fotoblukimo efektas, lyginant su pavieniais R6G sluoksniais, ženkliai sumažėja. (4.1 skyrius).

Kitoje šios disertacijos dalyje tiriamos struktūros su aukso nanogumbų gardelių matricomis, kuriose paviršiaus gardelės plazmonų rezonansas yra stipriojoje sąveikoje su kitais plazmoniniais sužadinimais bei organinių dažų eksitonais. TIRE metodas buvo naudojamas stipriosios sąveikos tarp TPP ir SPP tyrimui nanofotoninėse struktūrose, suformuotose iš 1D PC ir aukso nanogumbų gardelės. Išplitusių plazmoninių poliaritoninių būsenų su ištisiniu aukso sluoksniu ir aukso nanogumbų gardelių masyvo optinės dispersijos ir sklidimo ypatumai analizuoti taikant dviejų susietų osciliatorių modelį bei bangos vektoriaus išplitimo priklausomybę nuo energijos (4.2 skyrius).

Skyriuje 4.3. pristatomi stipriosios sąveikos režimo tarp Tamm‘o (TPP) ir sklindančių plazmonų poliaritonų, hibridinėse plazmoninėse būsenose, įtakos modų jautrumo aplinkos lūžio rodiklio pokyčiams tyrimai. TIRE metodas buvo naudojamas struktūrų su ištisiniu aukso sluoksniu bei su aukso nanogumbų gardele, suformuota naudojant tiesioginio lazerio įrašymo metodą, optiniam atsakui ištirti. Hibridinių plazmoninių rezonansų optinio signalo jautrumas buvo lyginamas su tradiciniu SPR ant ištisinio aukso sluoksnio.

TIKSLAI

- Ištirti stipriosios sąveikos režimą tarp SPP ir eksitonų hibridinėje plazmono-eksitono poliaritono struktūroje, pagrindinį dėmesį skiriant energijos lygmenų ir optinės dispersijos pokyčiams.
- Ištirti stipriosios sąveikos režimo įtaką fotoblukimo slopinimui fluorescencinėse molekulėse (R6G dažai), pritaikant paviršiaus plazmonų-eksitonų poliaritonus FLIM metodui.
- Ištirti paviršinių gardelių matricų poveikį Tamm‘o plazmonų ir paviršiaus plazmonų poliaritonų sąveikai bei jų įtaką sklidimo ilgiui, Q-factoriui ir koherentiškumo savybėms.
- Išanalizuoti hibridinių TPP-SPP modų optinės dispersijos savybes ir jautrumą lūžio rodiklio pokyčiams, lyginant ištisinius aukso sluoksnius su nanogumbų gardelių struktūromis.

Uždaviniai tikslams pasiekti

- Išmatuoti elipsometrinių parametrų (Ψ ir Δ) TIRE spektrus, įvertinti hibridinio eksitono-SPP sužadinimo spektrines savybes ir palyginti jų optinį atsaką su pavieniu SPP ir struktūrą su SPP bei dažų eksitonais. Nustatyti poslinkius atspindžio intensyvumo žemėlapiuose.
- Naudojant FLIM metodą įvertinti fotoblukimo efektą fluorescencijos gyvavimo trukmei, stipriojoje bei silpnojoje sąveikoje esančiose struktūrose. Nustatyti fotoblukimo slopinimo pokytį, esant stipriajai sąveikai tarp SPP ir R6G dažo eksitonų.
- Kiekybiškai įvertinti Rabi tarpo ir stipriosios sąveikos stiprumą modeliuojant ir tinkinant viršutinių ir apatinių poliaritonų šakų dispersijos kreives. Palyginti sistemos ryšio stiprumą (g) su slopinimu (γ), stipriosios sąveikos režimui patvirtinti.
- Atlikti elipsometrinių parametrų (Ψ ir Δ) TIRE spektrinę analizę struktūrose su ištisiniu aukso sluoksniu bei su aukso nanogumbų gardele. Nustatyti bangos ilgio poslinkį ir jautrumą aplinkos lūžio rodiklio (dejonizuotas vanduo ir etanolis) pokyčiams.
- Palyginti spektrines savybes bei Q-faktorių hibridinių TPP-SPP ir PSLPR modų gautą atspindžio intensyvumo pasiskirstymą nuo optinės dispersijos struktūroms su ir be nanogumbų gardelės.
- Palyginti elipsometrinių parametrų (Ψ ir Δ) jautrumą aplinkos lūžio rodiklio pokyčiams ant ištisinių sluoksnių bei nanogumbų gardelių. Nustatyti jautrumo ir Q-faktoriaus pokytį dėl nanogumbų gardelės modifikacijų.

- Išmatuoti ir palyginti ištisinių aukso sluoksnių ir nanogumbų gardelių struktūrų spektrus bei elipsometrinius parametrus (Ψ ir Δ), įvertinti spektrinius poslinkius bei naujų hibridinių plazmoninių modų generavimą stipriosios sąveikos režime.
- Sumodeliuoti hibridinių TPP-SPP ir Bragg‘o modų optinę dispersiją, naudojant sąveikaujančių osciliatorių modelį, ištirti nanogumbų gardelės įtaką Rabi skilimui ir TPP-SPP komponenčių sąveikos stiprumui.
- Kiekybiškai įvertinti SPP ir TPP komponenčių Q-faktorių ir sklidimo ilgio (δ) pokyčius, nustatyti rezonanso išplitimo, bangos vektoriaus neapibrėžtumo (Δk) ir koherentiškumo savybių skirtumus tarp ištisinio aukso sluoksnio ir gardelės struktūrų.

MOKSLINIS NAUJUMAS

Šioje disertacijoje atlikti eksperimentiniai tyrimai priklauso nanofotoninių įtaisų sričiai, kuriuose naudojamos poliaritoninės būsenos su išplitusiomis koherentiškumo savybėmis.

Pagrindinis šios disertacijos naujumas – pademonstruota stipriosios sąveikos tarp šviesos ir medžiagos savybė slopinti organinių dažų molekulių fotoblukimą ir stabilizuoti fluorescencijos intensyvumą hibridinėje SPP ir R6G dažų eksitono modoje (SPP-eksitonas) bei šio efekto pritaikymas FLIM metodui.

Ankstesni eksperimentai parodė, kad lokalūs plazmonai bei J-agregatai, esantys stiprioje sąveikoje, slopina fotoblukimo efektą [18]. Šiuose tyrimuose naudojami du matavimo metodai: TIRE bei FLIM metodas, kurie papildo vienas kitą ir abu patvirtina stipriosios sąveikos tarp paviršiaus plazmono poliaritono ir eksitono poliaritono įtaką fotoblukimo efektui. Parodyta, kad hibridinėse SPP-eksitono būsenoje fotoblukimas sumažėja maždaug 6 kartus, o tai rodo stipriojoje sąveikoje esančių SPP-eksitonų poliaritonų teigiamą poveikį poliaritoninių prietaisų kūrimui, kurie pasižymėtų didesniu stabilumu bei našumu. Šio tyrimo metu TIRE metodas buvo naudojamas stipriosios sąveikos režimui tarp SPP ir R6G eksitonų nustatymui, pritaikant optinių filtrų metodą. Šis filtrų metodas ankstesniuose tyrimuose buvo pritaikytas skirtingiems plazmonų sužadinimams, esantiems stipriojoje sąveikoje [23]. Tuo tarpu FLIM metodas parodė, kad stiprioji sąveika sumažina fotoblukimo efektą. Stipriosios sąveikos režime esančios poliaritoninės nanostruktūros buvo pirmą kartą pritaikytos fotoblukimo slopinimui naudojant FLIM metodą.

Eksperimentiniai rezultatai parodė, kad naudojant paviršiaus gardelių matricas galima kontroliuoti ir keisti hibridinio plazmoninio sužadinimo sklidimo ilgį, esant stipriai sąveikai tarp TPP ir SPP komponenčių.

Nanofotoninės-plazmoninės struktūros suformuotos DLW metodu, kuris yra pigus, greitas metodas ir gali būti naudojamas didelio ploto integruotiems fotoniniams įtaisams kurti. DLW metodu suformuotos nanogumbų gardelės leidžia valdyti sklidimo ilgį ir koherentiškumo savybes hibridiniame plazmoniniame sužadinime. Paviršiaus gardelės rezonansų taikymas stipriosios sąveikos režime lemia sumažėjusius nuostolius, dėl kurių didėja tokių plazmoninių sužadinimų sklidimo ilgis ir pagerėja koherentiškumo savybės, o tai žada pažangius beslenksčius, plazmonais grįstus koherentinės spinduliuotės nanošaltinius. Didelis susidomėjimas nanofotoninėmis – plazmoninėmis struktūromis, pasižyminčiomis koherentiškumo savybėmis, dėl galimo tokių struktūrų pritaikymo plazmoninių lazerių kūrime, informacijos apdorojimui bei tokių poliaritoninių struktūrų panaudojimui naujos kartos biojutikliams.

PRAKTINIS PRITAIKYMAS

Stipriosios sąveikos režime esančių plazmoninių ir eksitoninių poliaritoninių būsenų taikymas fluorescencijos gyvavimo trukmės mikroskopijoje leidžia žymiai sumažinti fotoblukimo efektą organinių dažų molekulėse ir taip sumažinti įtaką fluorescencijos gyvavimo trukmės matavimams. Pastebėta, kad stipriosios sąveikos režimas tarp SPP ir dažų eksitonų vaidina pagrindinį vaidmenį slopinant fotoblukimo efektą, kuris dažnai trukdo atlikti fluorescencijos tyrimus. Plazmoninės-eksitoninės poliaritoninės nanostruktūros pasižymi gebėjimu stabilizuoti fotoblukimo mechanizmus, tokiu būdu suteikdamos plačias galimybes kurti kvantinius daugiadalelius nanofotoninius prietaisus su organinėmis molekulėmis.

Aukso nanogumbų gardelių matricų gamyba ant struktūrų, palaikančių stipriosios sąveikos režimą (TPP-SPP), leidžia modifikuoti išplitusių plazmoninių poliaritoninių būsenų sklidimo ilgį.

Parodyta, stipriosios sąveikos režimo, tarp TPP ir sklindančio SPP išplitusiose plazmoninėse poliaritoninėse modose, įtaką pakitusiam aplinkos lūžio rodiklio jautrumui. Ši optinė savybė buvo sėkmingai pritaikyta realaus laiko nedestruktyvioms optinio jutiklio technologijoms.

GINAMIEJI TEIGINIAI

- Stipriosios sąveikos režime gautas Rabi tarpas (90meV) tarp paviršiaus plazmonų ir R6G molekulių eksitonų rezonansinių dažnių viršija nuostolius (52meV), kurie yra lygūs abiejų sužadinimų pločių ketvirčio sumai.
- Stipriosios sąveikos režimas tarp plazmono ir eksitono slopina R6G molekulių fotoblukimo efektą, dėl to fluorescencijos gyvavimo trukmės signalo intensyvumas gęsta 25% mažiau nei bandiniuose esančiuose silpnojoje sąveikoje.
- Paviršiaus gardelės plazmoniniai rezonansai stipriosios sąveikos režime lemia mažesnius poliaritoninių būsenų nuostolius, dėl to didėja jų sklidimo ilgis ir erdvinis koherentiškumas.
- Stipriosios sąveikos režimas pagerina hibridinių TPP-SPP modų optinio signalo jautrumą 27% aplinkos lūžio rodiklio pokyčiams, lyginant su tradiciniais plazmonų rezonanso jutikliais.

LITERATŪROS APŽVALGA

Šiame skyriuje pateikiama literatūros apžvalga su disertacijoje pristatomais darbo tikslais bei uždaviniais. Literatūros apžvalga suskirstyta į poskyrius, kuriuose aptariami: stipriosios sąveikos rėžimas, plazmoniniai sužadinimai, fotoniniai kristalai, fotoblukimas, organinės fluorescuojančios molekulės, PL bei spinduliavimas.

Poskyris 2.1. Stipriosios sąveikos režimas tarp harmoninių osciliatorių sukuria naujus hibridinius sužadinimus ir nulemia energijos lygmenų modifikaciją, turinčius įtakos fotonikos ir kvantinių technologijų sritims. Šis reiškinys yra svarbus fotocheminių reakcijų kinetikų valdyme bei kuriant pažangius įrenginius, tokius kaip kvantiniai kompiuteriai, plazmoniniai lazeriai. Rabi skilimas indikuoja stipriosios sąveikos režimą, kai sąveikos stiprumas viršija nuostolius sistemoje, todėl energijos mainai tarp molekulės ir rezonansinės modos įvyksta per koherentiškumo laiką. SPP ir eksitonai, ypač organiniuose dažuose, pasižymi dideliu Rabi skilimu, tačiau jų Q-faktoriaus kokybę riboja SPP nuostoliai metale. Nuostolių mažinimas naudojant išplitusias SPP ir SLPR modas pagerina sistemų stabilumą bei našumą, jas taikant fotoblukimo slopinimui ir jutiklių jautrumo didinimui. Tokiais tyrimais siekiama pagerinti erdvinį ir laikinį koherentiškumą, ištirti stipriosios sąveikos režimo savybes bei taikyti jas kvantinėse sistemose.

Poskyris 2.2. Bragg‘o veidrodžiai (1D fotoniniai kristalai) susideda iš periodiškai pasikartojančių dielektrinių sluoksnių porų, kurių optinio kelio

ilgis yra ketvirtis bangos ilgio kiekvienai sluoksnių porai. Kiekvieną porą sudaro dvi medžiagos, turinčios skirtingus lūžio rodiklius. Bragg‘o veidrodžiai turi mažą sugerties koeficientą. Didelis šviesos atspindys yra dėl konstruktyvios krentančios ir atspindėtos šviesos interferencijos (Fresnel‘io atspindys), kuri pasiekiama dėl daugkartinių Bragg‘o atspindžių nuo periodinės nanostruktūros. Šioms nanostruktūroms sukurti naudojami gamybos būdai: cheminis nusodinimas garais, solgelis, terminis garinimas ir jonapluoštis dulkinimas. Dažniausiai naudojamos medžiagos: TiO_2 ir SiO_2, pasirenkami dėl didelio lūžio rodiklių kontrasto ir medžiagų stabilumo. Dėl didelio atspindžio ir mažų nuostolių DBR plačiai naudojami spinduliavimo efektyvumui didinti bei optiniuose filtruose, mikrorezonatoriuose, fotoniniuose kristaluose, organiniuose šviesos dioduose.

Poskyris 2.3. Paviršinis plazmonas yra kolektyvinis svyravimas, kurį sukelia laisvieji elektronai metale. Kai metalo paviršius sąveikauja su krintančiu išoriniu elektromagnetiniu lauku, paviršiuje generuojami SPP, kurie leidžia tiksliai valdyti šviesą nanometrų dydžio matmenyse. SPP yra plačiai taikomi biojutikliuose, fotoninėse grandinėse bei saulės elementuose, tačiau dėl metalo sluoksnio turi didelius nuostolius, kurie riboja jų efektyvumą. TPP atsirandantys metalo ir Bragg‘o reflektoriaus riboje dar labiau praplėtė plazmoninius tyrimus, dėl to, kad krintančios šviesos bangos vektorius visada yra didesnis už TPP bangos vektoriaus dydį, todėl nereikalingas papildomas optinis elementas, kaip pvz. SPP sužadinimams. TPP dėl savo savybių naudojami optiniuose įrenginiuose: lazeriuose bei jutikliuose. Panaudojus TPP struktūrą su stiklo prizme, kuri naudojama sužadinti SPP, galima žadinti hibridines TPP-SPP modas. Šie hibridiniai sužadinimai susidaro tarp TPP ir SPP, kai jų bangų vektoriai sutampa. Ši sąveika lemia koherentinius energijos mainus ir dispersinių sąryšių pokyčius, sukuriant naujus hibridinius režimus su pakitusiais energijos spektrais. Metalinės nanostruktūros, palaikančios paviršiaus gardelių plazmonus, gali būti suskirstytos į 1D ir 2D matricas, kuriuose gali susidaryti HLPP. Šios matricos sumažina energijos nuostolius ir palaiko gardelės plazmonų rezonansus su daug aukštesniais kokybės faktoriais ($Q > 200$), lyginant su netvarkingai išsidėsčiusiomis nanodalelėmis ($Q < 20$). Periodiškas nanodalelių išdėstymas leidžia efektyviai sujungti LSP ir paviršiaus gardelės plazmonų rezonansus, sukuriant hibridines paviršines būsenas. Sąveika tarp lokalizuotų plazmonų ir Bragg‘o atspindžių kompensuoja fazės pokytį, dėl to padidėja rezonanso Q-faktorius ir sumažėja energijos nuostoliai. Šis reiškinys yra naudingas optinėms sistemoms, kurioms reikalingas tikslumas ir maži energijos nuostoliai. Itin tvarkingos nanodalelių matricos pasižymi daug

siauresniu rezonanso puspločiu (apie >10 nm), palyginti su netvarkingomis matricomis, kurios paprastai viršija 80 – 100 nm.

Skirsnis 2.3.5. Hibridiniai eksitonų-poliaritonų sužadinimai susidaro tarp eksitonų (elektrono-skylės pora) ir fotonų esančių stiprioje sąveikoje, paprastai stebimi dielektriniuose mikrorezonatoriuose. Šios kvazidalelės pasižymi mišriomis šviesos-medžiagos savybėmis, mažesne efektyviąja mase ir ilgesniu sklidimo nuotoliu. Kai eksitonų ir fotonų sąveikos stiprumas viršija sistemos nuostolius, susidaro hibridiniai eksitonai-poliaritonai, dėl kurių atsiranda Rabi skilimas. Fotoninės rezonansinės modos dielektrikuose gali būti pakeistos plazmoninėmis modomis, kurios pasižymi itin mažais modų tūriais bei didesne elektrinio lauko lokalizacija, tai leidžia pasiekti didelį sąveikos stiprumą. Organiniuose dažuose, tokiuose kaip R6G, sąveika su paviršiaus plazmonais sudaro plazmono-eksitono poliaritonus, kurie pagerina optines savybes ir energijos perdavimo efektyvumą nanoskalėje. Šie hibridiniai režimai yra daug žadantys žemo slenksčio lazeriuose, jutikliuose ir kituose optoelektroniniuose įrenginiuose, todėl jie yra dabartinių fotonikos tyrimų dėmesio centre.

Skirsnis 2.3.5.1. PL yra šviesos spinduliavimas, kai energijos kvantą sugėręs elektronas šoka į sužadintą būseną iš kurios relaksuoja atgal į pagrindinę būseną išspinduliuodamas fotoną. Ji apima momentinę fluorescenciją ir uždelstą fosforescenciją, naudojama medžiagų charakterizavimui, biologiniam vaizdinimui, optoelektronikoje ir jutikliuose. PL savybės priklauso nuo cheminės molekulių struktūros, tirpiklių poveikio joms, koncentracijos ir temperatūros. Hibridinės plazmonų-eksitonų sistemos sustiprina emisiją dėl eksitonų-plazmonų sąveikos. Emisijos spektrus galima reguliuoti keičiant sąveikos stiprumą, o taikymo sritys apima optinį detektavimą, apšvietimą, ekranus ir kvantinę informaciją. Organiniai dažai gali būti panaudojami kaip aktyvioji terpė naujos kartos koherentiniams šviesos nanošaltiniams, veikiantiems stipriosios sąveikos tarp plazmono ir eksitono pagrindu. Vienos dažniausiai naudojamų molekulių yra R6G, Rhodaminas B (ksanteno (Xanthene) dažai), fluoresceinas. Svarbiausios jų savybės: didelis osciliatoriaus stipris, stipri sugertis esant sužadinimo bangos ilgiui ir minimali sugertis ties lazerio bangos ilgiu, t. y. minimalus sugerties ir emisijos spektrų persidengimas, didelis kvantinis efektyvumas (0,5 – 1,0), fotocheminis stabilumas, trumpa fluorescencijos trukmė (5 – 10 ns) ir didelis grynumas, nes priemaišos dažnai gesina lazerio išeigą. Tinkamai parinkus dažus, galima sukurti koherentinę, bet kokio bangos ilgio šviesą nuo 320 iki 1200 nm.

Skirsnis 2.3.5.2. Fotoblukimas yra negrįžtamas fluorescencijos praradimas dėl šviesos poveikio, slopinantis fluorescencijos signalo intensyvumą. Tai atsiranda dėl fotocheminių reakcijų, kurios skaido fluoroforus, kurie sąveikauja su aplinkoje esančiu deguonimi. Fotoblukimo efektas riboja fluorescencijos gyvavimo trukmės mikroskopijos matavimo galimybes. Stipriosios sąveikos tarp plazmonų ir eksitonų pritaikymas gali perskirstyti energiją, sumažinant fotoblukimą ir prailginti fluorescencijos gyvavimo trukmes. Šis metodas pagerina fluorescencija pagrįstų metodų patvarumą, naudingą biologiniam vaizdinimui ir medžiagų mokslui.

METODAI

Šiame tyrime buvo naudojama SE, siekiant apibūdinti plonų sluoksnių optines savybes bei sluoksnių storius. Buvo naudojamas J.A. Woollam gamintojo RC2 elipsometras, kuris pasižymi galimybe išmatuoti visą Miulerio matricą 210 – 1700 nm spektro diapazone, o krintančios šviesos kampų diapazonas yra nuo 20° iki 90°. TIRE matavimas naudotos 45° bei 70° prizmės, skirtos valdyti krintančią šviesą, ir reikiamam bangos vektoriaus dydžiui pasiekti, būtino plazmonui sužadinti, (1 pav. a). Išmatuotas poliarizuotos šviesos amplitudės santykis (Ψ) ir fazių skirtumas (Δ), leidžia tiksliai nustatyti sluoksnio lūžio rodiklį bei storį. Duomenų analizei naudojama CompleteEASE programinė įranga užtikrina tikslią ir visapusišką medžiagos analizę.

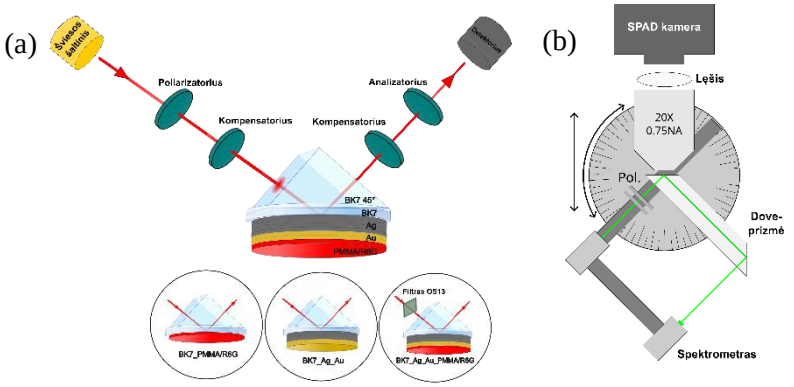

1 pav. (a) Hibridinio eksitono-SPP sužadinimo TIRE schema. (b) TIRF sistemos schema su apšvietimo / surinkimo svirtimi, pritvirtinta prie sukimosi ir transliacijos stovo ir Dove-prizme. Ši ranka juda nepriklausomai nuo prizmės ir mikroskopo objektyvo (pažymėta juodomis rodyklėmis)**.**

FLIM metodas naudojamas fluorescencijos gyvavimo trukmei išmatuoti (τ), parodantis kiek laiko fluoroforas išlieka sužadintoje būsenoje. Šis gyvavimo laikas yra jautrus lokaliai molekulinei aplinkai ir nepriklauso nuo fluoroforo koncentracijos. FLIM gali būti laikinis matavimo metodas, fiksuojantis gesimo laikus po trumpų žadinančios šviesos impulsų, arba dažninis metodas, matuojantis moduliuotos šviesos fazių poslinkį. Tyrimams naudota FLIM įranga apima tokius komponentus kaip Dove-prizmė ir pavienio fotono lavinos detektoriaus matrica (1 pav. b), todėl galima tiksliai analizuoti molekulinę fluoroforų sąveiką bei aplinkos sąlygas.

Bandiniai ruošiami naudojant pažangias gamybos technologijas. Jonapluoščio dulkinimo metodas naudojamas periodiškai pasikartojantiems TiO_2 ir SiO_2, atitinkamai 110 nm ir 200 nm sluoksnio storiams, nusodinti ant BK7 stiklinio padėklo. Ant viršaus papildomai suformuotas 30 nm TiO_2 sluoksnis. Magnetroninis dulkinimas naudojamas ploniems sidabro (35 nm 4.1 skyriuje) ir aukso (9 nm skyriuje 4.1 ir 50 nm skyriuje 4.2 ir 4.3) sluoksniams nusodinti, kurie yra būtini hibridinio paviršiaus plazmono-eksitono poliaritono modoms žadinti. Tiesioginis lazerinis įrašymas naudojamas aukso gardelių matricoms formuoti, naudojant Yb-femtosekundinį lazerį su 300 fs impulsais, esant 515 nm bangos ilgiui. Spinduliuotė buvo sufokusuota į $\approx$ 1 µm tašką, kurio energija yra 1,5 nJ vienam impulsui, o transliacijos greitis 2,8 mm/s ir impulso pasikartojimo dažnis 4 kHz, leidžia suformuoti ~0,7 µm periodo struktūras. Sluoksnio liejimo centrifūguojant metodas naudojamas suformuoti ~ 20 nm PMMA-R6G sluoksnį, esant 3000 aps./min. sukimosi greičiui, kai išsukimo laikas 30 s. PMMA ir R6G koncentracijos atitinkamai 1 x 10^{-5} mol/L ir 25 x 10^{-3} mol/L ir abi šios medžiagos tirpinamos etanolyje. Šie parametrai parinkti siekiant suformuoti vienodas ir aukštos kokybės dangas, būtinas optiniams tyrimams.

Aukso nanogumbų ir plono aukso sluoksnio morfologija įvertinta naudojant SEM metodą. SEM mikroskopinėse nuotraukose pavaizduotas vienodas 50 nm storio aukso sluoksnis ir nanogumbų gardelės masyvas ant to paties aukso sluoksnio. Struktūra buvo sudaryta iš aukso nanogumbų, kurių skersmuo yra apie 370 nm, o periodas apie 650 nm.

Tyrimuose aprašomuose 4.1. poskyryje daug dėmesio skiriama šviesos-medžiagos sąveikai, pavyzdžiui, siekiant sukurti plazmonines eksitonines struktūras kaip koherentinius šviesos šaltinius su žemu galios slenksčiu. Šiame tyrime nagrinėjama kambario temperatūros stipriosios sąveikos režimo tarp SPP ir eksitonų įtaka fluorescencijos gyvavimo trukmei ir fotoblukimo efektui. Suformuota plazmoninė fotoninė struktūra, sudaryta iš plonų sidabro ir aukso sluoksnių bei dažo R6G sluoksnio, parodė, aiškų plazmonų rezonanso ir R6G sugerties linijų pasislinkimą, keičiant šviesos kritimo kampą. Šioje struktūroje pasiektas stipriosios sąveikos režimas tarp plazmono ir eksitono, o gautas Rabi energijos tarpas buvo maždaug 90 meV (2 pav).

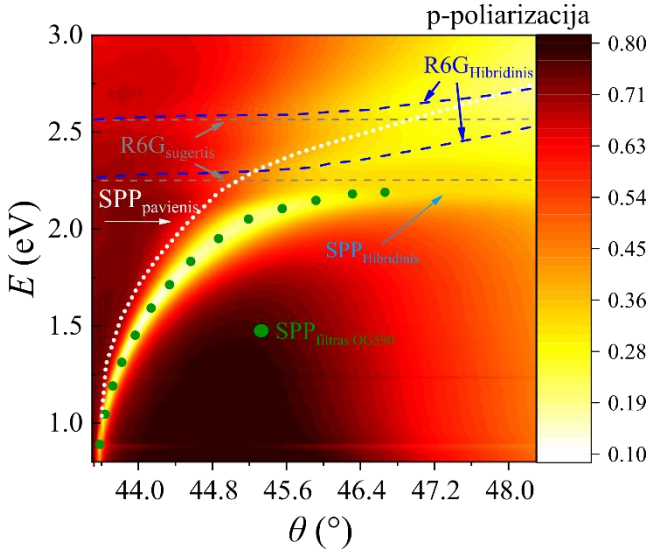

2 pav. Hibridinio sužadinimo (tamsiai mėlynos (R6G) ir šviesiai mėlynos (SPP) punktyrinės kreivės) ir pavienio SPP (baltos punktyrinės kreivės) bei R6G eksitonų (pilkos brūkšninės linijos) dispersiniai sąryšiai naudojant TIRE metodą. Matavimai panaudojant filtro (OG-590) metodą pažymėti žaliais taškais.

Fotoblukimo efektui įvertinti naudotas FLIM metodas. Šis metodas parodė, kad plazmoninėse-eksitoninėse struktūrose, kurios yra stipriojoje sąveikoje organinių R6G dažų molekulių fotoblukimą slopina net 6 kartus daugiau, lyginant su ištisiniais R6G sluoksniais (3 pav). Gauti rezultatai parodė, kad stipriosios sąveikos režimas tarp šviesos ir medžiagos vaidmuo yra esminis mažinant fotoblukimo efektą ir stabilizuojant fluorescencijos

intensyvumą. Tai pagerina kvantinių daugiadalelių nanofotoninių prietaisų kūrimą, pasižyminčiu didesniu stabilumu bei našumu.

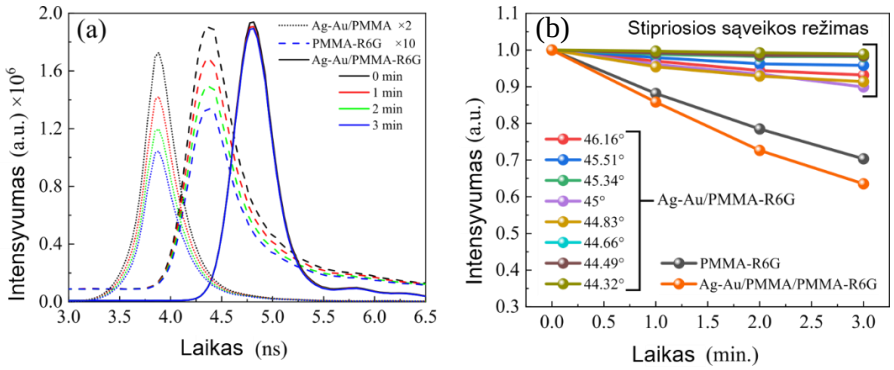

3 pav. (a) Fluorescencijos gyvavimo trukmės ir intensyvumo pokyčiai nuo 0 iki 3 minučių dėl R6G fotoblukimo plazmoninėse-nanofotoninėse struktūrose (vientisos kreivės) su atskiriamuoju sluoksniu tarp Ag-Au ir PMMA-R6G (punktyrinės linijos) bei atraminiu mėginiu (punktyrinės kreivės). (b) BK7/Ag-Au/PMMA-R6G struktūrų fotoblukimas laikui bėgant, esant skirtingiems kritimo kampams bei palyginama su pavieniu R6G dažų sluoksniu, ties 45 ° AOI (juodas).

4.2. poskyryje naudojamas TIRE metodas tiriant stipriosios saveikos režimą tarp TPP ir SPP nanofotoninėse struktūrose su 1D PC ir aukso nanogumbų gardelės matrica (4 pav.). Ištirtos dvi skirtingos mėginių konfigūracijos: su plonu ištisiniu aukso sluoksniu, o kita - su aukso nanogumbų gardelės matrica. TPP moda sužadinama PC/aukso sluoksnio sandūroje, o HSPP moda sužadinama aukso ir oro sandūroje, dėl SPP sužadinimo ir Bragg‘o modos sąveikos.

Tyrimai parodė, kad aukso nanogumbų gardelė suformavo papildomą Bragg‘o modą, susijusią su gardelės periodu. Išsami analizė parodė, kad SPP sklidimo nuotolis padidėjo, o TPP sumažėjo dėl papildomos Bragg‘o modos susidarymo. Optinės dispersijos bei sklidimo ypatybės struktūroms su 1D PC ir ištisiniu aukso sluoksniu bei aukso nanogumbų gardele, buvo analizuojamos taikant dviejų susietų osciliatorių modelį bei analizuojant bangos vektoriaus priklausomybės nuo energijos išplitimo duomenis (5 pav.).

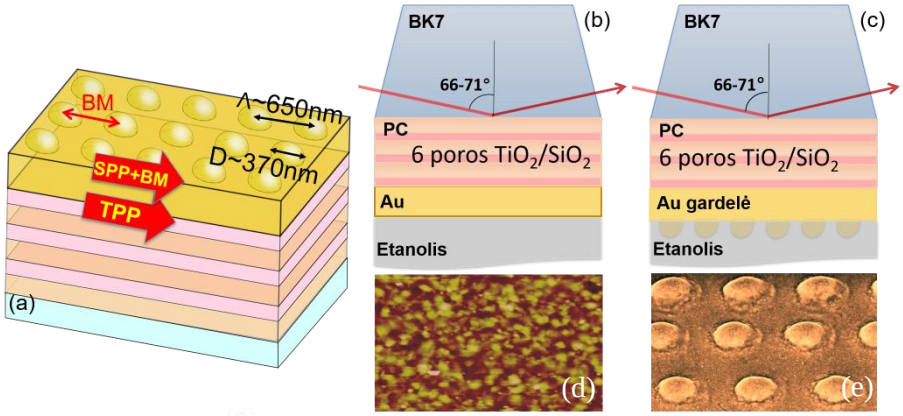

4 pav. Tiriama struktūra, sudaryta iš ~652 nm periodo aukso nanogumbelių gardelės (a). (b) hibridinio TPP–SPP sužadinimo ir (c) SPP–HSPP struktūrų sužadinimo visiško vidaus atspindžio konfigūracijoje schema, su 70° prizme. SEM mikrogramos (d) ištisinio Au (50 nm) sluoksnio ir (e) nanogumbų gardelės masyvo ant to paties plono aukso sluoksnio.

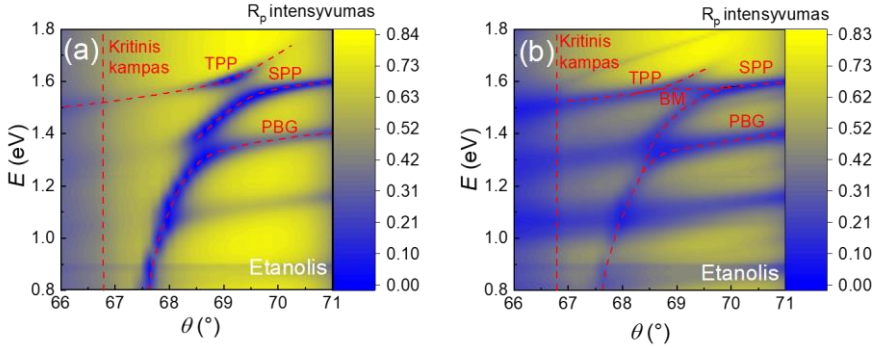

5 pav. (a) p-poliarizuotos šviesos atspindžio intensyvumo pasikirstymas *E(θ)*: struktūroje su ištisiniu aukso sluoksniu ir (b) struktūroje su aukso nanogumbų gardelės masyvu.

Palyginami sužadinimų sklidimo ilgiai (δ), kurie parodo atstumą, per kurį hibridinių plazmoninių modų elektrinio lauko amplitudė sumažėja per 1/e nuo pradinės vertės. Nanostruktūrose su ištisiniu aukso sluoksniu įvertintas sklidimo ilgis buvo $\delta_{SPP} \approx$ 5,5-6,5 μm ir $\delta_{TPP} \approx$ 6,5-9,5 μm atitinkamai SPP ir TPP komponentėms hibridinio poliaritoninio sužadinimo atveju. Tuo tarpu, dėl periodinės aukso gardelės sukeltų pokyčių SPP komponentės sklidimo ilgis padidėjo ($\delta_{SPPlattice} \approx$ 7-10,5 μm), o TPP - sumažėjo ($\delta_{TPPlattice} \approx$ 5,5-8,5 μm) (6 pav.).

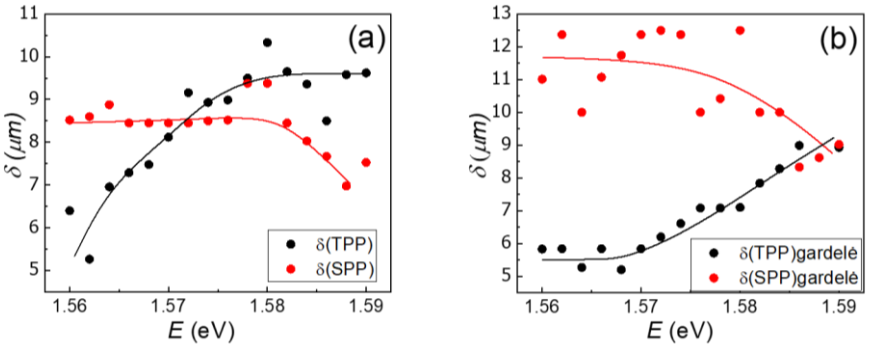

6 pav. Sklidimo ilgio (δ), priklausomybė nuo energijos. (a) struktūra be nano gumbų (juodi apskritimai – δ_{TPP}, raudoni apskritimai – δ_{SPP}) ir (b) su aukso nanogumbų gardele (juodi apskritimai – δ_{TPP}, raudoni apskritimai – δ_{SPP}). Vientisos juodos ir raudonos linijos rodo TPP ir SPP komponenčių sklidimo ilgio pokyčiai.

Gauti rezultatai atskleidžia naują metodą, kuris leidžia kontroliuoti ir keisti sklidimo ilgį, esant stipriosios sąveikos režimui tarp TPP ir SPP komponenčių hibridiniame plazmoniniame sužadinime, naudojant nanogardelių matricas. DLW metodas, leidžia pagaminti didelio ploto (cm^2) integruotas optines grandines su universaliomis Bragg‘o gardelėmis. Šios gardelės pasižymi siaurais plazmoninių rezonansų puspločiais bei palengvina naujas integruotos optikos taikymo galimybes. Paviršiaus gardelės rezonansų taikymas stipriosios sąveikos režime lemia nuostolių mažėjimą, todėl didėja tokių plazmoninių sužadinimų sklidimo ilgis ir erdvinis koherentiškumas. Tai žada pažangias savybes mažų elektros energijos sąnaudų arba be slenksčio veikiančių plazmoninių koherentinės emisijos nanošaltinių srityje.

Paskutiniame 4.3. poskyryje analizuojamas jautrumas aplinkos lūžio rodiklio pokyčiams, kur tyrimas atliekamas ant ištisinio aukso sluoksnio (~50 nm) su 1D PC iš penkių periodinių TiO_2 (~110 nm)/SiO_2 (~200 nm) dvisluoksnių ir aukso nanogumbų masyvo, suformuoto tiesioginio lazerinio įrašymo metodu ant to paties bandinio. Hibridinių plazmoninių rezonansų optinio signalo jautrumas buvo lyginamas su tradiciniu SPR ant ištisinio aukso sluoksnio. Analizuojama TPP ir hibridiniuose plazmoniniuose rezonansuose sklindančių plazmonų poliaritonų stipriosios sąveikos įtaka optiniam jautrumui. Tyrimai parodė labai didelį hibridinių plazmoninių modų jautrumą $S_{HSPP} \approx 26\ 000$ nm/RIU aplinkos lūžio rodiklio pokyčiui, struktūroje su ištisiniu aukso sluoksniu, tuo tarpu struktūroje su aukso gardele signalo jautrumas sumažėja, tačiau padidėja Q-faktorius (7 pav.). Nepaisant to, jautrumas elipsometriniams parametrams Ψ ir Δ ant aukso gardelės buvo gana

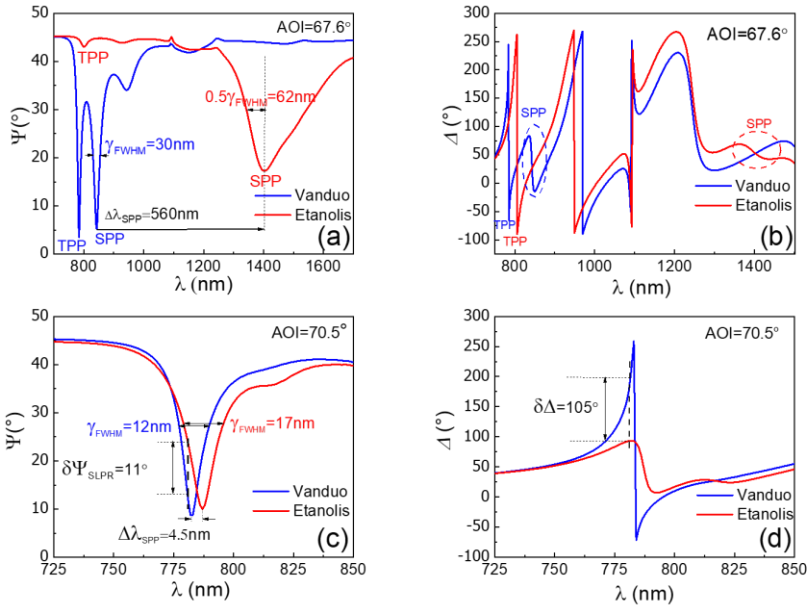

7 pav. Elipsometrinių parametrų Ψ(λ) ir Δ(λ) spektrai (a)-(b) struktūros su ištisiniu aukso sluoksniu, (c)-(d) struktūros su aukso nanogardele skirtinguose terpėse. Mėlyna kreivė atitinka struktūros spektro optinį atsaką vandenyje, raudona kreivė - etanolyje.

didelis dėl padidėjusio Q-faktoriaus. Palyginus plazmoninių rezonansų jautrumą hibridinio TPP-SPP sužadinimo ant ištisinio aukso sluoksnio lūžio rodiklio pokyčiams su tradiciniu SPR, paaiškėjo, kad hibridinis plazmoninis sužadinimas dėl stipriosios sąveikos režimo yra apie 27 % jautresnis nei tradicinis SPR.

IŠVADOS

- TIRE metodas panaudotas ištirti stipriosios sąveikos režimui tarp SPP ir eksitonų plazmoninėse-fotoninėse nanostruktūrose, kambario temperatūroje. Nustatytos optinės dispersijos (E(k) energijų susikirtimo taške) parodė, kad Rabi energijos tarpas lygus 90 meV ir yra didesnis nei plazmoninio ir eksitoninio rezonanso linijų pločiai (γ), kas patvirtina stiprios sąveikos režimą tokioje struktūroje.
- FLIM metodas parodė, kad naudojant poliaritonines nanostruktūras, kuriose plazmonai ir eksitonai yra stipriosios sąveikos režime, fluorescencijos intensyvumas sumažėja 5%, tuo tarpu silpnosios sąveikos režime fluorescencijos intensyvumas sumažėja apie 25-30%. Kas leidžia teigti, kad stipriosios sąveikos režimas tarp SPP ir dažų eksitonų slopina fotoblukimo efektą apie 6 kartus.
- Stipriosios sąveikos tarp TPP ir SPP nanofotoninėse struktūrose su 1D PC bei aukso nanogumbų gardelių masyvu sužadinimui buvo naudojamas TIRE metodas. Bangos vektoriaus Δk analizė parodė, kad SPP sklidimo ilgis ant aukso nanogumbų gardelės padidėjo apie 30%, o TPP komponentės sumažėjo ~10%, palyginti su hibridine plazmonine moda ant ištisinio aukso sluoksnio.
- Paviršiaus metalų nanogumbų gardelių matricos, pagamintos DLW metodu ant plono metalo sluoksnio, generuoja delokalizuotus koherentinius poliaritoninius sužadinimus. Stipriosios sąveikos režimas sumažina nuostolius, dėl to didėja tokių plazmoninių sužadinimų sklidimo ilgis, Q-faktorius bei pagerinamas erdvinis koherentiškumas. Gauti rezultatai parodo DLW metodo galimybes, formuojant reikiamų parametrų nanofotonines-plazmonines struktūras, šiuo atveju modifikuojant sklidimo nuotolį tarp TPP ir SPP komponenčių hibridinėje plazmoninėje modoje.
- Kretschmann‘o konfigūracija bei spektrinės elipsometrijos metodas buvo naudojamas stipriosios sąveikos režimui tarp TPP ir SPP nanofotoninėse struktūrose su 1D PC bei aukso nanogumbų gardelėmis sužadinti. Hibridinių plazmoninių poliaritoninių modų poslinkiai spektre parodė labai didelį hibridinio plazmoninio režimo jautrumą $S_{HSPP} \approx 26000$ nm/RIU ant ištisinio aukso sluoksnio aplinkos lūžio rodiklio pokyčiui.

- Aukso nanogumbų gardelės plazmoninėje-nanofotoninėje struktūroje sumažina signalo jautrumą lūžio rodiklio pokyčiui spektre, bet padidina plazmoninių rezonansų Q-faktorių. Jautrumas elipsometriniams parametrams Ψ ir Δ išauga dėl padidėjusio rezonansų Q-faktoriaus (Q_{HSLPP}=63.6), kas lemia mažėjančius sklidimo nuostolius.
- Plazmoninio rezonanso jautrumo palyginimas lūžio rodiklio pokyčiams ant ištisinio aukso sluoksnio su hibridiniu TPP-SPP sužadinimu, parodė, kad hibridinis plazmoninis sužadinimas dėl stipriosios sąveikos režimo yra apie 27 % jautresnis nei pavienis SPP.

7. PUBLIKACIJŲ SĄRAŠAS

Mokslinių publikacijų disertacijos tema sąrašas

P1. J. Anulytė, E. Bužavaitė-Vertelienė, V. Vertelis, E. Stankevičius, K. Vilkevičius, Z. Balevičius, Influence of gold nano-bumps surface lattice array to the propagation length of strongly coupled Tamm and surface plasmon polaritons, *Journal of Materials Chemistry C* (2022), 10, 13234 – 13241. Q1 (IF:8.067)

P2. J. Anulytė, E. Bužavaitė-Vertelienė, E. Stankevičius, K. Vilkevičius, Z. Balevičius, High Spectral Sensitivity of Strongly Coupled Hybrid Tamm-Plasmonic Resonances for Biosensing Application, *Sensors* (2022), 22(23), 9453. Q2 (IF:3.847)

P3. J. Anulytė, V. Žičkus, E. Bužavaitė-Vertelienė, D. Faccio, Z. Balevičius, Strongly coupled plasmon-exciton polaritons for photobleaching suppression, *Nanophotonics,* vol. 13, no. 22, 2024, pp. 4091-4099. Q1 (IF: 6.5).

Kitos doktorantūros metu išspausdintos mokslinės publikacijos

P4. E. Bužavaitė-Vertelienė, V. Mačiulis, I. Plikusienė, J. Anulytė, T. Tolenis, A. Baškys, Z. Balevičius, Total internal reflection ellipsometry approach for Bloch surface waves biosensor applications, *Biosensors* **12**(8), 584, (2022). Q1 (IF:5.743)

Konferencijos

C1. V. Gradauskas, J. Anulytė, E. Bužavaitė-Vertelienė, I. Plikusienė, Z. Balevičius. (In-situ) Study of immobilized receptor binding kinetics by using planar photonic-plasmonic nanostructures for biosensing. *64th International conference for students of physics and natural sciences "Open Readings"*, Vilnius, 2021, kovo 16-19d. (stendinis)

C2. J. Anulytė, E. Bužavaitė-Vertelienė, I. Plikusienė. Z. Balevičius. Hybrid Tamm-surface plasmon polaritons mode based on planar plasmonic photonic nonostructure for highly sensitive real time biosensing of GsCF and BSA proteins. *23-rd International Conference – School, "Advanced materials and technologies"*, Palanga, 2021, rugpjūčio 23-27 dienomis. (stendinis)

C3. J. Anulytė, E. Bužavaitė-Vertelienė, Z. Balevičius. Modelling of plasmon – exciton strong coupling in silver/gold film with R6G dye in polymethyl methacrylate layer. *65th International conference for students of physics and natural sciences "Open Readings"*, Vilnius, 2022, kovo 15-18d. (stendinis)

C4. J. Anulytė, E. Bužavaitė-Vertelienė, Z. Balevičius. Application of hybrid Tamm and surface plasmon polariton modes to optical sensors. Lietuvos mokslų akademijos *11-oji konferencija „Fizinių ir technologijos mokslų tarpdalykiniai tyrimai“* reikšmė ir rezultatai, Vilnius, 202, kovo 23d. (žodinis)

C5. J. Anulytė, E. Bužavaitė-Vertelienė, V. Vertelis, E. Stankevičius, K. Vilkevičius, Z. Balevičius. Optical response of the hybrid Tamm-surface plasmon polariton modes on the surface lattice array of gold nanobumbs. *66th International conference for students of physics and natural sciences "Open Readings",* Vilnius, 2023 balandžio 18-21d. (stendinis)

C6. J. Anulytė, E. Bužavaitė-Vertelienė, Z. Balevičius. Study of the strongly coupled Tamm-plasmon polariton states in the surface lattice array of gold nano-bumps. *6th International Conference on Optics, Photonics and Lasers (OPAL' 2023),* 2023 gegužės 17-19d. Funchal (Madeira island), Portugalija. (stendinis)

C7. E.Bužavaitė-Vertelienė, S. Juciūtė, I. Plikusienė, J. Anulytė, Z. Balevičius. Application of strongly coupled plasmonic excitation for sensing of dye-labelled Bovine Serum Albumin, *IOP Photon 2024, Swansea,* Didžioji Britanija, 2024 Rugsėjo 2-6 d. (stendinis)

C8. P. Jurkšaitis, J. Anulytė, D. Banevičius, E. Bužavaitė-Vertelienė, Z. Balevičius. Surface Plasmon Coupled Emission of Rhodamine 6G Dye in Strong Coupling Regime, *IOP Photon 2024, Swansea,* Didžioji Britanija, 2024 Rugsėjo 2-6 d.(stendinis)

PADĖKA

Būtų labai sunku įgyvendinti ir užbaigti doktorantūros studijas be kolegų ir šeimos narių paramos ir pagalbos, esu labai dėkinga, kad jie buvo šalia visus šiuos metus. Pirmiausia norėčiau padėkoti savo darbo vadovui prof. dr. Zigmui Balevičiui už suteiktą galimybę rengti disertaciją šia tema. Esu dėkinga už galimybę diskutuoti moksliniais klausimais, už palaikymą ir pagalbą analizuojant rezultatus bei ruošiant disertaciją. Taip pat esu dėkinga savo kolegei dr. Ernestai Bužavaitei-Vertelienei, kuri pakvietė mane į Plazmonikos ir nanofotonikos laboratoriją, dalijosi savo patirtimi bei žiniomis, padėjo įveikti sunkumus ir neleido pasiduoti. Džiaugiuosi turėdama galimybę dirbti su šiais mokslininkais.

Dėkoju visiems Fizinių ir technologijos mokslų centro kolegoms už pagalbą, patarimus ir draugišką aplinką. Ypač Dr. Viliui Verteliui už naudingą diskusiją apie modeliavimus bei patarimus rengiant rankraštį, Dr. Evaldui Stankevičiui ir dr. Linai Grinevičiūtei už mėginių paruošimą ir dr. Vytautui Žičkui už galimybę atvykti į Glazgo universitetą, susipažinti su daugybę puikių mokslininkų, išbandyti naujus matavimo metodus bei gauti naujų žinių ir rezultatų.

Galiausiai noriu padėkoti savo nuostabiai, įkvepiančiai šeimai, ypač seneliui, kurio tikėjimas manimi neleido pasiduoti ir padėjo kryptingai siekti savo tikslo. Taip pat noriu padėkoti savo bakalauro bei magistro studijų vadovui prof. habil. dr. Kęstučiui Arlauskui už motyvaciją, žinias ir galimybę pažinti mokslą. Noriu padėkoti visiems savo artimiesiems ir draugams už kantrybę ir begalinį palaikymą.

MOKSLINIS KŪRYBINIS VEIKLOS APRAŠYMAS

Vardas: Justina
Pavardė: Anulytė
El. paštas: justinaanulyte@gmail.com

Išsilavinimas:

2010-2014 m.	Klaipėdos „Ąžuolyno“ gimnazija.
2014-2018 m.	Vilniaus universitetas, Fizikos fakultetas. *Bakalauro laipsnis*.
2018-2020 m.	Vilniaus universitetas, Fizikos fakultetas. *Magistro laipsnis*.
2020-2024 m.	Vilniaus universitetas, Fizikos fakultetas bei VMTI Fizinių ir technologinių mokslų centras. *Doktorantūra*.

Darbo patirtis:

2016-2020 m.	Cheminės fizikos institutas. Kietojo kūno elektronikos katedra. *Laborantė*.
2020-2022 m.	Lazerinių technologijų skyrius. Plazmonikos ir nanofotonikos laboratorija. *Inžinierė*.
2022-11 (iki šiol)	Lazerinių technologijų skyrius. Plazmonikos nanofotonikos laboratorija. *Jaunesnioji mokslų darbuotoja.*

Kiti privalumai:

2021 m. liepos 17-24	International Physics Olympiad (IphO) vertintoja.
2022 m. lapkričio 12-26	Stažuotė „Extreme Light Group“ Glazgo Universitete.
2024 m. lapkričio 11-18	Komandiruotė „Extreme Light Group“ Glazgo Universitete

8. REFERENCES

[1] J. Bellessa, C. Bonnand, J. C. Plenet, and J. Mugnier, "Strong Coupling between Surface Plasmons and Excitons in an Organic Semiconductor," *Phys. Rev. Lett.*, vol. 93, no. 3, p. 036404, Jul. 2004, doi: 10.1103/PhysRevLett.93.036404.

[2] M. A. Noginov *et al.*, "Demonstration of a spaser-based nanolaser," *Nature*, vol. 460, no. 7259, pp. 1110–1112, Aug. 2009, doi: 10.1038/nature08318.

[3] T. K. Hakala *et al.*, "Bose–Einstein condensation in a plasmonic lattice," *Nature Phys*, vol. 14, no. 7, pp. 739–744, Jul. 2018, doi: 10.1038/s41567-018-0109-9.

[4] E. Verhagen, S. Deléglise, S. Weis, A. Schliesser, and T. J. Kippenberg, "Quantum-coherent coupling of a mechanical oscillator to an optical cavity mode," *Nature*, vol. 482, no. 7383, pp. 63–67, Feb. 2012, doi: 10.1038/nature10787.

[5] A. Lishchuk, C. Vasilev, M. P. Johnson, C. N. Hunter, P. Törmä, and G. J. Leggett, "Turning the challenge of quantum biology on its head: biological control of quantum optical systems," *Faraday Discuss.*, vol. 216, pp. 57–71, 2019, doi: 10.1039/C8FD00241J.

[6] P. Törmä and W. L. Barnes, "Strong coupling between surface plasmon polaritons and emitters: a review," *Rep. Prog. Phys.*, vol. 78, no. 1, p. 013901, Jan. 2015, doi: 10.1088/0034-4885/78/1/013901.

[7] D. G. Baranov, M. Wersäll, J. Cuadra, T. J. Antosiewicz, and T. Shegai, "Novel Nanostructures and Materials for Strong Light–Matter Interactions," *ACS Photonics*, vol. 5, no. 1, pp. 24–42, Jan. 2018, doi: 10.1021/acsphotonics.7b00674.

[8] E. M. Purcell, H. C. Torrey, and R. V. Pound, "Resonance Absorption by Nuclear Magnetic Moments in a Solid," *Phys. Rev.*, vol. 69, no. 1–2, pp. 37–38, Jan. 1946, doi: 10.1103/PhysRev.69.37.

[9] T. K. Hakala *et al.*, "Vacuum Rabi Splitting and Strong-Coupling Dynamics for Surface-Plasmon Polaritons and Rhodamine 6G Molecules," *Phys. Rev. Lett.*, vol. 103, no. 5, p. 053602, Jul. 2009, doi: 10.1103/PhysRevLett.103.053602.

[10] W. L. Barnes, "Surface plasmon–polariton length scales: a route to sub-wavelength optics," *J. Opt. A: Pure Appl. Opt.*, vol. 8, no. 4, pp. S87–S93, Apr. 2006, doi: 10.1088/1464-4258/8/4/S06.

[11] M. Hertzog, M. Wang, J. Mony, and K. Börjesson, "Strong light–matter interactions: a new direction within chemistry," *Chem.*

Soc. Rev., vol. 48, no. 3, pp. 937–961, 2019, doi: 10.1039/C8CS00193F.

[12] M. Pelton, S. D. Storm, and H. Leng, "Strong coupling of emitters to single plasmonic nanoparticles: exciton-induced transparency and Rabi splitting," *Nanoscale*, vol. 11, no. 31, pp. 14540–14552, 2019, doi: 10.1039/C9NR05044B.

[13] K. Santhosh, O. Bitton, L. Chuntonov, and G. Haran, "Vacuum Rabi splitting in a plasmonic cavity at the single quantum emitter limit," *Nat Commun*, vol. 7, no. 1, p. ncomms11823, Jun. 2016, doi: 10.1038/ncomms11823.

[14] W. Qin, A. F. Kockum, C. S. Muñoz, A. Miranowicz, and F. Nori, "Quantum amplification and simulation of strong and ultrastrong coupling of light and matter," *Physics Reports*, vol. 1078, pp. 1–59, Aug. 2024, doi: 10.1016/j.physrep.2024.05.003.

[15] D. S. Dovzhenko, S. V. Ryabchuk, Yu. P. Rakovich, and I. R. Nabiev, "Light–matter interaction in the strong coupling regime: configurations, conditions, and applications," *Nanoscale*, vol. 10, no. 8, pp. 3589–3605, 2018, doi: 10.1039/C7NR06917K.

[16] S. I. Azzam *et al.*, "Ten years of spasers and plasmonic nanolasers," *Light Sci Appl*, vol. 9, no. 1, p. 90, May 2020, doi: 10.1038/s41377-020-0319-7.

[17] V. G. Kravets, A. V. Kabashin, W. L. Barnes, and A. N. Grigorenko, "Plasmonic Surface Lattice Resonances: A Review of Properties and Applications," *Chem. Rev.*, vol. 118, no. 12, pp. 5912–5951, Jun. 2018, doi: 10.1021/acs.chemrev.8b00243.

[18] D. G. Lidzey, D. D. C. Bradley, A. Armitage, S. Walker, and M. S. Skolnick, "Photon-Mediated Hybridization of Frenkel Excitons in Organic Semiconductor Microcavities," *Science*, vol. 288, no. 5471, pp. 1620–1623, Jun. 2000, doi: 10.1126/science.288.5471.1620.

[19] D. G. Lidzey, D. D. C. Bradley, M. S. Skolnick, T. Virgili, S. Walker, and D. M. Whittaker, "Strong exciton–photon coupling in an organic semiconductor microcavity," *Nature*, vol. 395, no. 6697, pp. 53–55, Sep. 1998, doi: 10.1038/25692.

[20] P. Berini, "Long-range surface plasmon polaritons," *Adv. Opt. Photon.*, vol. 1, no. 3, p. 484, Nov. 2009, doi: 10.1364/AOP.1.000484.

[21] B. Munkhbat, M. Wersäll, D. G. Baranov, T. J. Antosiewicz, and T. Shegai, "Suppression of photo-oxidation of organic chromophores by strong coupling to plasmonic nanoantennas," *Sci. Adv.*, vol. 4, no. 7, p. eaas9552, Jul. 2018, doi: 10.1126/sciadv.aas9552.

[22] N. Nefedkin, E. Andrianov, and A. Vinogradov, “The Role of Strong Coupling in the Process of Photobleaching Suppression,” *J. Phys. Chem. C*, vol. 124, no. 33, pp. 18234–18242, Aug. 2020, doi: 10.1021/acs.jpcc.0c05518.

[23] S. D. Hart, G. R. Maskaly, B. Temelkuran, P. H. Prideaux, J. D. Joannopoulos, and Y. Fink, “External Reflection from Omnidirectional Dielectric Mirror Fibers,” *Science*, vol. 296, no. 5567, pp. 510–513, Apr. 2002, doi: 10.1126/science.1070050.

[24] H. Shen, Z. Wang, Y. Wu, and B. Yang, “One-dimensional photonic crystals: fabrication, responsiveness and emerging applications in 3D construction,” *RSC Adv.*, vol. 6, no. 6, pp. 4505–4520, 2016, doi: 10.1039/C5RA21373H.

[25] M. Ibanescu, Y. Fink, S. Fan, E. L. Thomas, and J. D. Joannopoulos, “An All-Dielectric Coaxial Waveguide,” *Science*, vol. 289, no. 5478, pp. 415–419, Jul. 2000, doi: 10.1126/science.289.5478.415.

[26] V. A. Tolmachev, T. S. Perova, and R. A. Moore, “Method of construction of composite one-dimensional photonic crystal with extended photonic band gaps,” *Opt. Express*, vol. 13, no. 21, p. 8433, 2005, doi: 10.1364/OPEX.13.008433.

[27] B. Gao, J. P. George, J. Beeckman, and K. Neyts, “Design, fabrication and characterization of a distributed Bragg reflector for reducing the étendue of a wavelength converting system,” *Opt. Express*, vol. 28, no. 9, p. 12837, Apr. 2020, doi: 10.1364/OE.391080.

[28] N. Kumar and B. Suthar, Eds., *Advances in photonic crystals and devices*. Boca Raton: CRC Press, 2020.

[29] Y. Mei, H.-Z. Wang, and S.-Y. Wang, “Transformation one-dimensional photonic crystal omnidirectional reflector,” *Optics Communications*, vol. 549, p. 129911, Dec. 2023, doi: 10.1016/j.optcom.2023.129911.

[30] S. Rabaste *et al.*, “Sol–gel fabrication of thick multilayers applied to Bragg reflectors and microcavities,” *Thin Solid Films*, vol. 416, no. 1–2, pp. 242–247, Sep. 2002, doi: 10.1016/S0040-6090(02)00722-8.

[31] A. Convertino, A. Valentini, and R. Cingolani, “Organic multilayers as distributed Bragg reflectors,” *Applied Physics Letters*, vol. 75, no. 3, pp. 322–324, Jul. 1999, doi: 10.1063/1.124363.

[32] S. Y. Choi, M. Mamak, G. Von Freymann, N. Chopra, and G. A. Ozin, “Mesoporous Bragg Stack Color Tunable Sensors,” *Nano*

Lett., vol. 6, no. 11, pp. 2456–2461, Nov. 2006, doi: 10.1021/nl061580m.

[33] V. Mikhelashvili and G. Eisenstein, "Effects of annealing conditions on optical and electrical characteristics of titanium dioxide films deposited by electron beam evaporation," *Journal of Applied Physics*, vol. 89, no. 6, pp. 3256–3269, Mar. 2001, doi: 10.1063/1.1349860.

[34] L. Persano *et al.*, "Monolithic polymer microcavity lasers with on-top evaporated dielectric mirrors," *Applied Physics Letters*, vol. 88, no. 12, p. 121110, Mar. 2006, doi: 10.1063/1.2179611.

[35] I. E. Shaaban, A. S. Samra, S. Muhammad, and S. Wageh, "Design of Distributed Bragg Reflectors for Green Light-Emitting Devices Based on Quantum Dots as Emission Layer," *Energies*, vol. 15, no. 3, p. 1237, Feb. 2022, doi: 10.3390/en15031237.

[36] N. Bilgili and A. Çetin, "1D photonic crystal biosensor for detection of SARS-CoV-2," Mar. 24, 2023. doi: 10.21203/rs.3.rs-2709079/v1.

[37] H.-J. Joo *et al.*, "1D photonic crystal direct bandgap GeSn-on-insulator laser," *Applied Physics Letters*, vol. 119, no. 20, p. 201101, Nov. 2021, doi: 10.1063/5.0066935.

[38] A. Bananej, R. Shiri H Shahrikhabadi, and T. Fathollahi Khalkhali, "Slow light generation by using one-dimensional photonic crystals for quantum memory applications," *ijpr*, vol. 21, no. 4, Dec. 2022, doi: 10.47176/ijpr.21.4.31225.

[39] L. Xu, F. Li, Y. Liu, F. Yao, and S. Liu, "Surface Plasmon Nanolaser: Principle, Structure, Characteristics and Applications," *Applied Sciences*, vol. 9, no. 5, p. 861, Feb. 2019, doi: 10.3390/app9050861.

[40] R. H. Ritchie, "Plasma Losses by Fast Electrons in Thin Films," *Phys. Rev.*, vol. 106, no. 5, pp. 874–881, Jun. 1957, doi: 10.1103/PhysRev.106.874.

[41] M. Aftab, M. S. Mansha, T. Iqbal, and M. Farooq, "Surface Plasmon Excitation: Theory, Configurations, and Applications," *Plasmonics*, Nov. 2023, doi: 10.1007/s11468-023-02095-2.

[42] A. G. Brolo, "Plasmonics for future biosensors," *Nature Photon*, vol. 6, no. 11, pp. 709–713, Nov. 2012, doi: 10.1038/nphoton.2012.266.

[43] M. A. Garcia, "Surface plasmons in metallic nanoparticles: fundamentals and applications," *J. Phys. D: Appl. Phys.*, vol. 44, no. 28, p. 283001, Jul. 2011, doi: 10.1088/0022-3727/44/28/283001.

[44] S. A. Maier, *Plasmonics: Fundamentals and Applications*. New York, NY: Springer US, 2007. doi: 10.1007/0-387-37825-1.

[45] Y.-C. Yeo, T.-J. King, and C. Hu, "Metal-dielectric band alignment and its implications for metal gate complementary metal-oxide-semiconductor technology," *Journal of Applied Physics*, vol. 92, no. 12, pp. 7266–7271, Dec. 2002, doi: 10.1063/1.1521517.

[46] C. Kar, S. Jena, D. V. Udupa, and K. D. Rao, "Tamm plasmon polariton in planar structures: A brief overview and applications," *Optics & Laser Technology*, vol. 159, p. 108928, Apr. 2023, doi: 10.1016/j.optlastec.2022.108928.

[47] M. Kaliteevski *et al.*, "Tamm plasmon-polaritons: Possible electromagnetic states at the interface of a metal and a dielectric Bragg mirror," *Phys. Rev. B*, vol. 76, no. 16, p. 165415, Oct. 2007, doi: 10.1103/PhysRevB.76.165415.

[48] M. E. Sasin *et al.*, "Tamm plasmon polaritons: Slow and spatially compact light," *Applied Physics Letters*, vol. 92, no. 25, p. 251112, Jun. 2008, doi: 10.1063/1.2952486.

[49] A. Kumari *et al.*, "Coupling to Tamm-plasmon-polaritons: dependence on structural parameters," *J. Phys. D: Appl. Phys.*, vol. 51, no. 25, p. 255103, Jun. 2018, doi: 10.1088/1361-6463/aac474.

[50] Z.-Y. Yang *et al.*, "Narrowband Wavelength Selective Thermal Emitters by Confined Tamm Plasmon Polaritons," *ACS Photonics*, vol. 4, no. 9, pp. 2212–2219, Sep. 2017, doi: 10.1021/acsphotonics.7b00408.

[51] B. I. Afinogenov, A. A. Popkova, V. O. Bessonov, and A. A. Fedyanin, "Measurements of the femtosecond relaxation dynamics of Tamm plasmon-polaritons," *Applied Physics Letters*, vol. 109, no. 17, p. 171107, Oct. 2016, doi: 10.1063/1.4966288.

[52] M. K. Shukla and R. Das, "Tamm-plasmon polaritons in one-dimensional photonic quasi-crystals," *Opt. Lett.*, vol. 43, no. 3, p. 362, Feb. 2018, doi: 10.1364/OL.43.000362.

[53] H. Lu, Y. Li, Z. Yue, D. Mao, and J. Zhao, "Topological insulator based Tamm plasmon polaritons," *APL Photonics*, vol. 4, no. 4, p. 040801, Apr. 2019, doi: 10.1063/1.5088033.

[54] Sk. S.-U. Rahman, T. Klein, S. Klembt, J. Gutowski, D. Hommel, and K. Sebald, "Observation of a hybrid state of Tamm plasmons and microcavity exciton polaritons," *Sci Rep*, vol. 6, no. 1, p. 34392, Oct. 2016, doi: 10.1038/srep34392.

[55] K. Hinrichs and K.-J. Eichhorn, Eds., *Ellipsometry of Functional Organic Surfaces and Films*, vol. 52. in Springer Series in Surface Sciences, vol. 52. Berlin, Heidelberg: Springer Berlin Heidelberg, 2014. doi: 10.1007/978-3-642-40128-2.

[56] V. G. Bordo and H. Rubahn, *Optics and Spectroscopy at Surfaces and Interfaces*, 1st ed. Wiley, 2005. doi: 10.1002/9783527618699.

[57] R. F. Oulton, "Surface plasmon lasers: sources of nanoscopic light," *Materials Today*, vol. 15, no. 1–2, pp. 26–34, Jan. 2012, doi: 10.1016/S1369-7021(12)70018-4.

[58] V. Vaicikauskas, G. Babonas, Z. Kuprionis, G. Niaura, and V. Šablinskas, *Paviršiaus optine spektroskopija*. TEV, Vilnius, 2008.

[59] A. P. Vinogradov, A. V. Dorofeenko, A. A. Pukhov, and A. A. Lisyansky, "Exciting surface plasmon polaritons in the Kretschmann configuration by a light beam," *Phys. Rev. B*, vol. 97, no. 23, p. 235407, Jun. 2018, doi: 10.1103/PhysRevB.97.235407.

[60] H. Raether, *Surface Plasmons on Smooth and Rough Surfaces and on Gratings*, vol. 111. in Springer Tracts in Modern Physics, vol. 111. Berlin, Heidelberg: Springer Berlin Heidelberg, 1988. doi: 10.1007/BFb0048317.

[61] C. L. Haynes, A. D. McFarland, and R. P. Van Duyne, "Surface-Enhanced Raman Spectroscopy," *Anal. Chem.*, vol. 77, no. 17, p. 338 A-346 A, Sep. 2005, doi: 10.1021/ac053456d.

[62] S. Azzini *et al.*, "Generation and Spatial Control of Hybrid Tamm Plasmon/Surface Plasmon Modes," *ACS Photonics*, vol. 3, no. 10, pp. 1776–1781, Oct. 2016, doi: 10.1021/acsphotonics.6b00521.

[63] R. Das, T. Srivastava, and R. Jha, "On the performance of Tamm-plasmon and surface-plasmon hybrid-mode refractive-index sensor in metallo-dielectric heterostructure configuration," *Sensors and Actuators B: Chemical*, vol. 206, pp. 443–448, Jan. 2015, doi: 10.1016/j.snb.2014.09.032.

[64] Y. Chen *et al.*, "Tamm plasmon- and surface plasmon-coupled emission from hybrid plasmonic–photonic structures," *Optica*, vol. 1, no. 6, p. 407, Dec. 2014, doi: 10.1364/OPTICA.1.000407.

[65] E. Buzavaite-Verteliene *et al.*, "Hybrid Tamm-surface plasmon polariton mode for highly sensitive detection of protein interactions," *Opt. Express*, vol. 28, no. 20, p. 29033, Sep. 2020, doi: 10.1364/OE.401802.

[66] E. Bužavaitė-Vertelienė, V. Vertelis, and Z. Balevičius, “The experimental evidence of a strong coupling regime in the hybrid Tamm plasmon-surface plasmon polariton mode,” *Nanophotonics*, vol. 10, no. 5, pp. 1565–1571, Mar. 2021, doi: 10.1515/nanoph-2020-0660.

[67] B. I. Afinogenov, V. O. Bessonov, A. A. Nikulin, and A. A. Fedyanin, “Observation of hybrid state of Tamm and surface plasmon-polaritons in one-dimensional photonic crystals,” *Applied Physics Letters*, vol. 103, no. 6, p. 061112, Aug. 2013, doi: 10.1063/1.4817999.

[68] M. Sarkar *et al.*, “Hybrid Plasmonic Mode by Resonant Coupling of Localized Plasmons to Propagating Plasmons in a Kretschmann Configuration,” *ACS Photonics*, vol. 2, no. 2, pp. 237–245, Feb. 2015, doi: 10.1021/ph500351b.

[69] A. Paulauskas, S. Tumenas, A. Selskis, T. Tolenis, A. Valavicius, and Z. Balevicius, “Hybrid Tamm-surface plasmon polaritons mode for detection of mercury adsorption on 1D photonic crystal/gold nanostructures by total internal reflection ellipsometry,” *Opt. Express*, vol. 26, no. 23, p. 30400, Nov. 2018, doi: 10.1364/OE.26.030400.

[70] I. Plikusienė, E. Bužavaitė-Vertelienė, V. Mačiulis, A. Valavičius, A. Ramanavičienė, and Z. Balevičius, “Application of Tamm Plasmon Polaritons and Cavity Modes for Biosensing in the Combined Spectroscopic Ellipsometry and Quartz Crystal Microbalance Method,” *Biosensors*, vol. 11, no. 12, p. 501, Dec. 2021, doi: 10.3390/bios11120501.

[71] A. Cuartero-González, S. Sanders, L. Zundel, A. I. Fernández-Domínguez, and A. Manjavacas, “Super- and Subradiant Lattice Resonances in Bipartite Nanoparticle Arrays,” *ACS Nano*, vol. 14, no. 9, pp. 11876–11887, Sep. 2020, doi: 10.1021/acsnano.0c04795.

[72] S. Derom, R. Vincent, A. Bouhelier, and G. Colas Des Francs, “Resonance quality, radiative/ohmic losses and modal volume of Mie plasmons,” *EPL*, vol. 98, no. 4, p. 47008, May 2012, doi: 10.1209/0295-5075/98/47008.

[73] A. Yang *et al.*, “Unidirectional Lasing from Template-Stripped Two-Dimensional Plasmonic Crystals,” *ACS Nano*, vol. 9, no. 12, pp. 11582–11588, Dec. 2015, doi: 10.1021/acsnano.5b05419.

[74] W. Wang, M. Ramezani, A. I. Väkeväinen, P. Törmä, J. G. Rivas, and T. W. Odom, “The rich photonic world of plasmonic nanoparticle arrays,” *Materials Today*, vol. 21, no. 3, pp. 303–314, Apr. 2018, doi: 10.1016/j.mattod.2017.09.002.

[75] D. Wang, J. Guan, J. Hu, M. R. Bourgeois, and T. W. Odom, “Manipulating Light–Matter Interactions in Plasmonic Nanoparticle Lattices,” *Acc. Chem. Res.*, vol. 52, no. 11, pp. 2997–3007, Nov. 2019, doi: 10.1021/acs.accounts.9b00345.

[76] E. Stankevičius, K. Vilkevičius, M. Gedvilas, E. Bužavaitė-Vertelienė, A. Selskis, and Z. Balevičius, “Direct Laser Writing for the Formation of Large-Scale Gold Microbumps Arrays Generating Hybrid Lattice Plasmon Polaritons in Vis–NIR Range,” *Advanced Optical Materials*, vol. 9, no. 12, p. 2100027, Jun. 2021, doi: 10.1002/adom.202100027.

[77] H. Deng, H. Haug, and Y. Yamamoto, “Exciton-polariton Bose-Einstein condensation,” *Rev. Mod. Phys.*, vol. 82, no. 2, pp. 1489–1537, May 2010, doi: 10.1103/RevModPhys.82.1489.

[78] M. Ramezani, M. Berghuis, and J. Gómez Rivas, “Strong light–matter coupling and exciton-polariton condensation in lattices of plasmonic nanoparticles [Invited],” *J. Opt. Soc. Am. B*, vol. 36, no. 7, p. E88, Jul. 2019, doi: 10.1364/JOSAB.36.000E88.

[79] A. I. Väkeväinen *et al.*, “Plasmonic Surface Lattice Resonances at the Strong Coupling Regime,” *Nano Lett.*, vol. 14, no. 4, pp. 1721–1727, Apr. 2014, doi: 10.1021/nl4035219.

[80] W. Lin *et al.*, “Physical mechanism on exciton-plasmon coupling revealed by femtosecond pump-probe transient absorption spectroscopy,” *Materials Today Physics*, vol. 3, pp. 33–40, Dec. 2017, doi: 10.1016/j.mtphys.2017.12.001.

[81] S. Ghosh *et al.*, “Microcavity exciton polaritons at room temperature,” *Photonics Insights*, vol. 1, no. 1, p. R04, 2022, doi: 10.3788/PI.2022.R04.

[82] M. Kautto, *Spectroscopic Study of Strong Coupling between R6G-dye and optical cavities*. University of Jyväskylä, 2018.

[83] Y. Niu, L. Gao, H. Xu, and H. Wei, “Strong coupling of multiple plasmon modes and excitons with excitation light controlled active tuning,” *Nanophotonics*, vol. 12, no. 4, pp. 735–742, Feb. 2023, doi: 10.1515/nanoph-2022-0701.

[84] M. Ramezani *et al.*, “Plasmon-exciton-polariton lasing,” *Optica*, vol. 4, no. 1, p. 31, Jan. 2017, doi: 10.1364/OPTICA.4.000031.

[85] S. Kéna-Cohen and S. R. Forrest, “Room-temperature polariton lasing in an organic single-crystal microcavity,” *Nature Photon*, vol. 4, no. 6, pp. 371–375, Jun. 2010, doi: 10.1038/nphoton.2010.86.

[86] B. Valeur and M. N. Berberan-Santos, *Molecular fluorescence: principles and applications*, Second edition. Weinheim,

Germany : [Chichester, England]: Wiley-VCH ; Wiley-VCH Verlag GmbH & Co. KGaA, 2012.
[87] V. I. Klimov, Ed., *Nanocrystal Quantum Dots*, 2nd ed. CRC Press, 2017. doi: 10.1201/9781420079272.
[88] C. W. Tang and S. A. VanSlyke, "Organic electroluminescent diodes," *Applied Physics Letters*, vol. 51, no. 12, pp. 913–915, Sep. 1987, doi: 10.1063/1.98799.
[89] D. A. B. Miller, "Optical Physics of Quantum Wells," pp. 239–266, 1996.
[90] J. R. Lakowicz, Ed., "Instrumentation for Fluorescence Spectroscopy," in *Principles of Fluorescence Spectroscopy*, Boston, MA: Springer US, 2006, pp. 27–61. doi: 10.1007/978-0-387-46312-4_2.
[91] E. M. Purcell, "Spontaneous emission probabilities at radio frequencies," *Physical Review*, vol. 69, no. 11–1, p. 681, 1946.
[92] G. Khitrova, H. M. Gibbs, M. Kira, S. W. Koch, and A. Scherer, "Vacuum Rabi splitting in semiconductors," *Nature Phys*, vol. 2, no. 2, pp. 81–90, Feb. 2006, doi: 10.1038/nphys227.
[93] J. R. Lakowicz, "Radiative decay engineering 5: metal-enhanced fluorescence and plasmon emission," *Analytical Biochemistry*, vol. 337, no. 2, pp. 171–194, Feb. 2005, doi: 10.1016/j.ab.2004.11.026.
[94] J. A. Schuller, E. S. Barnard, W. Cai, Y. C. Jun, J. S. White, and M. L. Brongersma, "Plasmonics for extreme light concentration and manipulation," *Nature Mater*, vol. 9, no. 3, pp. 193–204, Mar. 2010, doi: 10.1038/nmat2630.
[95] L. Novotny and N. Van Hulst, "Antennas for light," *Nature Photon*, vol. 5, no. 2, pp. 83–90, Feb. 2011, doi: 10.1038/nphoton.2010.237.
[96] V. Giannini, A. I. Fernández-Domínguez, S. C. Heck, and S. A. Maier, "Plasmonic Nanoantennas: Fundamentals and Their Use in Controlling the Radiative Properties of Nanoemitters," *Chem. Rev.*, vol. 111, no. 6, pp. 3888–3912, Jun. 2011, doi: 10.1021/cr1002672.
[97] J. Homola, S. S. Yee, and G. Gauglitz, "Surface plasmon resonance sensors: review," *Sensors and Actuators B: Chemical*, vol. 54, no. 1–2, pp. 3–15, Jan. 1999, doi: 10.1016/S0925-4005(98)00321-9.
[98] N. Liu, M. L. Tang, M. Hentschel, H. Giessen, and A. P. Alivisatos, "Nanoantenna-enhanced gas sensing in a single tailored nanofocus," *Nature Mater*, vol. 10, no. 8, pp. 631–636, Aug. 2011, doi: 10.1038/nmat3029.

[99] M. S. Tame, K. R. McEnery, S. K. Ozdemir, J. Lee, S. A. Maier, and M. S. Kim, "Quantum Plasmonics," 2013, doi: 10.48550/ARXIV.1312.6806.
[100] P. Berini and I. De Leon, "Surface plasmon–polariton amplifiers and lasers," *Nature Photon*, vol. 6, no. 1, pp. 16–24, Jan. 2012, doi: 10.1038/nphoton.2011.285.
[101] S. I. Bozhevolnyi, V. S. Volkov, E. Devaux, J.-Y. Laluet, and T. W. Ebbesen, "Channel plasmon subwavelength waveguide components including interferometers and ring resonators," *Nature*, vol. 440, no. 7083, pp. 508–511, Mar. 2006, doi: 10.1038/nature04594.
[102] O. G. Peterson, J. P. Webb, W. C. McColgin, and J. H. Eberly, "Organic Dye Laser Threshold," *Journal of Applied Physics*, vol. 42, no. 5, pp. 1917–1928, Apr. 1971, doi: 10.1063/1.1660468.
[103] G. H. Patterson and D. W. Piston, "Photobleaching in Two-Photon Excitation Microscopy," *Biophysical Journal*, vol. 78, no. 4, pp. 2159–2162, Apr. 2000, doi: 10.1016/S0006-3495(00)76762-2.
[104] R. Bonnett and G. Martínez, "Photobleaching of sensitisers used in photodynamic therapy," *Tetrahedron*, vol. 57, no. 47, pp. 9513–9547, Nov. 2001, doi: 10.1016/S0040-4020(01)00952-8.
[105] I. Georgakoudi, M. G. Nichols, and T. H. Foster, "The Mechanism of Photofrin Photobleaching and Its Consequences for Photodynamic Dosimetry," *Photochem & Photobiology*, vol. 65, no. 1, pp. 135–144, Jan. 1997, doi: 10.1111/j.1751-1097.1997.tb01889.x.
[106] X. Kong, E. Nir, K. Hamadani, and S. Weiss, "Photobleaching Pathways in Single-Molecule FRET Experiments," *J. Am. Chem. Soc.*, vol. 129, no. 15, pp. 4643–4654, Apr. 2007, doi: 10.1021/ja068002s.
[107] P. Jönsson, M. P. Jonsson, J. O. Tegenfeldt, and F. Höök, "A Method Improving the Accuracy of Fluorescence Recovery after Photobleaching Analysis," *Biophysical Journal*, vol. 95, no. 11, pp. 5334–5348, Dec. 2008, doi: 10.1529/biophysj.108.134874.
[108] D. M. Soumpasis, "Theoretical analysis of fluorescence photobleaching recovery experiments," *Biophysical Journal*, vol. 41, no. 1, pp. 95–97, Jan. 1983, doi: 10.1016/S0006-3495(83)84410-5.
[109] T. Zal and N. R. J. Gascoigne, "Photobleaching-Corrected FRET Efficiency Imaging of Live Cells," *Biophysical Journal*, vol. 86, no. 6, pp. 3923–3939, Jun. 2004, doi: 10.1529/biophysj.103.022087.

[110] R. Del Vecchio and N. V. Blough, “Photobleaching of chromophoric dissolved organic matter in natural waters: kinetics and modeling,” *Marine Chemistry*, vol. 78, no. 4, pp. 231–253, Jun. 2002, doi: 10.1016/S0304-4203(02)00036-1.
[111] H. Fujiwara, *Spectroscopic Ellipsometry: Principles and Applications*, 1st ed. Wiley, 2007. doi: 10.1002/9780470060193.
[112] J. Xie *et al.*, “Optical properties of chemical vapor deposition-grown PtSe $_2$ characterized by spectroscopic ellipsometry,” *2D Mater.*, vol. 6, no. 3, p. 035011, Apr. 2019, doi: 10.1088/2053-1583/ab1490.
[113] R. M. A. Azzam and N. M. Bashara, *Ellipsometry and polarized ligth*, Snd ed. rev. in North-Holland personal library. Amsterdam: North-Holland, 1989.
[114] D. E. Aspnes, *Spectroscopic Ellipsometry of Solids*, vol. 15. Optical Properties of Solids, 1976.
[115] H. G. Tompkins and E. A. Irene, Eds., *Handbook of ellipsometry*. Norwich, NY : Heidelberg, Germany: William Andrew Pub. ; Springer, 2005.
[116] J. A. Woollam and P. G. Snyder, *Variable Angle Spectroscopic Ellipsometry*, vol. 401–411. Boston: Buttrerworth-Heinemann, 1992.
[117] H. Arwin, M. Poksinski, and K. Johansen, “Total internal reflection ellipsometry: principles and applications,” *Appl. Opt.*, vol. 43, no. 15, p. 3028, May 2004, doi: 10.1364/AO.43.003028.
[118] A. Nabok and A. Tsargorodskaya, “The method of total internal reflection ellipsometry for thin film characterisation and sensing,” *Thin Solid Films*, vol. 516, no. 24, pp. 8993–9001, Oct. 2008, doi: 10.1016/j.tsf.2007.11.077.
[119] V. M. Agranovich and D. L. Mills, *Surface polaritons: electromagnetic waves at surfaces and interfaces*. in Modern problems in condensed matter sciences. Amsterdam New York: North-Holland Pub. Co. Sole distributors for the USA and Canada, Elsevier Science Pub. Co, 1982.
[120] V. M. Shalaev, Ed., *Nanophotonics with surface plasmons*, 1st ed. in Advances in nano-optics and nano-photonics, no. 2. Amsterdam ; Boston, MA: Elsevier, 2007.
[121] R. N. Hall, G. E. Fenner, J. D. Kingsley, T. J. Soltys, and R. O. Carlson, “Coherent Light Emission From GaAs Junctions,” *Phys. Rev. Lett.*, vol. 9, no. 9, pp. 366–368, Nov. 1962, doi: 10.1103/PhysRevLett.9.366.

[122] G. G. Stokes, “XXX. On the change of refrangibility of light,” *Phil. Trans. R. Soc.*, vol. 142, pp. 463–562, Dec. 1852, doi: 10.1098/rstl.1852.0022.
[123] G. Weber, “Fluorescence-polarization spectrum and electronic-energy transfer in proteins.,” *Biochemical Journal*, vol. 51(2), pp. 155–167, 1952.
[124] D. L. Farkas, M. D. Wei, P. Febbroriello, J. H. Carson, and L. M. Loew, “Simultaneous imaging of cell and mitochondrial membrane potentials,” *Biophysical Journal*, vol. 56, no. 6, pp. 1053–1069, Dec. 1989, doi: 10.1016/S0006-3495(89)82754-7.
[125] M. Chalfie, Y. Tu, G. Euskirchen, W. W. Ward, and D. C. Prasher, “Green Fluorescent Protein as a Marker for Gene Expression,” *Science*, vol. 263, no. 5148, pp. 802–805, Feb. 1994, doi: 10.1126/science.8303295.
[126] W. Becker, “Fluorescence lifetime imaging – techniques and applications,” *Journal of Microscopy*, vol. 247, no. 2, pp. 119–136, Aug. 2012, doi: 10.1111/j.1365-2818.2012.03618.x.
[127] R. Datta, T. M. Heaster, J. T. Sharick, A. A. Gillette, and M. C. Skala, “Fluorescence lifetime imaging microscopy: fundamentals and advances in instrumentation, analysis, and applications,” *J. Biomed. Opt.*, vol. 25, no. 07, p. 1, May 2020, doi: 10.1117/1.JBO.25.7.071203.
[128] J. T. Gudmundsson and D. Lundin, “Introduction to magnetron sputtering,” in *High Power Impulse Magnetron Sputtering*, Elsevier, 2020, pp. 1–48. doi: 10.1016/B978-0-12-812454-3.00006-1.
[129] C. H. Shon and J. K. Lee, “Modeling of magnetron sputtering plasmas,” *Applied Surface Science*, vol. 192, no. 1–4, pp. 258–269, May 2002, doi: 10.1016/S0169-4332(02)00030-2.
[130] V. Stranak *et al.*, “Deposition of thin titanium–copper films with antimicrobial effect by advanced magnetron sputtering methods,” *Materials Science and Engineering: C*, vol. 31, no. 7, pp. 1512–1519, Oct. 2011, doi: 10.1016/j.msec.2011.06.009.
[131] D. Pavlov, A. Zhizhchenko, L. Pan, and A. A. Kuchmizhak, “Tuning Collective Plasmon Resonances of Femtosecond Laser-Printed Metasurface,” *Materials*, vol. 15, no. 5, p. 1834, Mar. 2022, doi: 10.3390/ma15051834.
[132] A. Selimis, V. Mironov, and M. Farsari, “Direct laser writing: Principles and materials for scaffold 3D printing,” *Microelectronic Engineering*, vol. 132, pp. 83–89, Jan. 2015, doi: 10.1016/j.mee.2014.10.001.

[133] Z.-L. Wu *et al.*, “Polymer-Based Device Fabrication and Applications Using Direct Laser Writing Technology,” *Polymers*, vol. 11, no. 3, p. 553, Mar. 2019, doi: 10.3390/polym11030553.
[134] M. Moebius, K. Vora, S. Kang, P. Munoz, G. Deng, and E. Mazur, “Direct Laser Writing of 3D Gratings and Diffraction Optics,” in *CLEO: 2015*, San Jose, California: OSA, 2015, p. SW1K.6. doi: 10.1364/CLEO_SI.2015.SW1K.6.
[135] J. F. Galisteo-López, M. López-García, A. Blanco, and C. López, “Studying Light Propagation in Self-Assembled Hybrid Photonic–Plasmonic Crystals by Fourier Microscopy,” *Langmuir*, vol. 28, no. 24, pp. 9174–9179, Jun. 2012, doi: 10.1021/la300448y.
[136] M. Seo and M. Lee, “Surface plasmon resonance and coloration in stainless steel with a 2D periodic texture,” *Appl. Phys. A*, vol. 125, no. 9, p. 624, Sep. 2019, doi: 10.1007/s00339-019-2926-9.
[137] J. Guo, Z. Li, and H. Guo, “Near perfect light trapping in a 2D gold nanotrench grating at oblique angles of incidence and its application for sensing,” *Opt. Express*, vol. 24, no. 15, p. 17259, Jul. 2016, doi: 10.1364/OE.24.017259.
[138] T. Kerdcharoen and C. Wongchoosuk, “Carbon nanotube and metal oxide hybrid materials for gas sensing,” in *Semiconductor Gas Sensors*, Elsevier, 2013, pp. 386–407. doi: 10.1533/9780857098665.3.386.
[139] M. D. Tyona, “A theoritical study on spin coating technique,” *Advances in materials Research*, vol. 2, no. 4, pp. 195–208, Dec. 2013, doi: 10.12989/AMR.2013.2.4.195.
[140] T. Karstens and K. Kobs, “Rhodamine B and rhodamine 101 as reference substances for fluorescence quantum yield measurements,” *J. Phys. Chem.*, vol. 84, no. 14, pp. 1871–1872, Jul. 1980, doi: 10.1021/j100451a030.
[141] P. Hildebrandt and M. Stockburger, “Surface-enhanced resonance Raman spectroscopy of Rhodamine 6G adsorbed on colloidal silver,” *J. Phys. Chem.*, vol. 88, no. 24, pp. 5935–5944, Nov. 1984, doi: 10.1021/j150668a038.
[142] H. Kogelnik and C. V. Shank, “STIMULATED EMISSION IN A PERIODIC STRUCTURE,” *Applied Physics Letters*, vol. 18, no. 4, pp. 152–154, Feb. 1971, doi: 10.1063/1.1653605.
[143] S. Franzen, “Surface Plasmon Polaritons and Screened Plasma Absorption in Indium Tin Oxide Compared to Silver and Gold,” *J. Phys. Chem. C*, vol. 112, no. 15, pp. 6027–6032, Apr. 2008, doi: 10.1021/jp7097813.

[144] P. Vasa *et al.*, “Real-time observation of ultrafast Rabi oscillations between excitons and plasmons in metal nanostructures with J-aggregates,” *Nature Photon*, vol. 7, no. 2, pp. 128–132, Feb. 2013, doi: 10.1038/nphoton.2012.340.
[145] A. Graf, L. Tropf, Y. Zakharko, J. Zaumseil, and M. C. Gather, “Near-infrared exciton-polaritons in strongly coupled single-walled carbon nanotube microcavities,” *Nat Commun*, vol. 7, no. 1, p. 13078, Oct. 2016, doi: 10.1038/ncomms13078.
[146] J. Galego, F. J. Garcia-Vidal, and J. Feist, “Suppressing photochemical reactions with quantized light fields,” *Nat Commun*, vol. 7, no. 1, p. 13841, Dec. 2016, doi: 10.1038/ncomms13841.
[147] A. Lyons *et al.*, “Fluorescence lifetime Hong-Ou-Mandel sensing,” *Nat Commun*, vol. 14, no. 1, p. 8005, Dec. 2023, doi: 10.1038/s41467-023-43868-x.
[148] G. Sun, J. B. Khurgin, and R. A. Soref, “Practical enhancement of photoluminescence by metal nanoparticles,” *Applied Physics Letters*, vol. 94, no. 10, p. 101103, Mar. 2009, doi: 10.1063/1.3097025.
[149] D. A. Helmerich, G. Beliu, S. S. Matikonda, M. J. Schnermann, and M. Sauer, “Photoblueing of organic dyes can cause artifacts in super-resolution microscopy,” *Nat Methods*, vol. 18, no. 3, pp. 253–257, Mar. 2021, doi: 10.1038/s41592-021-01061-2.
[150] R. Eckenstaler and R. A. Benndorf, “A Combined Acceptor Photobleaching and Donor Fluorescence Lifetime Imaging Microscopy Approach to Analyze Multi-Protein Interactions in Living Cells,” *Front. Mol. Biosci.*, vol. 8, p. 635548, May 2021, doi: 10.3389/fmolb.2021.635548.
[151] W. Hwang, D. Kim, S. Lee, Y. J. Won, S. Moon, and D. Y. Kim, “Analysis of biexponential decay signals in the analog mean-delay fluorescence lifetime measurement method,” *Optics Communications*, vol. 443, pp. 136–143, Jul. 2019, doi: 10.1016/j.optcom.2019.02.059.
[152] V. M. Agranovich, M. Litinskaia, and D. G. Lidzey, “Cavity polaritons in microcavities containing disordered organic semiconductors,” *Phys. Rev. B*, vol. 67, no. 8, p. 085311, Feb. 2003, doi: 10.1103/PhysRevB.67.085311.
[153] M. Köllner and J. Wolfrum, “How many photons are necessary for fluorescence-lifetime measurements?,” *Chemical Physics Letters*, vol. 200, no. 1–2, pp. 199–204, Nov. 1992, doi: 10.1016/0009-2614(92)87068-Z.

[154] J. M. McMahon, J. Henzie, T. W. Odom, G. C. Schatz, and S. K. Gray, “Tailoring the sensing capabilities of nanohole arrays in gold films with Rayleigh anomaly-surface plasmon polaritons,” *Opt. Express*, vol. 15, no. 26, p. 18119, 2007, doi: 10.1364/OE.15.018119.

[155] G. C. Schatz, J. M. McMahon, and S. K. Gray, “Tailoring the parameters of nanohole arrays in gold films for sensing applications,” presented at the NanoScience + Engineering, M. I. Stockman, Ed., San Diego, California, USA, Sep. 2007, p. 664103. doi: 10.1117/12.731368.

[156] S. Zou, N. Janel, and G. C. Schatz, “Silver nanoparticle array structures that produce remarkably narrow plasmon lineshapes,” *The Journal of Chemical Physics*, vol. 120, no. 23, pp. 10871–10875, Jun. 2004, doi: 10.1063/1.1760740.

[157] V. A. Markel, “Coupled-dipole Approach to Scattering of Light from a One-dimensional Periodic Dipole Structure,” *Journal of Modern Optics*, vol. 40, no. 11, pp. 2281–2291, Nov. 1993, doi: 10.1080/09500349314552291.

[158] K. T. Carron, H. W. Lehmann, W. Fluhr, M. Meier, and A. Wokaun, “Resonances of two-dimensional particle gratings in surface-enhanced Raman scattering,” *J. Opt. Soc. Am. B*, vol. 3, no. 3, p. 430, Mar. 1986, doi: 10.1364/JOSAB.3.000430.

[159] B. Liedberg, C. Nylander, and I. Lundström, “Biosensing with surface plasmon resonance — how it all started,” *Biosensors and Bioelectronics*, vol. 10, no. 8, pp. i–ix, Jan. 1995, doi: 10.1016/0956-5663(95)96965-2.

[160] V. G. Kravets *et al.*, “Singular phase nano-optics in plasmonic metamaterials for label-free single-molecule detection,” *Nature Mater*, vol. 12, no. 4, pp. 304–309, Apr. 2013, doi: 10.1038/nmat3537.

[161] Y. Tsurimaki *et al.*, “Topological Engineering of Interfacial Optical Tamm States for Highly Sensitive Near-Singular-Phase Optical Detection,” *ACS Photonics*, vol. 5, no. 3, pp. 929–938, Mar. 2018, doi: 10.1021/acsphotonics.7b01176.

[162] Y. Nishijima, N. To, A. Balčytis, and S. Juodkazis, “Absorption and scattering in perfect thermal radiation absorber-emitter metasurfaces,” *Opt. Express*, vol. 30, no. 3, p. 4058, Jan. 2022, doi: 10.1364/OE.447885.

[163] U. Koch *et al.*, “Plasmonics—high-speed photonics for co-integration with electronics,” *Jpn. J. Appl. Phys.*, vol. 60, no. SB, p. SB0806, May 2021, doi: 10.35848/1347-4065/abef13.

[164] R.-M. Ma, R. F. Oulton, V. J. Sorger, G. Bartal, and X. Zhang, “Room-temperature sub-diffraction-limited plasmon laser by total internal reflection,” *Nature Mater*, vol. 10, no. 2, pp. 110–113, Feb. 2011, doi: 10.1038/nmat2919.
[165] U. Kreibig and M. Vollmer, *Optical properties of metal clusters*. in Springer series in materials science, no. 25. Berlin Heidelberg: Springer, 2010.
[166] V. Reshetnyak, I. Pinkevych, T. Bunning, and D. Evans, “Influence of Rugate Filters on the Spectral Manifestation of Tamm Plasmon Polaritons,” *Materials*, vol. 14, no. 5, p. 1282, Mar. 2021, doi: 10.3390/ma14051282.
[167] N. K. Gupta, A. K. Tiwari, H. Wanare, and S. A. Ramakrishna, “Near singular-phase optical biosensing with strongly coupled modes of a plasmonic–photonic trimer,” *J. Opt.*, vol. 23, no. 6, p. 065003, Jun. 2021, doi: 10.1088/2040-8986/abf8ce.
[168] Z. Balevicius and A. Baskys, “Optical Dispersions of Bloch Surface Waves and Surface Plasmon Polaritons: Towards Advanced Biosensors,” *Materials*, vol. 12, no. 19, p. 3147, Sep. 2019, doi: 10.3390/ma12193147.
[169] A. Sinibaldi *et al.*, “Direct comparison of the performance of Bloch surface wave and surface plasmon polariton sensors,” *Sensors and Actuators B: Chemical*, vol. 174, pp. 292–298, Nov. 2012, doi: 10.1016/j.snb.2012.07.015.
[170] E. Bužavaitė-Vertelienė *et al.*, “Total Internal Reflection Ellipsometry Approach for Bloch Surface Waves Biosensing Applications,” *Biosensors*, vol. 12, no. 8, p. 584, Jul. 2022, doi: 10.3390/bios12080584.
[171] C. Amra *et al.*, “Energy density engineering via zero-admittance domains in all-dielectric stratified materials,” *Phys. Rev. A*, vol. 97, no. 2, p. 023819, Feb. 2018, doi: 10.1103/PhysRevA.97.023819.
[172] D. Niu *et al.*, “Excitation of Bloch Surface Waves in Zero-Admittance Multilayers for High-Sensitivity Sensor Applications,” *Phys. Rev. Applied*, vol. 13, no. 5, p. 054064, May 2020, doi: 10.1103/PhysRevApplied.13.054064.
[173] V. G. Kravets, F. Schedin, A. V. Kabashin, and A. N. Grigorenko, “Sensitivity of collective plasmon modes of gold nanoresonators to local environment,” *Opt. Lett.*, vol. 35, no. 7, p. 956, Apr. 2010, doi: 10.1364/OL.35.000956.
[174] J. Anulytė, E. Bužavaitė-Vertelienė, V. Vertelis, E. Stankevičius, K. Vilkevičius, and Z. Balevičius, “Influence of a gold nano-bumps surface lattice array on the propagation length of strongly

coupled Tamm and surface plasmon polaritons," *J. Mater. Chem. C*, vol. 10, no. 36, pp. 13234–13241, 2022, doi: 10.1039/D2TC02174A.
[175] V. G. Kravets, F. Schedin, and A. N. Grigorenko, "Extremely Narrow Plasmon Resonances Based on Diffraction Coupling of Localized Plasmons in Arrays of Metallic Nanoparticles," *Phys. Rev. Lett.*, vol. 101, no. 8, p. 087403, Aug. 2008, doi: 10.1103/PhysRevLett.101.087403.
[176] C. V. Hoang *et al.*, "Interplay of hot electrons from localized and propagating plasmons," *Nat Commun*, vol. 8, no. 1, p. 771, Oct. 2017, doi: 10.1038/s41467-017-00815-x.
[177] Z. Balevičius, "Strong Coupling between Tamm and Surface Plasmons for Advanced Optical Bio-Sensing," *Coatings*, vol. 10, no. 12, p. 1187, Dec. 2020, doi: 10.3390/coatings10121187.
[178] H. Arwin, *Ellipsometry of functional organic surfaces and films*, 1st edition. in Springer series in surface sciences, no. 52. New York: Springer, 2013.
[179] Z. Balevicius *et al.*, "In situ study of ligand–receptor interaction by total internal reflection ellipsometry," *Thin Solid Films*, vol. 571, pp. 744–748, Nov. 2014, doi: 10.1016/j.tsf.2013.10.090.
[180] Z. Balevicius *et al.*, "Study of optical anisotropy in thin molecular layers by total internal reflection ellipsometry," *Sensors and Actuators B: Chemical*, vol. 181, pp. 119–124, May 2013, doi: 10.1016/j.snb.2013.01.059.
[181] C. Rhodes *et al.*, "Surface plasmon resonance in conducting metal oxides," *Journal of Applied Physics*, vol. 100, no. 5, p. 054905, Sep. 2006, doi: 10.1063/1.2222070.

Vilnius University Press
9 Saulėtekio Ave., Building III, LT-10222 Vilnius
Email: info@leidykla.vu.lt, www.leidykla.vu.lt
bookshop.vu.lt, journals.vu.lt
Print run 16